Friedrich-Schiller-University Jena

Institute for Geography

Department for Earth Observation

in cooperation with

Max Planck Institute for Biogeochemistry Jena

GEO 512: Master thesis

Retrieval of structural properties of vegetation in a Mediterranean ecosystem using TLS

by Ekaterina Bogdanovich

Course of studies: M.Sc. Geoinformatics

Matriculation number: 148087

Trierer Straße 28

99423 Weimar

Germany

e-Mail: ekaterina.manakhova@uni-jena.de

Reviewers:

Prof. Dr. Christiane Schmullius

(Friedrich-Schiller-University Jena)

Dr. Oscar Peréz-Priego

(Max Planck Institute for Biogeochemistry Jena)

Handover date: 10.08.2018

Contents

List of Figures

List of figures in Appendix.

List of tables:

List of abbreviations:

GIS	Geographical Information Systems
LiDAR	Light Detection and Ranging
TLS	Terrestrial Laser Scanner
DBH	Diameter at the Breast Height
UAS	Unmanned Aerial Systems
TIN	Triangulated Irregular Network
CHM	Canopy Height Model
DH	Dendrometer Height
LL	Low Level (80 cm from the ground)
MT	Main eddy-covariance Tower
ST	South eddy-covariance Tower
NT	North eddy-covariance Tower
CM	Method of DBH calculation from circumference
PR	Method of DBH calculation from perpendiculars
HP	Hemispherical Photography
EC tower	Eddy-Covariance tower
LAI	Leaf Area Index
eLAI	Effective Leaf Area Index
DEM	Digital Elevation Model
DTM	Digital Terrain Model
NASA	National Aeronautics and Space Administration

List of symbols:

Ω	Clumping index
π	Pi number

Units:

ha	Hectare
km	Kilometer
m	Meter
cm	Centimeter
nm	Nanometer
mg m^{-2}	Milligram per quadrat meter
m^2	Quadrat meter
GB	Gigabyte
n*ha-1	Number per hectare

Acknowledgement

The present master thesis was carried out at the Department for Earth Observation at the Friedrich-Schiller-University in cooperation with Max-Planck-Institute for Biogeochemistry in Jena. I am very grateful Prof. Dr. Christiane Schmullius and all members of academic staff or the comprehensive education in the last years.

I would like to extend my deepest gratitude to my supervisor Dr. Oscar Peréz-Priego for all the support and guidance of my study from the first steps to the day of handover. I have been lucky to have a supervisor who was so generous with his time and knowledge. ¡Muchas gracias!

I am also grateful to Dr. Marcus Guderle for his helpful practical advices. Special thanks to The Biosphere-Atmosphere Experimentation and Interactions Group (BAIE), especially to the group leader Dr. Mirco Migliavacca, for sharing their valuable suggestions and experience with me. Moreover, my sincere thanks to Dr. Arthur Maxwell Sayler for the proofreading.

Finally, I thank my beloved husband for supporting me in the resent years.

1 Introduction

Ecosystem functions and processes are largely determined by structural parameters of vegetation (WIEZIK et al. 2011, GAITAN et al. 2014). Biometrical parameters of vegetation such as plant height, plant volume, diameter at the breast height etc. and their spatial distribution are fundamental variables in ecosystem research and modeling of plant functional types, diversity, carbon accounting, as well as ecophysiology (BROWN & LUGO 1992, HOUGHTON et al. 2001, CHAVE et al. 2005, GIBBS et al. 2007). For instance, the amount of light used for photosynthesis is largely determined by the amount and distribution of leaves within a vegetative canopy, and therefore, leaf area index (LAI; amount of leaves per unit of ground area) and clumping index (Ω; variable defining leaf distribution) are key structural variables in modeling of biosphere-atmosphere exchanges of energy, water vapor and carbon dioxide (ASNER et al. 2003, BREDA 2003). Thus, proper estimation of vegetation structure is necessary for understanding the ecological processes in an ecosystem.

Light Detection and Ranging (LiDAR) is a remote sensing technique that has been used successfully to estimate vegetation structural parameters (VAN LEEUWEN & NIEUWENHUIS 2010, HILL et al. 2011). LiDAR is an active sensor that measures distance to the object by generating beam of light. Its major advantage over optical sensors is its ability to obtain the 3D structure of objects (LEFSKY et al. 2002, HILL et al. 2011). LiDAR instruments can be classified according to the placement of the scanner: spaceborne, airborne and ground-based LiDAR (also termed as Terrestrial Laser Scanner, TLS) (LEMMENS 2011). Whereas spaceborne LiDAR is mostly used for land cover classification and estimation of terrain elevation on global scale, airborne and ground-based LiDAR provides information about vegetation structure at the scale of a single tree to the whole ecosystem. It is worth remarking that TLS acquires not only height level vegetation like airborne LiDAR, but also the structure of understory, which play an important role. (VAN LEEUWEN & NIEUWENHUIS 2010, DASSOT et al. 2011). The use of TLS is, therefore, essential when targeting tree-grass ecosystems.

The ability of TLS to provide the information of vegetation structure on different levels is especially useful for research of savanna ecosystem, which is characterized by existence of two separated layers: sparse trees (typically between 10-40 tree/ha) and a well-stablished herbaceous stratum. Savanna is one of most important ecosystems of our planet as it covers a quarter (27 million km^2) of Earth's land surface and is credited as the main source of food (via pastoral industry) for almost a quarter of the world's human

population. The productivity of savanna is about 25% of total Gross Primary Production (SCHOLES & ARCHER 1997) and can vary depending on different factors, e.g. seasonal moisture variability, annual solar radiation budget, fires or spatial heterogeneity of vegetation (BERINGER et al. 2007, KANNIAH et al. 2011, KANNIAH et al. 2013, MOORE et al. 2015). The contribution of trees to the productivity of the ecosystem depends to some extent on how trees and grass compete each other for resources (e.g. water, nutrients, light etc.), which is strongly regulated by their spatial distribution and temporal dynamic. The trees influence the herbaceous productivity by storing water and nutrients and via protection from overheating (JOFFRE & RAMBAL 1993, BELSKY 1994, VALLADARES & PUGNAIRE 1999, MOORE et al. 2015). In fact, divergent patterns of the grass have been described in space, with clear differences in structure and functions between the grass underneath and between the crowns. This has been associated with structural relations between the tree crown projections and properties (i.e. gap fraction), soil moisture and nutrient availability and tree root development capacity. TLS provides an accurate estimation of tree parameters and their spatial distribution, which is critical for modeling of savanna ecosystem (HILL et al. 2011). CHEN et al. (2006) used LiDAR-derived Canopy Height Model (CHM) for delineation of trees in open oak savanna in California. GARCÍA et al. (2015) calculated Clumping index for oak trees in Spanish savanna based on gap fraction using TLS. The combination of airborne LiDAR and hyperspectral data were applied to classification and mapping tree species in African savannas (CHO et al. 2012, COLGAN et al. 2012, NAIDOO et al. 2012).

In practice, the application of TLS to heterogeneous ecosystems such as savannas remains challenging (HILL et al. 2011). One of the technical problems is occluded areas in laser scans that complicates estimation of trees' locations and diameter retrieval in the areas with high tree density (MOSKAL & ZHENG 2011). Additionally, TLS has the tendency to underestimate tree height, because of low point density in the upper canopy (HOPKINSON et al. 2004). Moreover, proper filtering and classification of points in the point cloud can be difficult, especially in areas covered by low-level vegetation (LIM et al. 2003). To improve the efficiency of LiDAR measurements the researchers have suggested the combination of TLS with optical sensors, development of new more effective approaches, as well as improvement of LiDAR technology itself (LIM et al. 2003, VAN LEEUWEN & NIEUWENHUIS 2010, DASSOT et al. 2011).

The objectives of this thesis are:

   i.   Evaluate and develop approaches for retrieval of structural parameters of vegetation (i.e. tree height, canopy projected area and perimeter, diameter at the breast height and canopy clumping index).

   ii. Characterize structural properties of ecosystem. The spatial distribution of tree structural parameters and their biometrical relationships is to be evaluated.

The thesis is divided in several different chapters described below. Chapter 2 describes the basics of LiDAR measurements and its application and gives an overview of Mediterranean savanna ecosystem (Dehesa). Chapter 3 provides the state of research in retrieval of structural vegetation properties. Chapter 4 introduces the study area, the data sets used and methodology. The results are presented in chapter 5. Finally, in chapter 6 there is a discussion of the findings and conclusions (chapter 7) close the thesis.

2 Theoretical background

2.1 LiDAR application

Remote sensing technology has been successfully used for different research purposes since the 1920s, when aerial photographic cameras were used to map the land cover and land cover changes. In the early 1960s the era of space-borne sensors began and since then over a hundred satellite-based sensors have been launched (COOPS & TOOKE 2017). Development of new techniques and instruments, such as unmanned aerial systems (UAS), improvement of spatial and radiometric resolution of satellites sensors makes remote sensing more effective for ecosystem research (TURNER et al. 2003, COLOMINA & MOLINA 2014).

One of these remote sensing instruments is Light Detection and Ranging (LiDAR), which an active sensor that emits a beam of electromagnetic energy (light) for measuring the distance to object (LEMMENS 2011). The object is represented as a 3D point cloud, where every point has the specific coordinates.

The idea to use the LiDAR as a remote sensing instrument goes back to the 1960s when LiDARs were first used in topography and bathymetry (ST-ONGE et al. 2003). The forest application of LiDAR began in the early 1980s when researchers used laser developed for bathymetrical works to accurately assess terrain elevation and forest canopy profile (KRABILL et al. 1984). Further development of the use of LiDAR forest application consisted of biomass, tree height and stand volume estimation (ST-ONGE et al. 2003). With the development of Geographical Information Systems (GIS), LiDAR became geo-data technology, which is used for the estimation of three-dimensional (3D) information for a variety of topographic and industrial objects (LEMMENS 2011). The utility of LiDAR prompted commercial development of Terrestrial Laser Scanners (e.g. RIEGL LMS Z210 and CYRAX 2200) in the late 1990s (NEWNHAM et al. 2015).

LiDAR and its outputs are used for different research purposes. Digital elevation model (DEM) and digital terrain model (DTM) are two of the most important LiDAR products that allow for the production of high-resolution topographic maps. Examples of application of LiDAR products include: for planning and designing roads (PEREIRA & JANSSEN 1999, SCHIESS & KROGSTAD 2003), detecting archeological features in woodland (DEVEREUX et al. 2005, DONEUS et al. 2008), estimating surface geometry in geology, studying the active processes in hard rock coastal cliffs, controlling erosion etc. (BUCKLEY et al. 2008). LiDARs are applied to forest management and forest fire

management, because of its high spatial resolution. Accurately measures of vegetation height is used to estimate post- and pre-fire fuel conditions: crown bulk density, differences in vertical structure and 3D canopy fuel measurements (LENTILE et al. 2006). LiDAR is also applied to fire smoke detection (FROMM et al. 2000, UTKIN et al. 2002). A special Instantaneous-Profile Laser Scanner is used to measure soil surface microtopography (DARBOUX & HUANG 2003). Airborne and terrestrial LiDARs are used for soil surface roughness estimation (PEREZ-GUTIERREZ et al. 2007, TURNER et al. 2014). Oceanographic LiDARs are used for water target detection, surface roughness measurements, bathymetry, measurements of chlorophyll and other waterborne pigments (HOGE & SWIFT 1981, CHURNSIDE 2013)

The ability of LiDAR to determine the vertical structure of scanned objects and to detect water droplets and ice particles in the atmosphere is relevant to cloud profiling (TAKEUCHI 2005). National Aeronautics and Space Administration (NASA) has LiDAR application group (https://science.larc.nasa.gov/LiDAR/), which uses airborne LiDARs to research the atmosphere, its chemical composition, radiation and dynamical processes: DIAL (Differential Absorption LiDAR) for ozone and aerosol/cloud profiles, LASE (LiDAR Atmospheric Sensing Experiment) for water vapor and aerosol/cloud profiles and HSRL (High Spectral Resolution LiDAR) to improve DIAL system for more quality of measurements.

The geoscience laser altimeter system (GLAS) onboard of the ICESat satellite was operated by NASA from 2003 to 2009 (https://icesat.gsfc.nasa.gov/). This spaceborne LiDAR was used for studies of ice-sheet mass, cloud and atmospheric properties over polar areas. It also provided topography and vegetation data around the globe.

2.2   Principles of measurement

LIDAR is an active sensor that emits a beam of electromagnetic energy (light) for measuring the distance to an object (LEMMENS 2011). These systems typically include the following components: high-frequency pulsed laser (the transmitter), solid-state photo-detector (the receiver) and optics that modify laser beam and collect backscattered light (LEDINGHAM & CAMPBELL 1997, ST-ONGE et al. 2003). The transmitter emits a laser beam, which is corrected by optic (O1 see Figure 2-1) and hits a target object (S) at the distance (R). This object generates backscattered light collected by further optic (O2) and received by the detector. The backscattered signal can be shown as a time function (t) with a peak at t=2R/c, where R is a range distance to the object and c is the velocity of light (LEDINGHAM & CAMPBELL 1997).

Legend:

S – target object
R – range distance to
object
Q1, Q2 – optics
c – speed of light
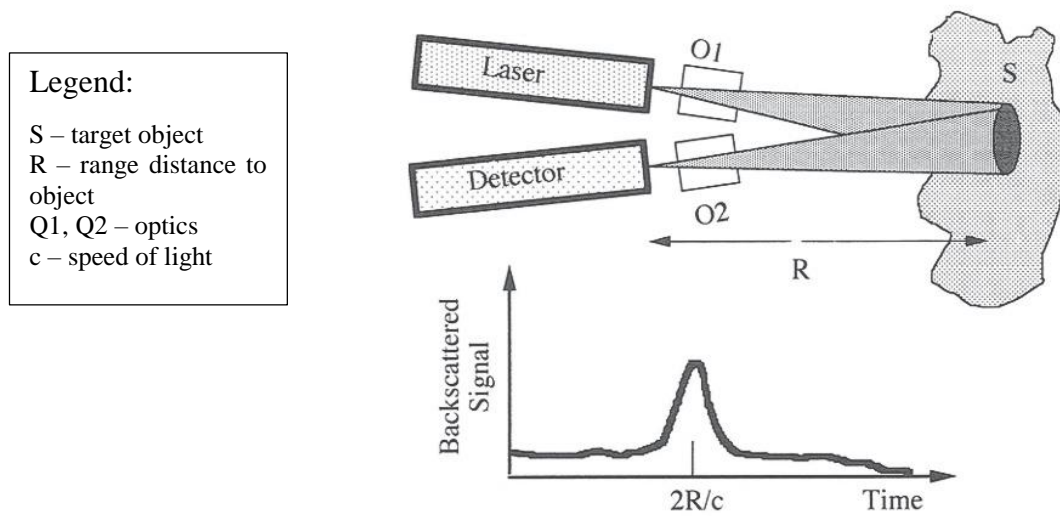
Figure 2-1: LiDAR principles of measurement

(LEDINGHAM & CAMPBELL 1997)

The resulting data set of laser scanning is a point cloud that consists of massive amount of points, each with 3D coordinates. These points define the positions of LiDAR echo (or pulse return) from each target (ST-ONGE et al. 2003). The 3D coordinates are the result of combining measured range, scan angles and position and orientation of the scanner. The raw data are then typically converted into a geodetic reference system (LEMMENS 2011).

The scan's mirror of TLS rotates vertically and deflects a laser beam that provides vertical plane scanning. The head part of the scan rotates 360 degrees horizontally and provides hemispherical scanning (DASSOT et al. 2011, SOUDARISSANANE 2016). The result of scanning is represented as 3D point cloud covering almost 360 degrees in spherical domain.

TLSs can be divided in two groups according to their range measurement principle: phase-shift and pulsed time-of-flight. Phase-shift scanners measure distances using a phase shift between the emitted and received laser beam and record only one return for each direction (Figure 2-2). Advantages of this kind of instrument are fast acquisition speeds, very high point quantities and wide fields of view (DASSOT et al. 2011).
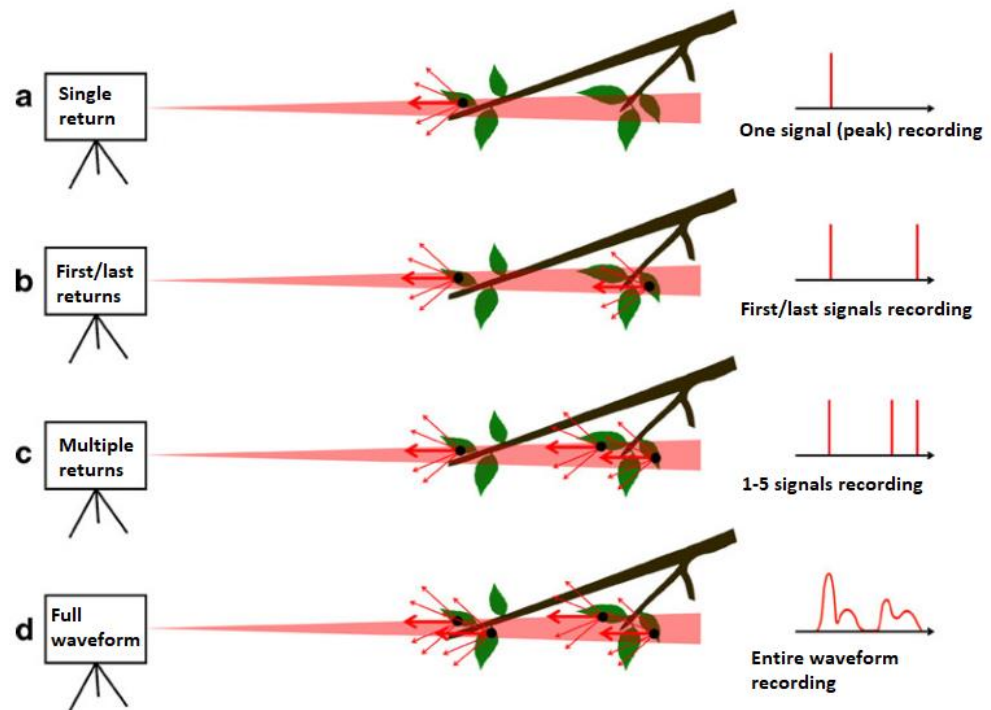
Figure 2-2: Types of laser returns. Depending on sensor capabilities, one or more

signals can be recorded by the scanner

(DASSOT et al. 2011)

Time-of-flight instruments estimate the distances based on the measure of the time emission and reception of a laser pulse. Dassot et al (2011) described four recording methods of time-of-flight LiDARs according to the number of return signals:

- single return recording (for the first object that reflects a portion of the laser pulse, Figure 2-2a);
- first/last return recording (the first, the last or both reflected signals are recordable, Figure 2-2b);
- multiple return recording (up to five signals, Figure 2-2 c);
- full waveform recording (continuous signal echo recording)

Different to phase-shift LiDARs, which use visible light for scanning (600–800 nm), time-of-flight LiDARs use near-infrared wavelengths (900–1.500 nm). The acquisition speeds of these instruments are relative low, but very long measurement distances are possible (over 100m). The vertical field of view is usually narrow.

There are three kinds of instrument according to the placement of scanner: airborne, spaceborne and ground-based LiDAR (Figure 2-3). An airborne LiDAR scanner is mounted on aircrafts or helicopters and spaceborne LiDAR is mounted on satellites. Ground-based LiDAR (also called terrestrial laser scanner or TLS) is placed on tripod over the ground or on the top of a car (LEMMENS 2011).
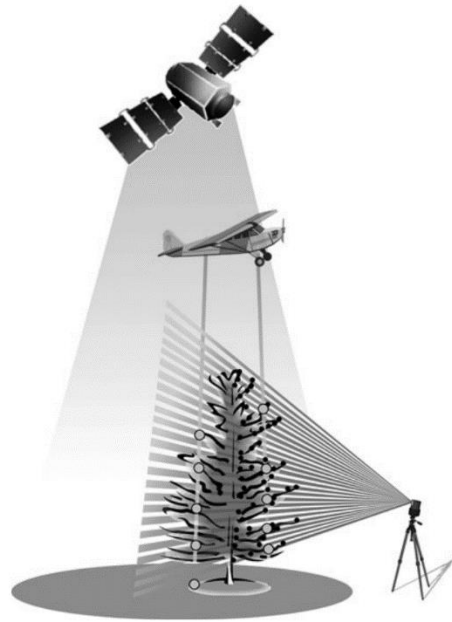
Figure 2-3: Spaceborne, airborne, and terrestrial LiDAR remote sensing and their

inherent scales of operation

(VAN LEEUWEN & NIEUWENHUIS 2010)

The major advantage of TLS is the possibility to get the information at the tree scale and under the canopy, which allows determining the structure of a single tree (DASSOT et al. 2011). However, TLS has several disadvantages. First, laser scans have a large file size that leads to slow file processing and an increased hardware requirement. The second problem is low point density in the occluded areas: the upper part of crown or even the entire tree can be hidden by low branches, understory or surrounded trees. Additionally, the quality of laser scans depends on weather conditions. Thus, wind, rain and snow lead to increase of noise points. Moreover, standard instruments cannot be used during extreme temperatures: under 0 and over 40°C (DASSOT et al. 2011).

2.3   Clumping index

Leaf area index (LAI) and clumping index (Ω) are key parameters in ecosystem modeling of biosphere-atmosphere exchanges of energy, water vapor and carbon dioxide. The amount of light used for photosynthesis is largely determined by the amount and distribution of leaves within a vegetative canopy, i.e. canopy architecture. Optic instruments (i.e. LI-COR LAI-2000) and hemispherical photos are usually used to estimate LAI in the field (GOWER et al. 1999). They measure the diffuse radiation that penetrates through the canopy, a.k.a. gap fraction. The measurement is based on the

assumption that all foliage element and live parts within canopy are randomly distributed. The overlapping and clumping of leaves are not taken into account (CHEN et al. 2005, ZHENG & MOSKAL 2009, KOENIG et al. 2013).

However, foliage elements are seldomly random distributed, and, therefore, LAI is typically underestimated in clumped canopies. In order to describe the results of LAI estimation from the gap fraction more accurately the term, effective LAI (eLAI), was developed (CHEN et al. 1991):

$$eLAI = \Omega \cdot LAI \tag{1}$$

where Ω is the clumping index, that evaluates a foliage grouping within single canopy structures such as tree crowns, shrubs and row crops, relative to a random distribution. Further, the 'true' LAI is defined as 'one half the total intercepting area per unit ground surface area' (CHEN & BLACK 1992).

Completely clumped canopy has a Ω value of 0 (leaves lay on each other), while $\Omega = 1$ represents a completely random canopy. $\Omega = 1$ means that canopy is uniform (leaves lay side by side). One of the methods to estimate the Ω is a gap size distribution. For a given LAI, clumped canopies have larger canopy gap fractions with different gap size distributions than that of random distribution (CHEN et al. 2005).

Thus, the Ω can be obtained from a gap fraction as (CHEN & CIHLAR 1995, LEBLANC 2002):

$$\Omega = \frac{\ln[F_m(0,\theta)]}{\ln[F_{mr}(0,\theta)]} \cdot \frac{[1 - F_{mr}(0,\theta)]}{[1 - F_m(0,\theta)]} \tag{2}$$

where Ω is canopy clumping index, $F_{mr}(\theta)$ is the gap fraction of a theoretical canopy with random spatial distribution, $F_m(\theta)$ is measured gap fraction, i.e. using Hemispherical Photography (HP) technology (TERRADAS 1999).

Some researches has estimated Ω using HP (WALTER et al. 2003, GONSAMO & PELLIKKA 2009, PUESCHEL et al. 2012, LIU et al. 2013). However, the optical instruments are limited in their 2D presentation of vegetation canopy. The ability of LiDAR to provide 3D point clouds and the resulting 3D canopy architecture is, therefore, used in many studies to better estimate the Ω and LAI.

GARCÍA et al. (2015) estimated Ω from combination of TLS and airborne UAS laser: the point cloud was converted into a 3D voxel-based model to obtain the gap size distribution (voxels are volumetric pixels). MOORTHY et al. (2011) calculated Ω direct from TLS points. They simulated point cloud with random distribution of points (laser returns) within the boundary of tree canopy derived from TLS data. Then they compared the densities of points in simulated and measured canopies. The Ω was calculated as a ratio of between simulated and measured canopy gap fractions.

2.4   Savanna type Dehesa

This study is focused on application of TLS in Mediterranean type of savanna named Dehesa. Spanish Dehesa is a landscape of the Southwestern Iberian Peninsula (Figure 2-4), that occupies more than 2 million ha (FERNÁNDEZ et al. 2018). Dehesa is covered by oaks, scattered among annual grasses and shrubs. The most representative Dehesa region in Spain is Extremadura, which is characterized by high oaks density (HUNTSINGER et al. 2013). Dehesas are result of human activities influence during more than 2000 years: their forming began at the ages of the Roman Empire. During many centuries it was managed by grazing (especially Iberian pigs), hunting and farming and as source for wood fuel. The most important was production of sweet acorns both for human food consumption and domestic animals feeding (JOFFRE et al. 1988). Today Dehesa is managed generally by livestock (sheep, goats, cattle or pigs) (ALAGONA et al. 2013).

This tree-grass ecosystem is located in Mediterranean climate zone, which is characterized by hot summer with drought and medium to low precipitation. The climatic factors such as temperature, drought and summer precipitation have influence on Dehesa's distribution. The researchers identify three Dehesa climate zones (Figure 2-5 a,b): zone 1, located in the southern and southwestern part of Spain, zone 2, covered central and south parts, and zone 3 in the northern part of the distribution of the Dehesa. The first zone is influenced by the humid winds from the Atlantic Ocean. The summer is characterized by a long drought period: July and August with their mean monthly precipitation value 3.0 and 5.0 mm and mean temperature 25.6 and 25.4 °C respectively are the hardest for vegetation growth. The zone 3 is coldest one: it is characterized by the lowest winter temperatures (coldest months are December and January with mean temperature 3.7 °C for each of them). Precipitation value in summer is about 14 mm. The second zone has intermediate climate characteristics in compare with others: the temperature of the coldest month (December) is 6.7 °C, the warmest month (July) hat
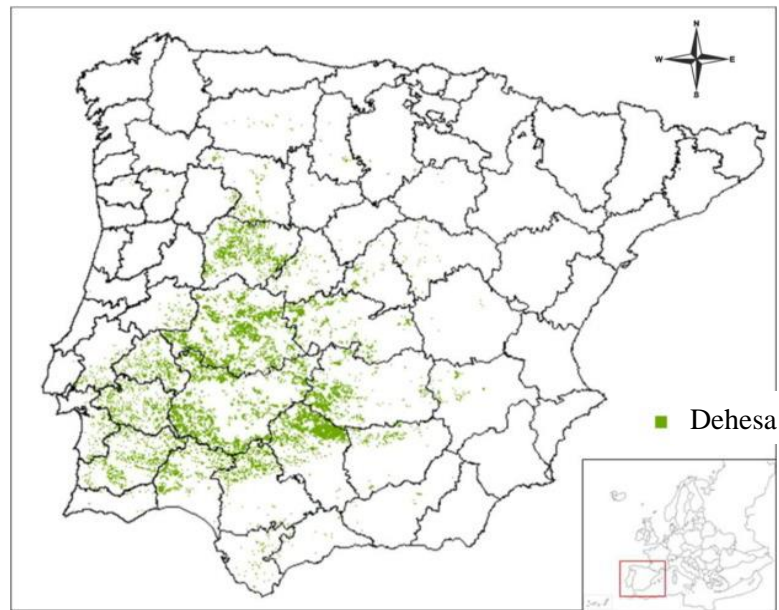
Figure 2-4: Location of the Dehesa areas in the Iberian Peninsula
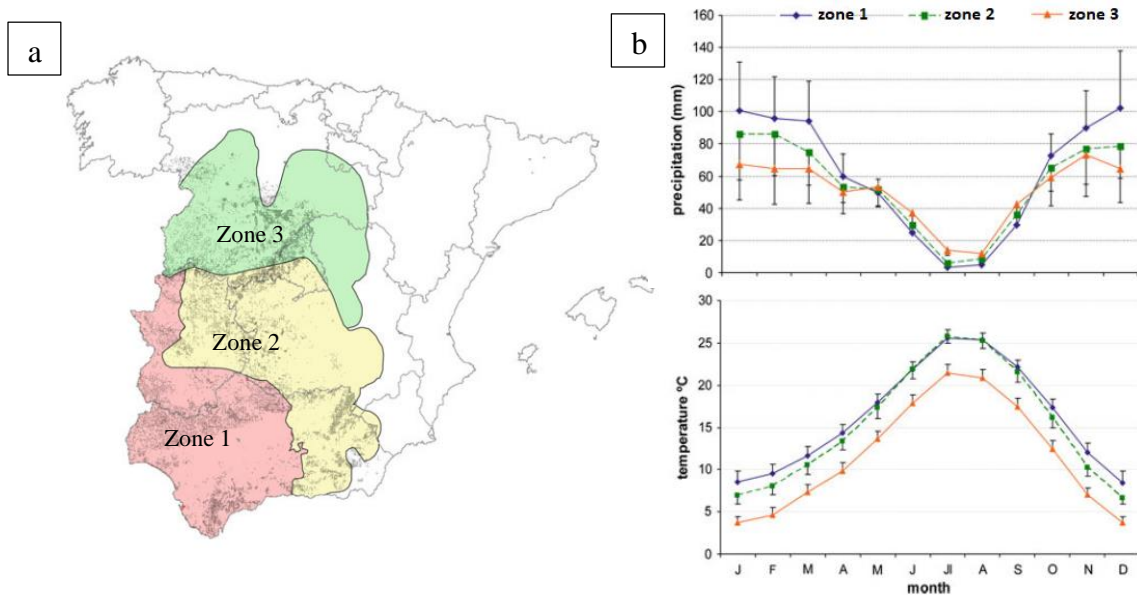
(HORRILLO et al. 2016)

Figure 2-5: Climatic characteristics of the Spanish Dehesa

(modified after ROIG et al. (2013)

a) location of the tree climatic zones of Dehesa in Spain (green, yellow and pink patches);

b) distribution of precipitation and mean temperature during the year at three climatic zones of the Spanish Dehesa. Bars show the standard deviation of the mean.

mean temperature of 25.8 ℃. The driest month (July) has 6.0 mm of precipitation (ROIG et al. 2013).

Holm oak (Figure 2-6a) is the dominant tree species of Dehesa: it is present in 84 % of the woodlands (HUNTSINGER et al. 2013). As a typically for Mediterranean plants it is evergreen and resistant to drought. Holm oak can reach a height 25-30 m with over 2 m of trunk diameter. However, trees having this height are rare, usually they are up to 15 m tall (TERRADAS 1999, DE RIGO & CAUDULLO 2016). Holm oaks are long-life trees: often they are over 300 years old (PLIENINGER et al. 2003). Holm oak forms a dense canopy during its slow growth and its stems are usually low. The crown is broad with ascending branches. Cracked into thin plates the bark has brownish-black color. The leaves are small, 3-7 cm long and their form is lanceolate to oval. The upper side is dark green, while the lower side is covered by white hairs. The leaves have relatively small stomata (length is 22-27 μm). Chlorophyll content is high: it ranges from 600-700 mg m-2 at the top of the canopy to 1000 mg m^{-2} at 3 m below the top (SABATÉ et al. 1999). Photosynthesis is highly dynamic throughout the year.

The roots of holm oak are deep, consisting of a complex system of spreading lateral roots growing from a thick, sometimes massive root crow. Deep complex root system of oaks (the roots expand as much 25 times the canopy volume into the soil) covers a larger soil area, stores more water and obtains more nutrients in areas with wide spacing between trees. Thus, the effect of duration and intensity of tree water stress is reduced that eventually helps them to survive and keep ability to growth even during the drought period (TERRADAS 1999, MORENO et al. 2013). The peak of vegetative growth, as well as maximum leaf fall, occurs during the spring season between April-June.

Holm oak is wind-pollinated tree. Flower buds and flowers appear mostly in May-June and last until late July (Figure 2-6b). Mature and fall of acorns take place in November- January. Sweet acorns are used for human and animal consumption (Figure 2-6c). Acorn production vary due to environmental factors, including rainfall and temperature, and biotic factors, such as birds, mammals and herbivores that eat or collect acorns (TERRADAS 1999, KOENIG et al. 2013).Holm oak is a hardwood tree, its wood is used for manufacturing of carpentry tools, parquets, etc. (TERRADAS 1999).

Undercover is represented by annual grasses and other herbaceous species, common species are rockrose (Cistus spp.), leguminous brooms (Retama, Genista and Cytisus sp.), gorse (Ulex spp.) and heather (Erica sp.). In total Dehesa has more than 100 species of herbaceous plants in 0.1 ha (DÍAZ 2009). DÍAZ (2009) concluded, that
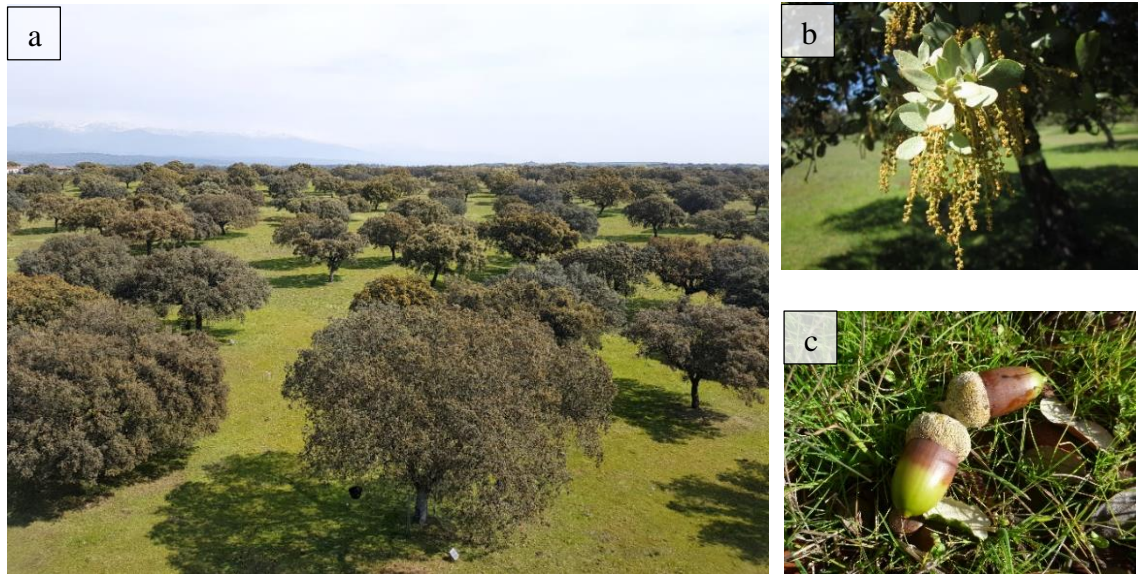
Figure 2-6: Dehesa ecosystem

(Max Planck institute photo archive)

a) typical Dehesa ecosystem near Majadas de Tiétar covered by holm oak;

b) flower buds of holm oak, c) acorns of the holm oak

Figure 2-7: Trees affect the understory: green grass beneath the canopies in dry

season

(Max Planck institute photo archive)

'the richness of species tends to be higher in Dehesas than in other types of habitat either natural or man-made'.

Soils were developed over acid slates and granites and characterized by low contents of organic matter, mineral nitrogen and available phosphorus (MORENO et al. 2013). Spatial distribution of trees in open tree-grass ecosystems like Dehesa can be characterized as scattered. MANNING et al. (2006) demonstrated the keystone role of scattered trees for savanna ecosystems and summarized their functions at local and landscape scales. Scattered trees influence water balance: complex root system storage the water during drought (SIMIONI et al. 2003). Trees influence the soil structure and composition. Recycling of leaf litter and circulation of the nutrients thought the deep root system makes soils beneath the canopy rich on organic matter, nutrients and water. This influence is proportional to the canopy projected area (JOFFRE & RAMBAL 1993, VALLADARES & PUGNAIRE 1999).

The trees affect understory layer, its species composition and phenology (Figure 2-7). The pants beneath the canopy have less light than in open areas: light reduction reaches 70 % close to trunks and decreases with the distance from the trunk (MONTERO et al. 2008). This light reduction play an important role during dry season protectiong the plants beneath the tree canopy from the overheating and damage of photosynthetic apparatus during high-light conditions (VALLADARES & PUGNAIRE 1999). Thus, the trees contribute to increase of pasture yield beneath the canopy. MARCOS et al. (2007) studied the effects of soil fertilisation on productivity of trees and grass. They showed the absence of any effect of soil fertilisation on nutrient status or acorn production of trees, while the productivity of understory increased. They concluded that tree-grass competition is limited. The grass takes nutrients from uppermost soil horizon, whereas complex deep root system of trees makes it possible to tap up nutrients from deeper soil layers. Similar results were demonstrated by BELSKY (1994) for African savannas. His study suggested that the competition is less intense in dry zones, because of root distribution into open grassland, and more intense in wet areas, where roots of tree are concentrated close to canopies.

Dehesas are a habitat for great number of birds and mammals. Among them are European red deer (Cervus elaphus), wild boar (Sus scrofa), Iberian lynx (Lynx pardinus), rabbits (Oryctolagus cuniculus), hares (Lepus granatensis), redlegged partridges (Alectoris rufa), pigeons (Columba palumbus, C. oenas) (DÍAZ et al. 2013). Seed-dispersing animals such as wood mouse (Apodemus sylvaticus) and Algerian mouse

(Mus spretus) as well as birds, e.g. Eurasian jay (Garrulus glandarius) helps regeneration of oaks through hoarding of acorns for their consummation (DÍAZ 2009).

3 Retrieval of vegetation structural parameters using LiDAR: state of the art

Forest structural parameters; such as tree height, crown perimeter, crown area, diameter at breast height (DBH), tree density and canopy fraction; are not only the key forest inventory attributes. They are also important for studies of the biomass, biogeochemical cycles, ecological functioning, spatial heterogeneity, exchange between mass and energy and water budgets of a forest ecosystem (WIEZIK et al. 2011, GAITAN et al. 2014). LiDAR technology also allows accurate estimation of vegetation structural parameters, LAI and aboveground biomass in high-biomass ecosystems (LEFSKY et al. 2002).

Terrestrial Laser Scanners (TLS) are common used for vegetation structure retrieval (BUCKLEY et al. 2008). TLS provide data with high point cloud density that allows retrieval of detailed 3D information on individual trees. There are various automatic data processing techniques that can be used to extract individual tree position, tree height, DBH and other forest structural parameters from LIDAR data. Many studies have reported the use of TLS for extraction of the main forest parameters.

Tree top detection and delineation are necessary for collection of information about forest stands. Accurate delineation of trees is important for the estimation of main metrics of a tree such as tree height, crown perimeter, tree volume etc. Some researches based their approaches to detect single trees on the analysis of horizontal slices of LiDAR point clouds. For example, BIENERT et al. (2006) used slices that were extracted from the point cloud at the height 1.30 m. Fitting the circles into these slices at a given height allowed to detect the tree location. Given the increasing importance of this variable in defining further tree structural attributes, this algorithm has been implemented into AutoStemTM software (DASSOT et al. 2011). Different fitting approaches and detection approaches have been proposed during last decade. HOPKINSON et al. (2004) used a similar approach: slicing the point cloud data at different height of the trunk. The center of circle of points was defined as the tree stem. Identification of individual trees is also implemented by detecting local maxima in a Canopy Maxima Model (CHEN et al. 2006) or in a Digital Crown Height Model (KOCH et al. 2006).

To delineate the trees CHEN et al. (2006) applied the watershed segmentation algorithm. The fundament of this algorithm is based on the representation a gray-scale image as a landscape model, where pixels with low values (basins) are isolated by pixels with high values (watershed) (VINCENT & SOILLE 1991, ROERDINK & MEIJSTER 2000). The tops of tree canopies are presented on Canopy Height Model (CHM) as the pixels

having maximum value. The delineation of tree canopies is implemented from inverted CHM, where the tree tops are represented via minimum pixel values, which correspond to the basins on landscape model (WANG et al. 2004) (this algorithm is presented in detail in methodology section of this thesis). KOCH et al. (2006) used pouring algorithm for tree delineation. This algorithm starts from local maxima (tree top) as center of grow and appends the neighboring pixels with the lower of the same height value. Overlapping regions became a tree crown boundary. POPESCU & ZHAO (2008) applied local maxima filtering to CHM in order of tree detection and delineation.

WANG et al. (2008) presented an alternative approach to delineate the tree crowns based on voxelization of point cloud. The points from a normalized point cloud are resampled to a local voxel space where a 2D raster image is extracted. The pixels of the 2D raster image have grey values that correspond to the number of points within the voxel. This allow tree crowns to be isolated based on brightness of the pixels (high brightness values representing a high point density is interpreted as a tree location.

Different methods have been proposed to estimate tree height. For example, BIENERT et al. (2006) calculated the tree height as the height difference between the highest point of the point cloud of a tree and the terrain model. Alternatively, HOPKINSON et al. (2004) estimated the tree height as the vector joining the lowest and highest elevation points within an individual tree point cloud. OLOFSSON et al. (2014) classified the whole point clouds of single trees into tree stem and tree canopy points and calculated height percentiles within the canopy point cloud. The tree height was estimated as the 100th height percentile. LEFSKY et al. (2002) pointed out two main difficulties by estimation of tree height: i) accurate determining the elevations in a terrain model using airborne LiDAR, ii) practical difficulties in detecting the upper layer of a tree canopy - for TLS. The largest uncertainties are associated with sites having dense understory, when sensor confounds the elevation of understory by the ground level. In addition, tree height may be also underestimated due to the widely observed of low point density of upper crown that complicates its accurate detection with a sensor.

Another important tree variable is Diameter at the breast height (DBH). This parameter is commonly used in volume functions and in estimating growing stock, thinning and increment. Location of the breast height is at 1.3 m from the base point along the axis of the stem (GSCHWANTNER et al. 2009). Caliper and diameter tape are typical instruments for field measurements (VAN LAAR & AKÇA 2007). Some studies have reported the estimation DBH from laser scans. The most common approach to retrieve DBH is the fitting of a cylinder or circle to the LiDAR point's slices (from now on we

refer it to as cuts) of individual trees. This approach is based on the assumption that a tree cut have a circular shape. BIENERT et al. (2006) used the fitting approach to estimate the DBH by the fitting circles into the 2D projection of the trunk cuts points. Following this approach, HOPKINSON et al. (2004) selected all LiDAR points lay between 1.25 and 1.75 m above the lowest point and fitted a cylinder primitive to the data as manner to retrieve DBH. OLOFSSON et al. (2014) proposed so called the Random Sample Consensus (RANSAC) method, which models a tree stem as number of cylinders. Fitting the circles to the laser points of tree stem, which lie inside of the model, allows to estimate DBH. Alternatively, MOSKAL & ZHENG (2011) developed the point cloud slicing algorithm that applies 3-D cylinder to the cuts that have been voxelized before the fitting.

These voxel-based algorithms are commonly used for estimating object volumes volume (MOSKAL & ZHENG 2011, HOSOI et al. 2013, BIENERT et al. 2014). The tree volume is obtained by integrating the volumes of all voxels (a.k.a. volumetric pixels) that represent the tree. Another method to estimate tree volume is via allometric equations, where tree volume is a function of different tree structural parameters. For example, POPESCU et al. (2004) used LiDAR-derived DBH and tree height to calculate individual tree volume. YAO et al. (2012) used crown area, tree height and crown height acquired from triangulated point cloud of single trees for the same purposes.

4 Methods

To meet with the proposed objectives of the study the methodology and analysis performed are summarized in Figure 4-1.
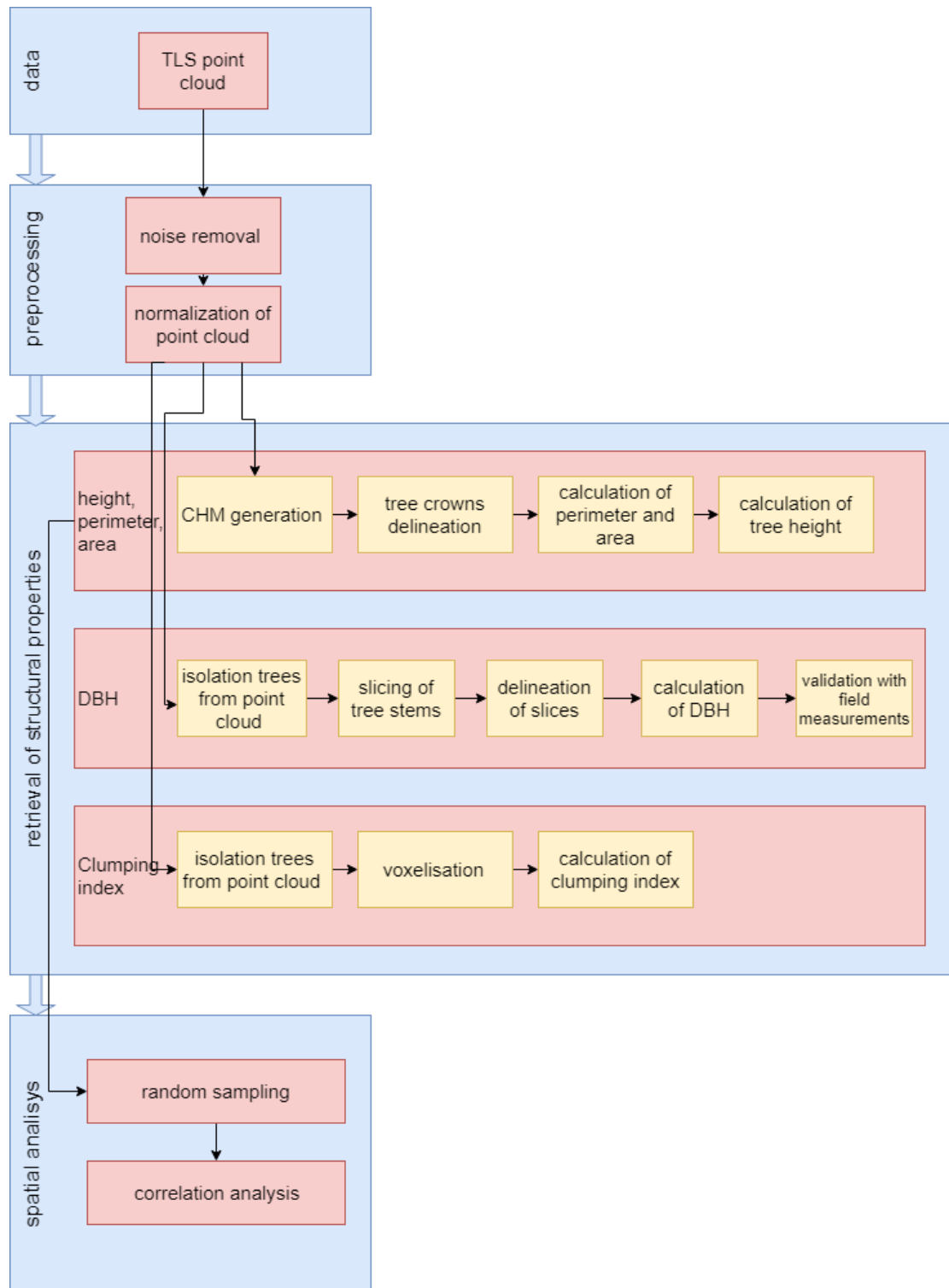

Figure 4-1: Methodology workflow

(own illustration)

i.   Evaluate and develop approaches for the retrieval- of structural parameters of vegetation (i.e. tree height, canopy projected area and perimeter, diameter at the breast height and canopy clumping index).

TLS data were obtained from Majadas study site in Spain (39°56´024.68´´ N, 5°45´50.27´´W; Majadas de Tiétar, Cáceres, Extremadura). After noise removal and normalization of TLS point clouds (preprocessing), a Canopy Height Model (CHM) was generated. The CHM provides the bases parameter estimates of the vegetation (canopy height, perimeter area, DBH and Ω) (Figure 4-2). The next step was the delineation of tree crowns, which allowed for the production of a shape file with the tree crown projections in the form of spatial polygons. The tree height was calculated from CHM as the highest pixel value within the canopy, while the crown projected area and the perimeter were obtained from the shape file. Given the observed inconsistences across the proposed methods, we test a new delineation-based approach for estimating DBH (see details below). On the other hand, we evaluate the sensitivity of the approach proposed by GARCÍA et al. (2015) in retrieving the Ω across a set of parameterizations. To this end, the Ω was calculated for 10 trees.
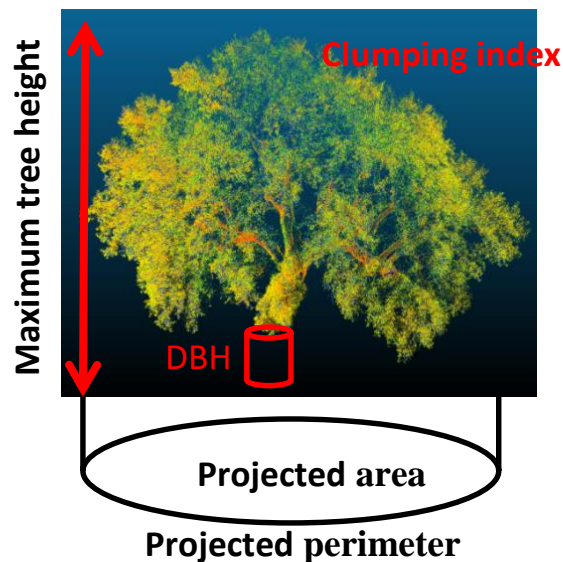
Figure 4-2: Tree structural parameters, obtained from TLS scans in this study

(own illustration)

ii.   Characterize structural properties of ecosystem. The spatial distribution of tree
structural parameters and their biometrical relationships is evaluated

A Monte-Carlo technique was used to randomly sample polygons. For each
polygon, the average values of the main trees structural parameters, as well as canopy
fraction and tree density were calculated. A 200 runs assured to cover the whole area
under study (>35 ha). The degree of heterogeneity was studied from the distribution of
the statistical properties extracted from the resampling analysis as well as the size of the
polygons. To this end, the analysis was replicated with three different polygons sizes
20x20m, 50x50m and 100x100m. For each set, we evaluate the biometric correlations
across the structural parameters.

4.1   Study site description

The study site Majadas (Figure 4-3) is located in the west of Spain (39°56´024.68´´ N,
5°45´50.27´´W; Majadas de Tiétar, Cáceres, Extremadura).

Figure 4-3: Study site location. Red triangles – EC towers

(own illustration)

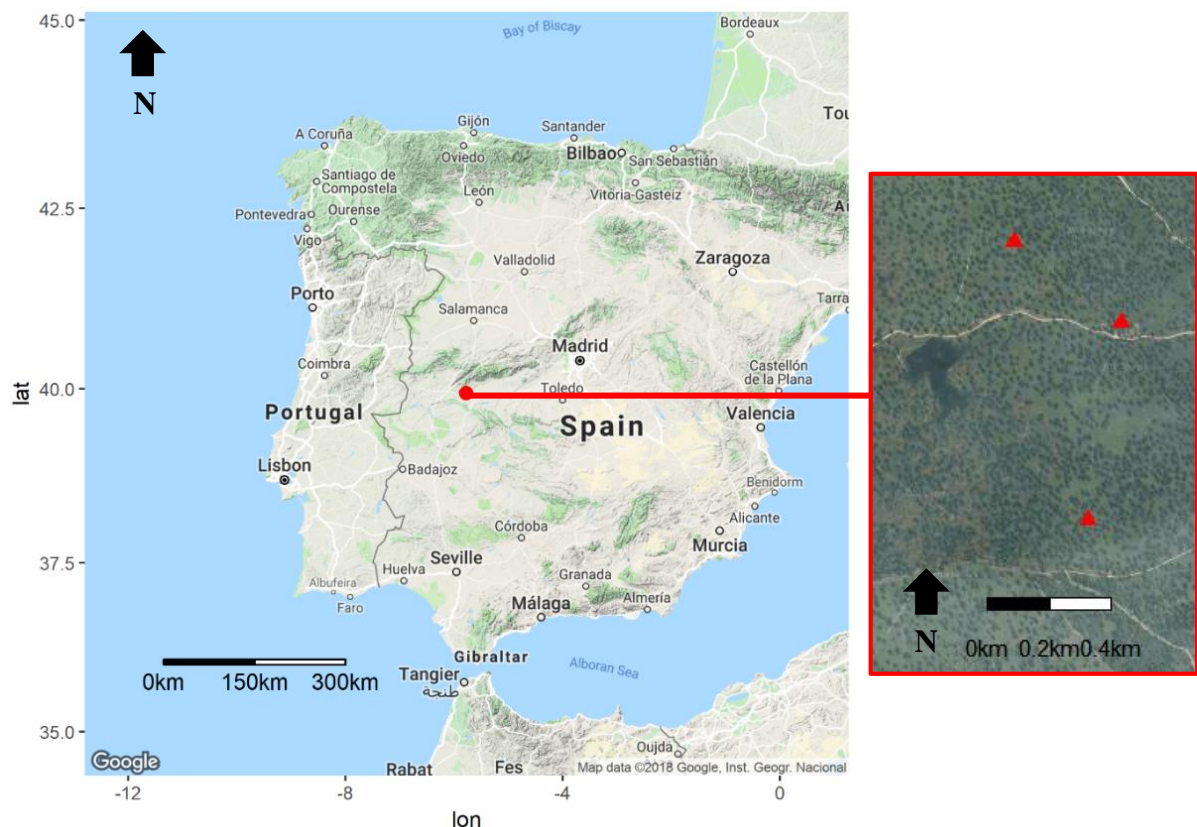The ecosystem type is savanna, called Spanish Dehesa. Climate is Mediterranean, characterized by a hot and dry summer. The annual precipitation value is 400–800 mm (falling mostly in spring and autumn) and mean annual temperature is 16°C. The study site is dominated by grass layer *(Vulpia bromoides (L.), Vulpia geniculate (L.), Trifolium subterraneum (L.), Ornithopus compressus (L.))* and wood vegetation is also present, i.e. evergreen and deciduous holm oak *(Quercus ilex ballota)* with low tree density (about 20 trees per ha), average height of 8 m and 0.4 m DBH. Typically for Dehesas, Majadas is managed by low-intensity grazing (<0.3 cows per ha).

Tree eddy-covariance towers are located on study site (main EC tower, north EC tower and south EC tower) and used for CO2, nitrogen and phosphorus measurements. Main tower (ES-LMa in FLUXNET) is a covariance FLUXNET site Majadas del Tietar and has been in operation since 2003. North and south towers (ES-LM1 and ES-LM2) have been operated since 2014.

4.2   Data collection and preprocessing

4.2.1 Data collection

For ground-validation, we used a consistent data set containing field DBH measurements (more than 200 hundred trees were sampled) against compare the DBH estimates from the TLS scans. Field data are presented in xlsx format. They included tree coordinates and DBH in cm obtained during the field campaign of 2015. The measurements were taken using tree caliper. The two measurements were taken perpendicular to each other and an average value recorded. Additionally, six trees of NT site were chosen in order to validate the method of DBH estimation. Diameter was measured in March 2018 at three different heights with measure tape: at the breast height (1.30m above the ground), at low level (0.80 m above ground) and at the height of dendrometers mounted on these trees (every tree has its own dendrometer height, usually between 0.90 – 1.20m). The diameter was calculated from circumference divided by π.

TLS data included three TLS point clouds acquired at Majadas in August 2016 using Riegl VZ 2000 laser measurement system (Figure 4-4a,b). This system is characterized by a maximum range of 2000 m and a wide field of view of 100° vertically and 360° horizontally with a measurement rate of up to 400000 measurements per second (RIEGL-LASER-MANAGEMENT-SYSTEMS-GMBH 2017).

TLS scans (Figure 4-4c) covered the area of about 19ha around south EC tower (ST scan), 23 ha around north EC tower (NT scan) and 25 ha around main EC tower. Area around each EC tower was scanned from different scan locations: 36 scan locations for

MT scan, 40 – for NT and 37 - for ST site. The scans have LAS file format, which is used to organize and systematize large LiDAR data (SRINIVASAN et al. 2014).
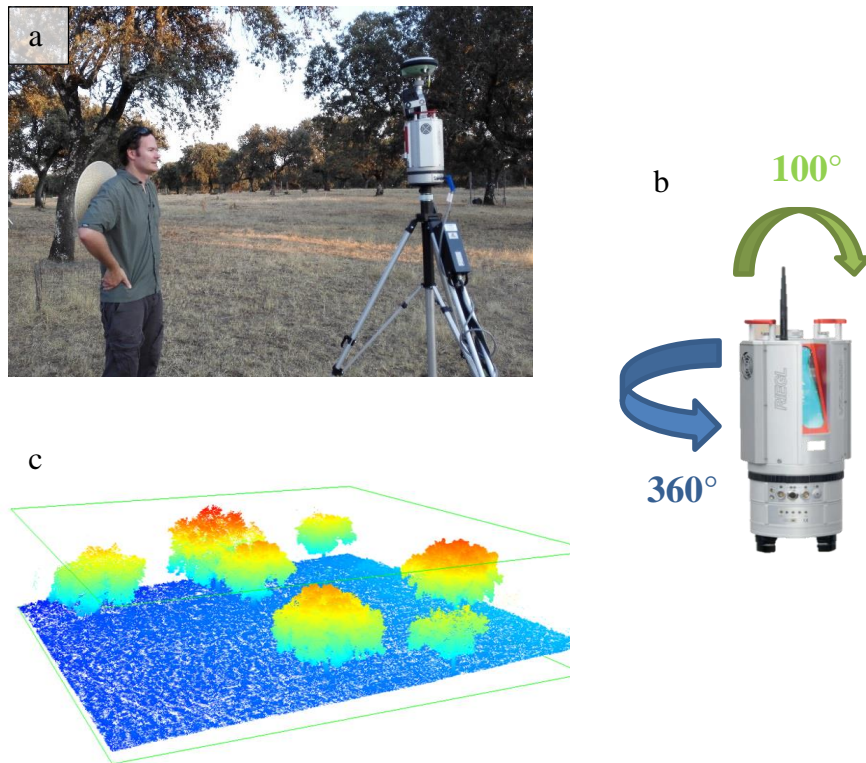
Figure 4-4: Data collection using TLS in Majadas study site

a) process of measurements (photo by M. Migliavacca),

b) Riegl VZ 2000 laser measurement system. Vertical field of view is 100 ˚,

horizontal – 360 ˚ (modified after RIEGL-LASER-MANAGEMENT-SYSTEMS-GMBH (2017),

c) TLS point cloud colored by elevation (own illustration)

4.2.2 Preprocessing

Preprocessing included noise removal and normalization of point clouds. Artificial objects such as flux-tower and fence were removed from the TLS data using Cloud Compare software. Mistake points (noise) were filtered from the scans using LAStools function lasnoise. This function creates a number of cells and looks for isolated points inside them according to user-defined criteria: cell size and maximal number of points for the cell. All the points, which amount in the cell is less than maximum threshold value, are removed.

Normalization of point clouds was done using LAStools software via command line with a batch script. First, the points from a point cloud were classified into ground (class 2) and non-ground (class 1) points using the lasground tool. This tool generates a Triangulated Irregular Network (TIN) surface from below to the sub-randomly distributed laser points and collects statistics about the distance to the TIN facets and angles to the nodes (Figure 4-5). These statistics are used to select seed points of ground class (red points in the Figure 4-5). Then the tool adds additional points to the surface (blue points in the Figure 4-5) using threshold values (AXELSSON 2000).

Second, elevation above the ground was computed for each point and non-ground points were additionally classified to high vegetation (trees) using the lasheight tool. Then the point cloud was height-normalized (lasheight): the z-coordinate was corrected for ground level value, which means that all the ground points have an elevation of zero and all other points have an elevation that equals their height above (or below) the ground.
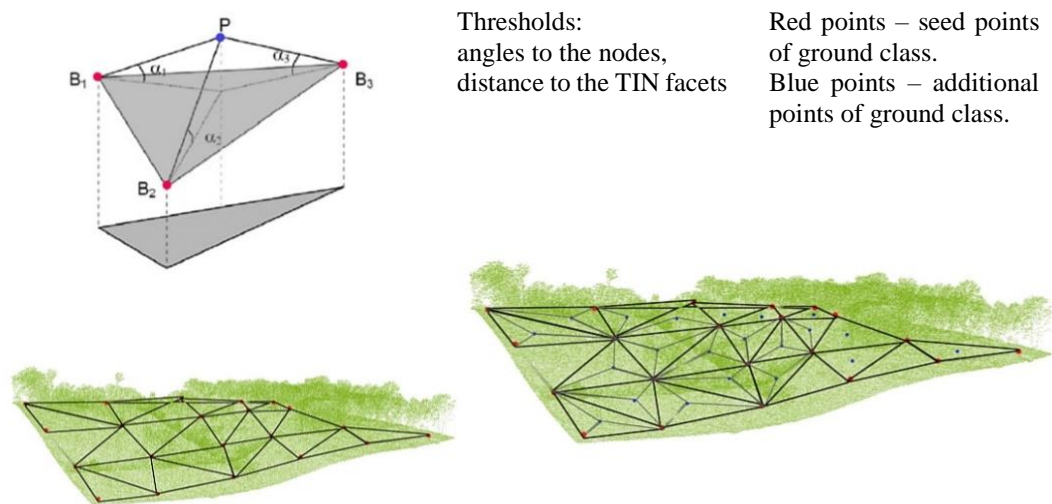

Figure 4-5: Lasground tool: principle of generating of Triangulated Irregular

Network

(Ludwig Boltzmann Institute 2018)

4.3   Retrieval of structural parameters

4.3.1 DBH

Most approaches for DBH estimation are based on the assumption that a tree cross section has a circular shape (PULKKINEN 2012). The most common method of DBH estimation is fitting a cylinder or circle primitive to the cut of the tree trunk's point cloud at 1.3 m height (HOPKINSON et al. 2004, BIENERT et al. 2007, MOSKAL & ZHENG 2011, OLOFSSON et al. 2014). In this study, we developed and tested an approach for estimation DBH based on the delineation of point cloud cuts of tree trunks.

Processing steps are shown in the Figure 4-6. A total of 36 trees were isolated from the denoised and normalized point cloud using LAStools: 16 from NT scan, 10 from MT scan and 10 from ST scan. Then, the points clouds were cleaned manually in Cloud Compare in order to remove the remaining understory vegetation. The point clouds of trees were then sliced at a height from 1.25 to 1.35 vertically above the lowest point in the file (LAStools). A slice thickness of 10 cm is commonly used for DBH retrieval from the laser data as it provides a sufficient number of points (BIENERT et al. 2007, SRINIVASAN et al. 2015). Additionally, the point clouds of six trees (NT scan) were sliced at the height from 0.75 to 0.85 m (named low level, LL) and at the dendrometer height (DH). The dendrometers are the instruments, which are mounted on the tree trunk for monitoring precisely small variations of the trunk size associated with tree growth or water storage measurements (DESLAURIERS et al. 2007). They are usually located close to the breast height. In our case DH varied from 0.88 to 1.20 m above the ground.

The trunk cuts of each tree are presented as rings of TLS points. Subsequent processing was then implemented in command-line form using batch script. The LAStools lasboundary tool was applied to delineate each tree cut. This tool computes a boundary polygon which encloses the points. The controlling parameter is "concavity": its value determines the minimum distance between points that fall into the generated spatial polygon. A concavity value of 0.15 was applied in this study: this value allows computing of closed ring-likely boundaries. This result is a shape file for every tree, which contains a spatial polygon with an "interior" hole.

The shapefiles were processed using SAGA GIS in batch script modus. Because the TLS points of tree cuts with different elevation values were projected into a 2D surface to get the closed ring-likely boundary of trunk cut, it is difficult to determine exactly where the 'real' boundary with the elevation 1.30 m is located. We assumed the location of this boundary is between the "interior" hole and the "exterior" polygon boundary.

Thus, it was decided to generate two polygons for every cut: the "interior" (from hole) and the "exterior" (from polygon boundary) and calculate the diameter as an average value of the two estimates. Finally, boundaries of these polygons were smoothed using Gaussian smoothing for better fitting of the real trunk cut form. Additionally, centroids for every polygon were found and saved in separated shape file.
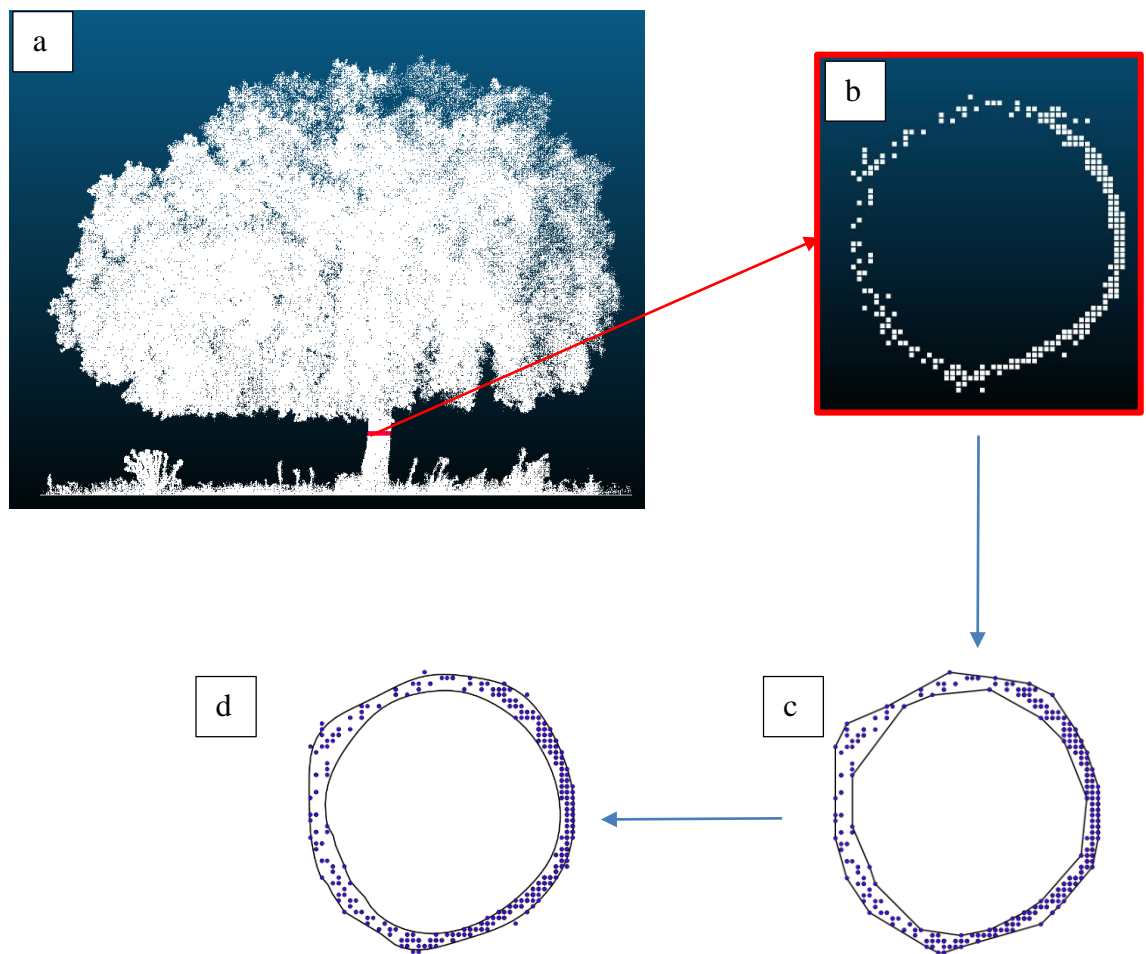

Figure 4-6: DBH estimation from TLS scans

(own illustration)

a) TLS point cloud of a tree, red line on the trunk – location of the breast height (1.3 m);

b) point cloud of trunk cut (up-down view); c) result of delineation;

d) result of smoothing

For the further processing R-studio was applied with the packages "rgeos", "rgdal" and "geophere". Diameters were calculated using two different methods, based on instrumental measurements manner: from circumference and as an average value of two taken perpendicular diameters. There are two commonly used field measurement methods: measuring with a tape or using a caliper (VAN LAAR & AKÇA 2007). In the case of tape measurement, DBH is calculated by dividing circumference by π. In the case of caliper, two measurements of diameter are taken and an average value is recorded. In our approach, for first calculation method (CM) perimeters of the "interior" and "exterior" polygons were divided by π and averaged. For the second method (PM) 10 randomly angled perpendiculars passing through the centroid were generated for each polygon (package 'geosphere'), both "interior" and "exterior" (Figure 4-7). Then the diameter was estimated as an average value of lengths of all perpendiculars. Results of the calculated diameters were validated against field measurements.
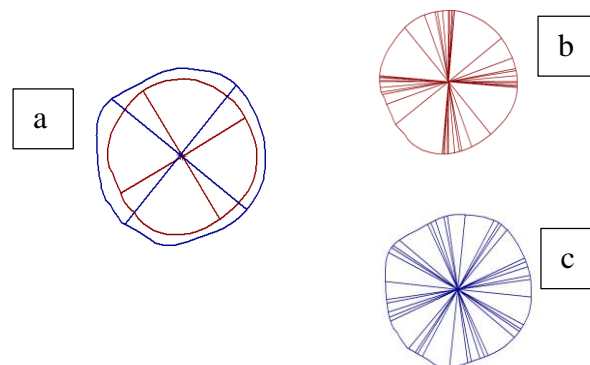
Figure 4-7: Calculation of diameter using random perpendicular diameters

(own illustration)

a) "exterior" (blue) and "interior" (red) polygons with perpendicular diameters, presenting trunk cut; b) random perpendiculars in "interior" polygon;

c) random perpendiculars in "exterior" polygon

4.3.2 Clumping index

The clumping index (Ω) was determined using the approach proposed by GARCÍA et al. (2015). The method is based on the retrieval of the gap size distribution in a 3D voxel-based model of a TLS point cloud of single trees. GARCÍA et al. (2015) positioned the

TLS (Leica HDS-6000) under a tree canopy and scanned the tree twice from opposite placements. They estimated Ω for four trees and compared TLS derived Ω with HP derived one. In our study we used scans from Riegl VZ 2000 TLS, where the instrument was positioned at different distances from the trees.

We isolated the canopies of ten trees having a high point density from the normalized and noise-free point cloud (MT scan) in Cloud Compare. Then, the point clouds were processed in Matlab using the code developed by Mariano García. First, the point clouds of tree canopies were voxelized. The concept of voxel model is shown in Figure 4-8. Voxels, or volumetric pixels, enclose laser points within 3D space. The LiDAR height bins are a 2D representation of voxels (POPESCU & ZHAO 2008).

Then a binary image was generated for each height bin within the voxelized canopy. A value of 1 was assigned to occupied voxels and value of 0 – to non-occupied ones. Non-occupied voxels represent the gaps. To evaluate the effect of voxel size on clumping index different resolutions were applied: 5, 10, 15, 20 and 25 cm (Figure 4-9). The Ω was calculated for each height bin using Equation 2 and then averaged. Large gaps were removed to simulate a random canopy.

The values of zenith angle were chosen following the study of GARCÍA et al. (2015): 30-60° and 55-60°. The range between 30-60° was used because the mean clumping index for this range and the mean clumping index for all zenith angles are similar. The range between 55-60° was chosen because at this range "the gap probability is nearly independent of the leaf angle distribution" (GARCÍA et al. 2015).
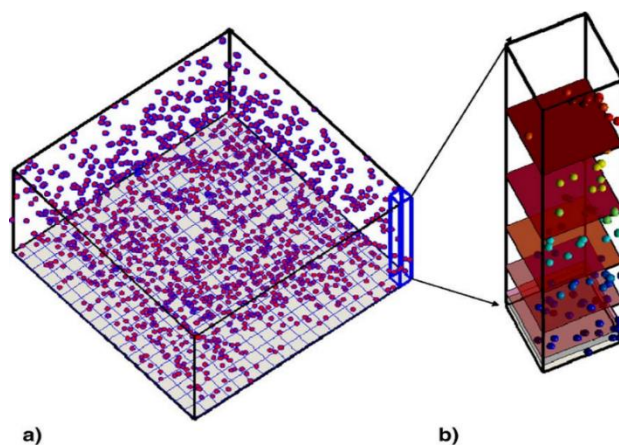

Figure 4-8: The concept of height bins and LiDAR voxels

(POPESCU & ZHAO 2008)

a) laser point cloud in 3-D space, b) vertical distribution of laser points over a 2-D pixel, in height bins (voxels) of varied user-defined height.
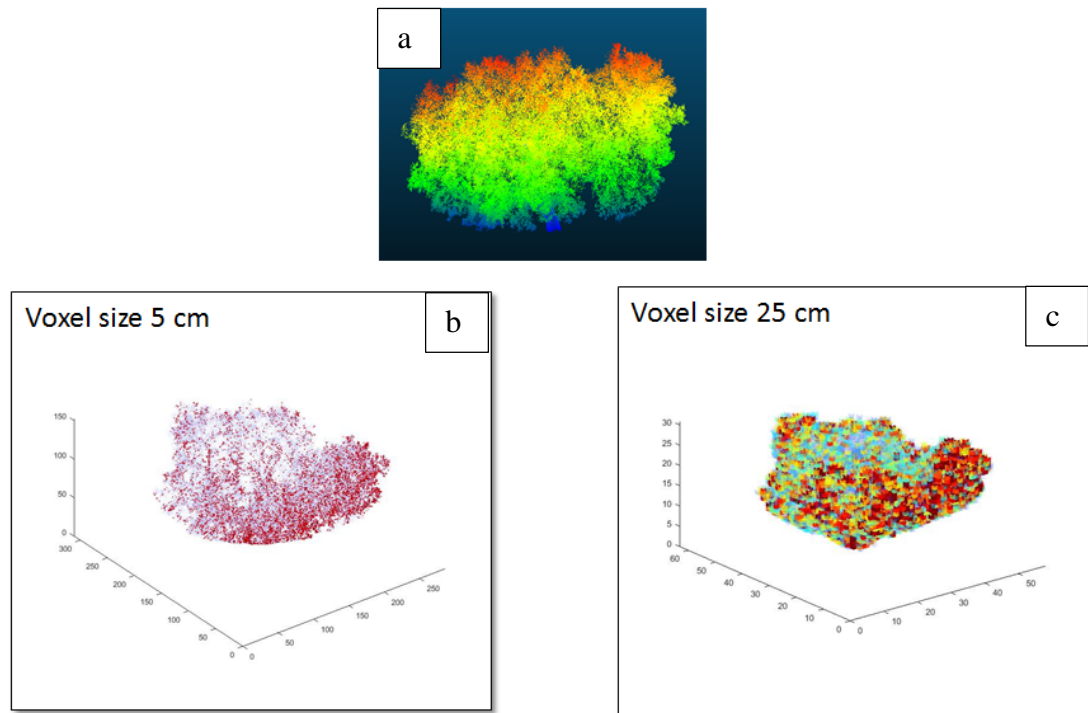
Figure 4-9: An example of voxelization

(own illustration)

a) tree point cloud colored by elevation; b) point cloud after voxelization, voxel size 5 cm; c) point cloud after voxelization, voxel size 25 cm. Voxels are colored by point density from low value (blue) to high value (red).

4.3.3 Estimation of tree perimeter, area and tree height

CHM is a base for tree delineation and estimation of structural parameters: maximum height, projected perimeter and projected area. To generate CHM an approach of KHOSRAVIPOUR et al. (2016) modified by ISENBURG (2014) was applied. This approach allows creating pit-free canopy model. "Pits" are empty pixels in resulting raster (Figure 4-10) that hamper the subsequent analysis, e.g. single tree detection and delineation, computing of tree height, projected perimeter and other structural parameters (ISENBURG 2014).

This algorithm uses an efficient combination of the blast2dem and lasgrid functions of LAStools. The algorithm consists of two steps. The first step is to keep only the highest returns due to Isenburg (lasthin) and interpolate them with a triangulated irregular network (TIN) and rasterize them into a grid (blast2dem) with a 5 cm pixel size to generate a standard CHM. Then, a number of partial CHMs are generated from highest returns on the same manner but below a certain height, so that each CHM represents only some higher part of the canopy (Figure 4-11). Then, all these CHMs are combined

together into one resulting CHM, presenting interpolated heights of all points in the canopy in the form of a raster with 5 cm pixel size (KHOSRAVIPOUR et al. 2016). The resulting standard and pit-free CHMs for the area around Main EC tower are shown in Figure 4-12 and Figure 4-13. Standard and pit-free CHMs for the area around North and South EC towers are presents in Appendix (Figure A-1 - Figure A-4).

Tree crown delineation was carried out using an approach Segmentation with Distance-Transformed Image using watershed algorithm (CHEN et al. 2006). All the calculations were implemented in the command line using SAGA GIS in batch script modus.
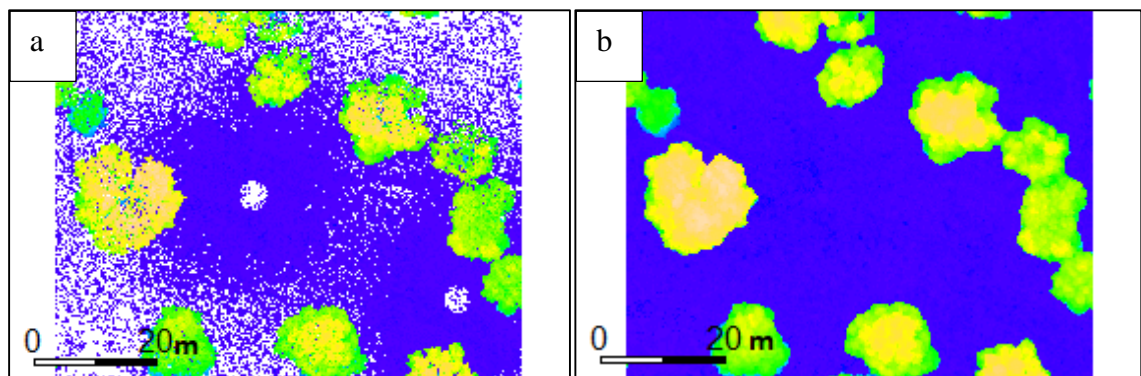

Figure 4-10: Data "pits" in CHM

(own illustration)

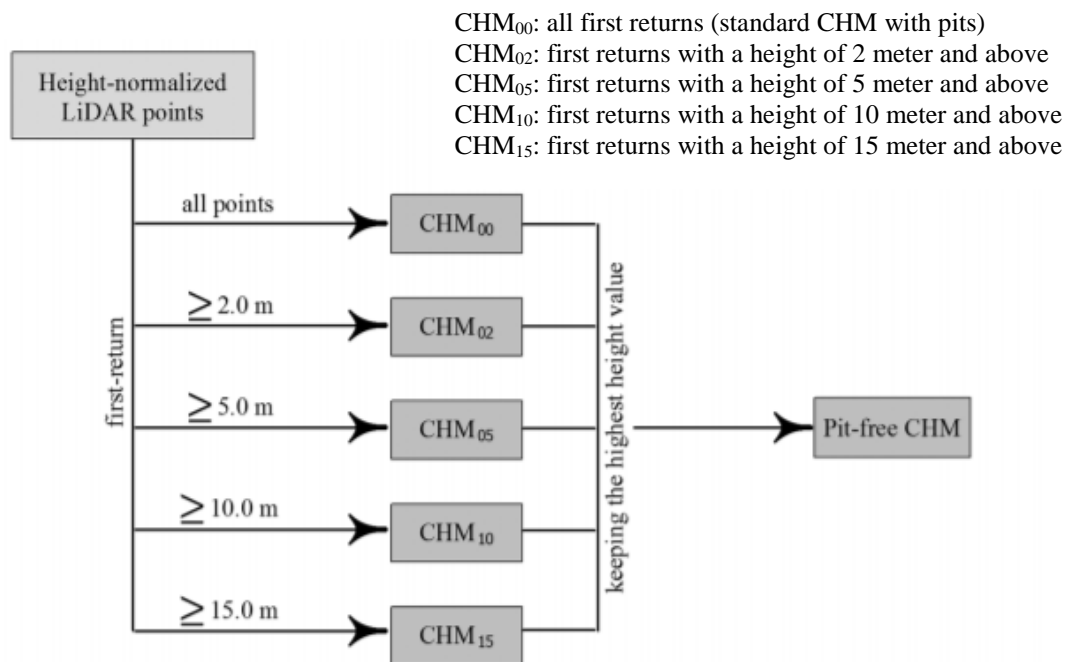a) fragment of general CHM with pits; b) fragment of pit-free CHM

Figure 4-11: Diagram of pit-free algorithm methodology

(KHOSRAVIPOUR et al. 2014)
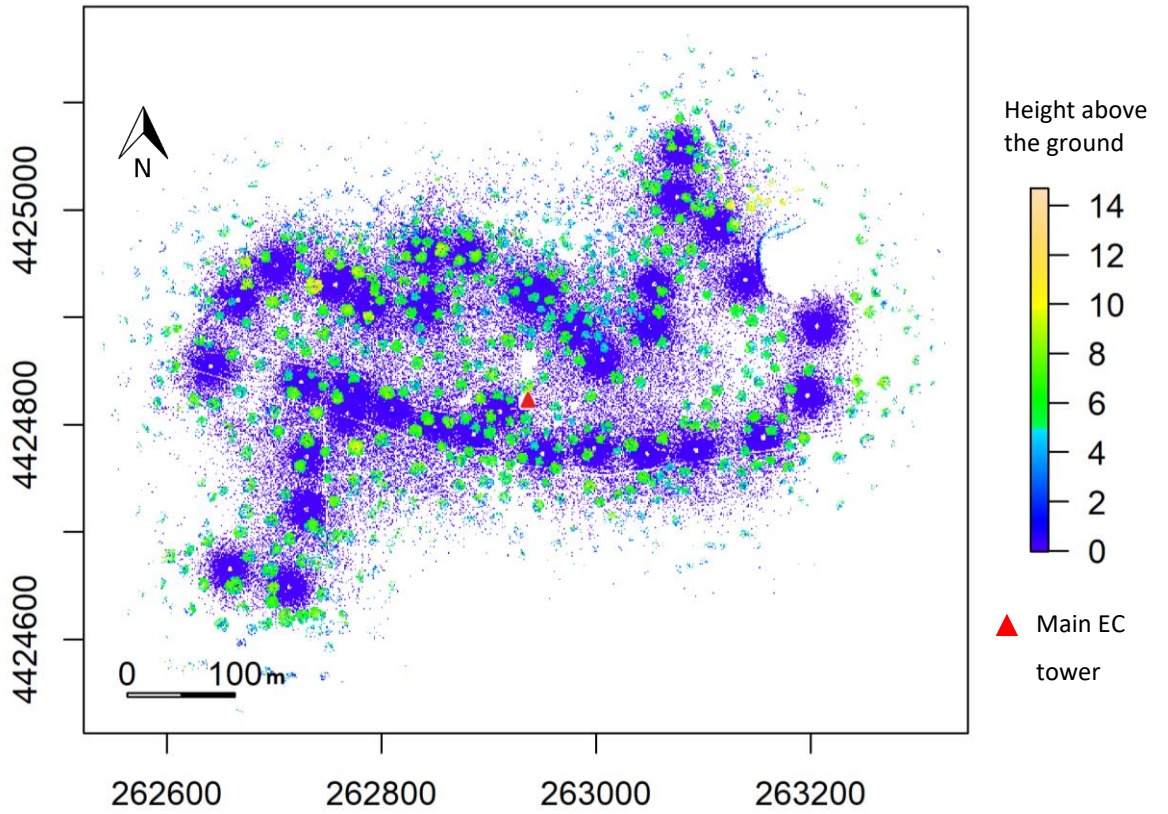
Figure 4-12: Standard CHM: area around main EC tower
(own illustration)
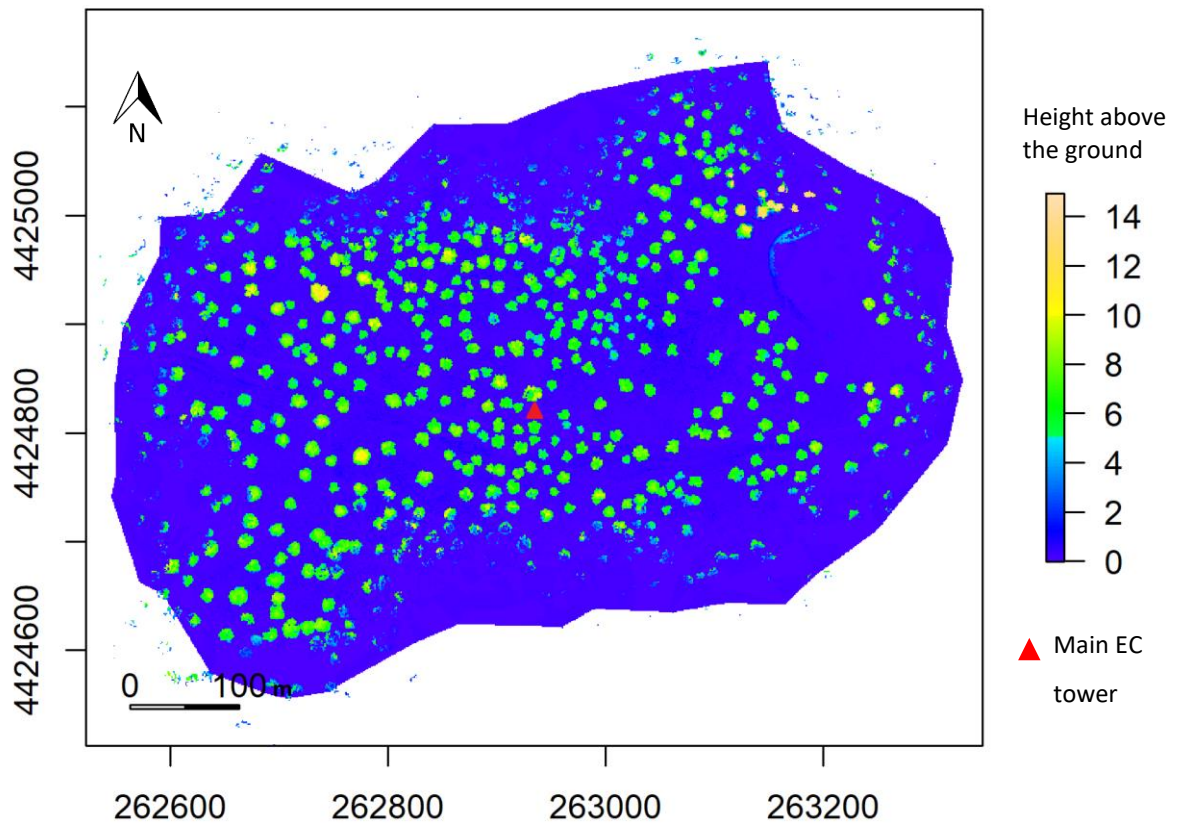
Figure 4-13: Pit-free CHM: area around main EC tower
(own illustration)

process begins from local minima and stopped when the water has reached the highest peak in the landscape. As a result, the landscape is segmented into basins isolated from each other by watersheds (ROERDINK & MEIJSTER 2000). The principle of a watershed algorithm for tree delineation is shown in Figure 4-15. A gray-scale image can be considered as a landscape model, where the gray tone of each pixel represents the elevation at the respective point (VINCENT & SOILLE 1991). The top of the tree has the maximum height inside of canopy and is represented on the image via pixel having maximum value (so-called local maxima). The inversion of the image converts the local maxima to local minima, which represents the basin on landscape model. The algorithm builds the watershed between the basins. Thus, the tree canopies on the resulting image are presented by closed contours, equivalent to water basins surrounded by watersheds (WANG et al. 2004).

Figure 4-14: Minima, catchment basins and watersheds

(VINCENT & SOILLE 1991)

Figure 4-15: An illustration of watershed segmentation algorithm

(modified after: CHEN et al. (2006)

a) CHM.; b) the complement of the CHM, c) dams built at the divide line

A relatively flat Holm oak canopy hamper the detection of the highest top layer of the tree from CHM. Therefore, the detection of the tree tops as local minima for application of watershed algorithm was obtained using distance transform of 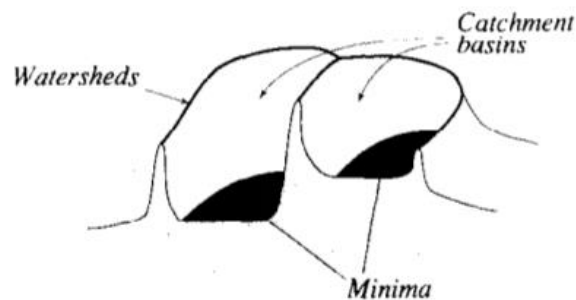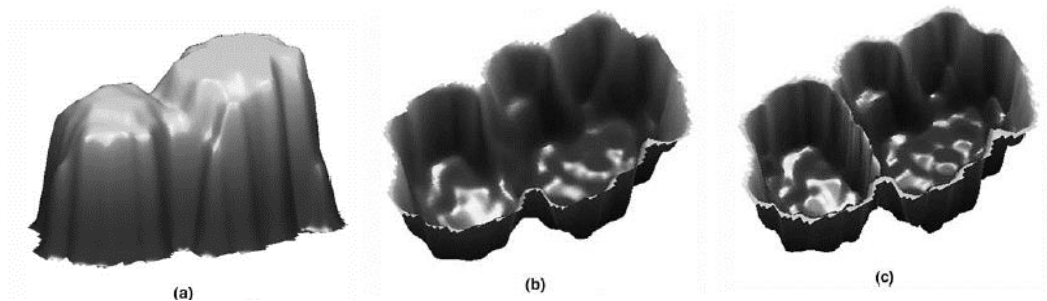a binary image and taking into account the fact that the tree top is located typically around the center of the canopy. The Distance transform approach calculates the distance between each pixel and nearest non-zero pixels of the image and replace pixel value with distance value (CHEN et al. 2006).

CHM was loaded into SAGA GIS software as a grid containing values of height. The first step was to separate the canopy and background by creating a binary image, where all the background cells have value 1. Using a logical ifelse function, the cells having value smaller than 1 (1m elevation from ground) are masked with 1, other cells get value -99999 (no data in SAGA GIS environment). The next step was to compute a Euclidian distance from each one-value pixel to the nearest one, so the resulting distance transformed image have the larger distance values for the crown center. Then this image was inverted, so that the crown center has minimum values, and the background is no data. Then the SAGA GIS watershed algorithm was implemented. Segmentation results were saved as a shapefile with the polygons as tree crowns.

The following issues were identified: 1. over-segmentation of some tree crowns, if there are more than two main branches. 2. under-segmentation of some trees having similar height in areas with high tree densities. Thus, the shapefile was cleaned manually using Qgis software.

Trees at the edges of scans with the low point density causes unaccurate estimation of the tree parameters and propagate errors to the spatial analysis. Therefore, it was decided to focus on the area close to EC towers with high point density. Finally, three sites were produced and named according to EC towers and TLS scans: MT site, ST site and NT site (Table 4-1). The MT site is presented in Figure 4-16. The ST site and the NT site are shown in Appendix (Figure A-5 and Figure A-6).

Table 4-1: Number of trees and area of each site

Site	Number of trees	Area of site, ha
MT site	260	12.8
ST site	260	12.1
NT site	298	14.9
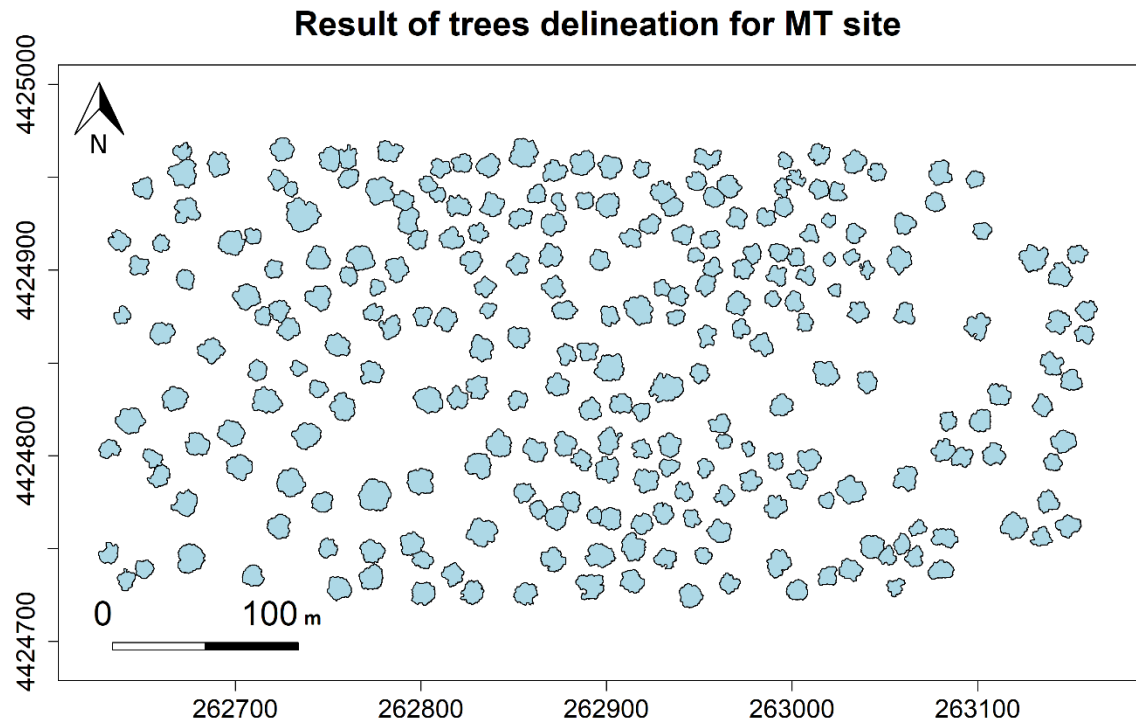
Figure 4-16: Result of trees delineation for MT site

(own illustration)

number of trees 260, area 12.8 ha

Each tree in shape files received ID number and coordinates of canopy centroid. To calculate crown projection perimeter and area the "Calculate geometry" function of the Qgis software was applied. The maximum height was calculated from the standard CHM as a maximum pixel value inside of each tree crown polygon. For further spatial analysis, field measured DBH was assigned to each tree.

4.4   Spatial analysis

The shape file containing the delineated tree crowns and information about tree parameters was processed in R-Studio for spatial analysis (packages "sp", "rgdal", "rgeos", "raster"). First, the shape file was converted to a raster brick. Raster brick is a multi-layer raster object. In our case the raster brick contains five raster layers, due to the number of fields in the shape file's attribute table: perimeter, area, ID, max height, DBH (Figure 4-17a). The resolution of each raster layer is 5 cm. Pixels related to the trees have values of correspondent attribute table's field. The background pixels have no data values (NA). Finally, three raster bricks for each sites were generated.
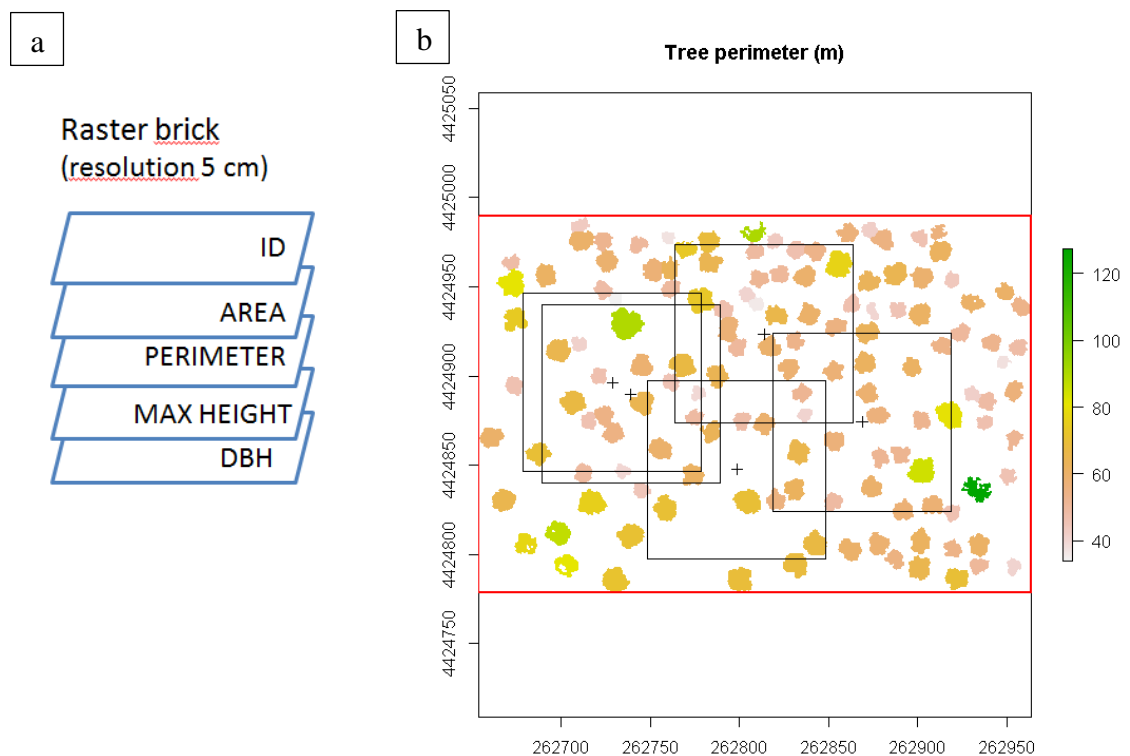
Figure 4-17: Random Sampling technique

(own illustration)

a) structure of raster brick; b) an example of 1ha polygons

To extract the information about spatial distribution of tree structural parameters from the raster brick, a random sampling technique was applied. Sample spatial quadrate polygons were randomly generated for each study site (Figure 4-17b). Sample number and polygon size are:

- for MT site 200 polygons of 100x100m, 200 polygons of 50x50m, 200 polygons of 20x20m
- for ST site 200 polygons of 100x100m, 200 polygons of 50x50m, 200 polygons of 20x20m
- for NT sit 200 polygons of 50x50m, 20x20m (polygon size 100x100m is not suitable for this site: some trees, located in the middle of site, were exclude from the study because of low point density of TLS point cloud)

The information was extracted from the raster brick as a large list containing pixel values from each raster layer for each sample polygon. For each polygon number of trees was calculated. For the trees located on the border of polygon the threshold value was applied: if more than 50% of tree pixel area was located out of the sample polygon, the tree was filtered out from this polygon.

For each polygon mean values of area, perimeter, DBH and maximum height were calculated. Ecosystem structural parameters such as tree density and tree canopy fraction were also obtained from the data. Tree density was calculated according its definition: the number of trees per one ha. The number of trees within a polygon was divided by its area and multiplied by one ha. The canopy fraction was obtained in the following way: the polygon area occupied by trees was divided by whole polygon area. Areas within sites with trees having low point density on TLS scans were avoided by random sampling.

To determine how tree structural parameters, tree density and canopy fraction relate to each other, simple correlation analysis (with the Pearson correlation coefficient) was applied to the results of the random sampling using RStudio.

5 Results

5.1   Retrieval of structural parameters

5.1.1 DBH

Figure 5-1 demonstrates the relationships between the TLS-derived and measured DBH. Validation against field measurements indicates a high R^2 value of 0.91 for the circumference calculation method CM (RMSE = 2.8 cm, n=36). Another calculation method (PM) showed a better accuracy in diameter prediction: $R^2 = 0.92$, RMSE = 2.4 cm. The proposed approach has a tendency to overestimate measured tree diameter, in particular CM method tends to overestimate diameter value more than PM calculation. At the same time, no significant differences were found between the diameters obtained at LL, DH or at the breast height. Our results suggest that the source of uncertainties is associated with irregular (non-circular) shapes of trunk cuts. This was further evaluated through a residual analysis where the residuals of DBH, obtained using PM method, were plotted against the standard deviation of 10 perpendicular diameters (Figure 5-2a). Based on visual inspection, the presence of some outliers is clear from this plot, which belong to the cuts with the highest standard deviation of perpendicular diameters. Note that a higher standard deviation of perpendicular diameters results from irregular shapes while a low value corresponds to cylindrical shapes. To better illustrate this, we have chosen four trunk cuts with the high residuals and one with low residual values and plotted their shapes (Figure 5-2b). The shape of the cuts with tree id "i-iv" is irregular, while the cut with id "v" is regular (circular). Comparison of diameter variation of these cuts shows that the diameter variation for irregular shape is significantly higher than one for irregular shape (Figure 5-2c).
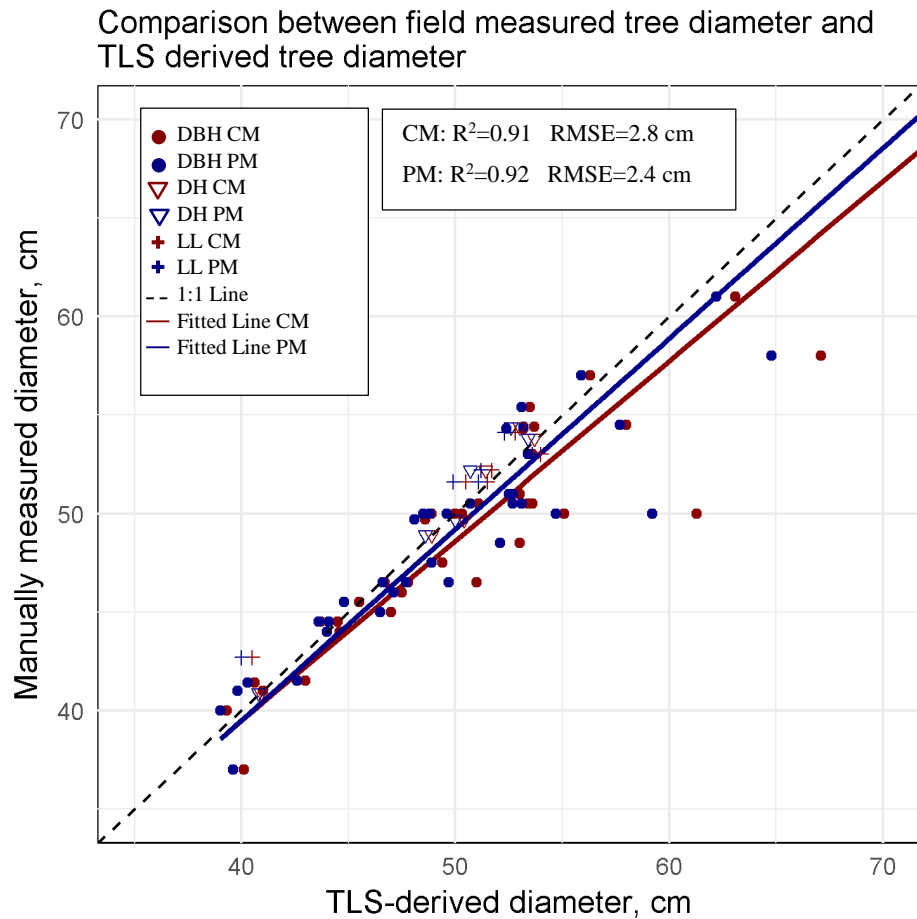
Comparison between field measured tree diameter and
TLS derived tree diameter

Figure 5-1: Comparison between field measured tree diameter and TLS derived tree
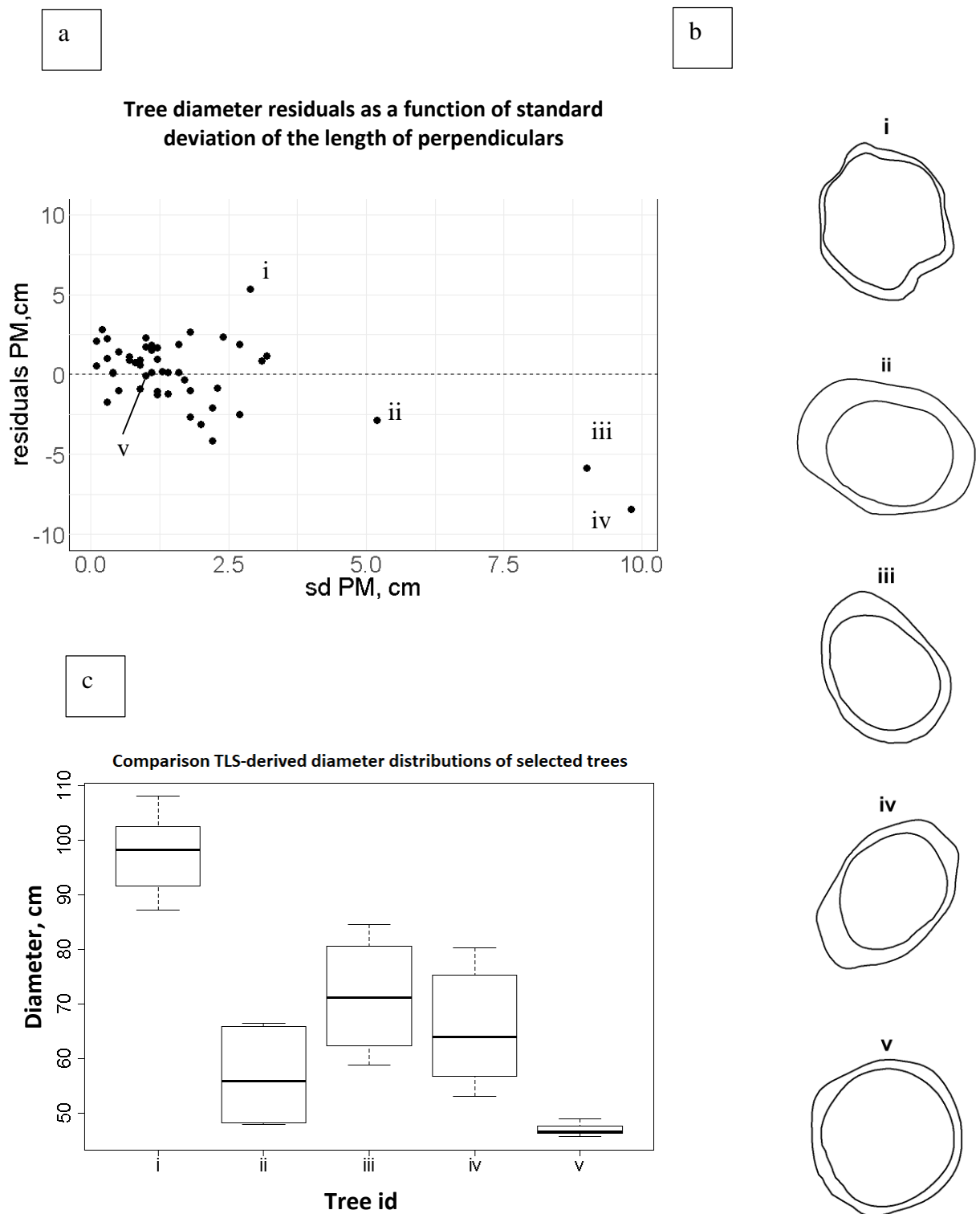diameter

(own illustration)

Figure 5-2: Tree diameter residuals and tree cuts shapes

(own illustration)

a) Scatter plot between residuals of DBH, obtained using PM method and standard deviation of the ten perpendicular diameters that were taken for each tree cut; b) shapes of trunk slices; c) comparison TLS-derived diameter distributions of selected trees

5.1.2 Clumping index

Table 5-1 and Table 5-2 include the results of clumping index (Ω) calculated with voxel sizes from 5 to 25 cm and zenith angles ranges 30-60˚ and 55-60˚. Apparently, the Ω decreases with increasing voxel sizes for both zenith angle ranges. For instance, the Ω for tree SAP4 decreases by 50%: 0.9416 for voxel size 5 cm to 0.2502 (Table 5-1) for zenith angle 30-60˚ and 0.8783 to 0.2027 for zenith angle 55-60˚ (Table 5-2). In common, the distribution of the Ω values for all trees for a voxel size 5 cm is narrower for a zenith angles 30-60˚ than for 55-60˚, whereas the distribution of Ω for 25 cm voxels is wider for 30-60˚ (Figure 5-3).

Table 5-1: Results of clumping index calculation for zenith angle range 30-60 degrees

Tree ID	Clumping index, zenith angle 30-60				
	voxel 5	voxel 10	voxel 15	voxel 20	voxel 25
SAP1	0.9522	0.8207	0.7397	0.6415	0.5523
SAP4	0.9416	0.7254	0.5261	0.3950	0.2502
SAP5	0.9739	0.8824	0.7457	0.5566	0.4466
SAP6	0.9426	0.7443	0.5470	0.4205	0.3462
Pot1	0.9886	0.9359	0.8468	0.7284	0.6083
Pot2	0.9880	0.9543	0.8920	0.8054	0.7340
Pot3	0.9902	0.9589	0.8628	0.7019	0.5564
Pot4	0.9807	0.9061	0.7695	0.5727	0.4221
Pot5	0.9805	0.9086	0.7430	0.5636	0.4494
Pot6	0.9681	0.8751	0.7252	0.5670	0.4773

Table 5-2: Results of clumping index calculation for zenith angle range 55-60 degrees

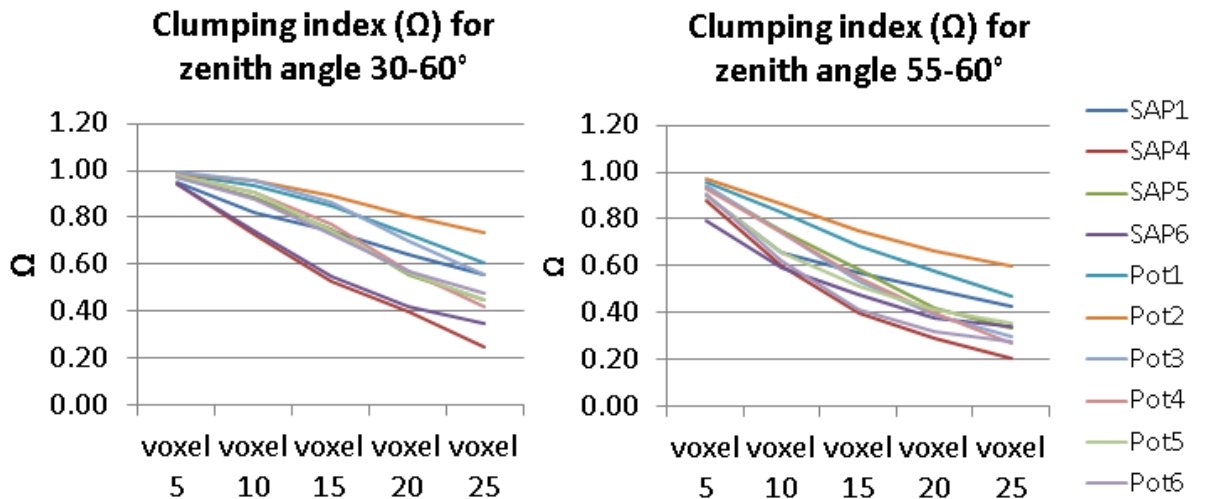| Tree ID	Clumping index, zenith angle 55-60				
	voxel 5	voxel 10	voxel 15	voxel 20	voxel 25
SAP1	0.8965	0.6546	0.5708	0.4959	0.4251
SAP4	0.8783	0.5981	0.3978	0.2896	0.2027
SAP5	0.9342	0.7464	0.5842	0.4192	0.3340
SAP6	0.7923	0.5944	0.4750	0.3783	0.3405
Pot1	0.9590	0.8274	0.6843	0.5759	0.4717
Pot2	0.9697	0.8631	0.7523	0.6602	0.6010
Pot3	0.9446	0.7420	0.5359	0.3903	0.2953
Pot4	0.9256	0.7391	0.5453	0.3996	0.2692
Pot5	0.8982	0.6549	0.5113	0.4119	0.3543
Pot6	0.9045	0.6189	0.4107	0.3173	0.2761

Figure 5-3: Results of clumping index calculation for different voxel sizes and

zenith angle ranges 30-60˚ and 55-60˚

(own illustration)

Lines are coloured by tree ID

5.2 Spatial analysis

Figure 5-4 shows the distribution of structural parameters of the 260 trees at the MT site. The projected perimeters of tree crowns vary from 31 m to 91m, projected areas – from 34 to 237 m^2. Tree height ranged from 5.4 m to 12 m. The observed DBH in 222 trees: spanned from 25 cm to 95 cm.

The spatial distribution of structural parameters for NT and ST sites is shown in Figure 5-5 and Figure 5-6. Some trees (shown in white color) were excluded from the analysis when the point density of TLS scans were not sufficiently high for a good retrieval of tree parameters. The ST site includes 260 trees and the structural parameters were calculated for 235 trees. The tallest tree is 10.8 m, the shortest one is 7.3 m. The maximum projected perimeter is 75 m with an area of 160 m^2. The minimum values are 45 m and 65 m^2 respectively. Diameters were measured for 219 trees and vary from 21 to 104 cm. Tree parameters were calculated for 298 trees of NT site (total number of trees is 337). Projected perimeter varies from 44 to 80 m, area from 64 to 170m^2. Maximum tree height 10.3 m, minimum – 6.8 m. DBH was measured for 245 trees. Maximum value is 54, minimum - 22.5 cm.
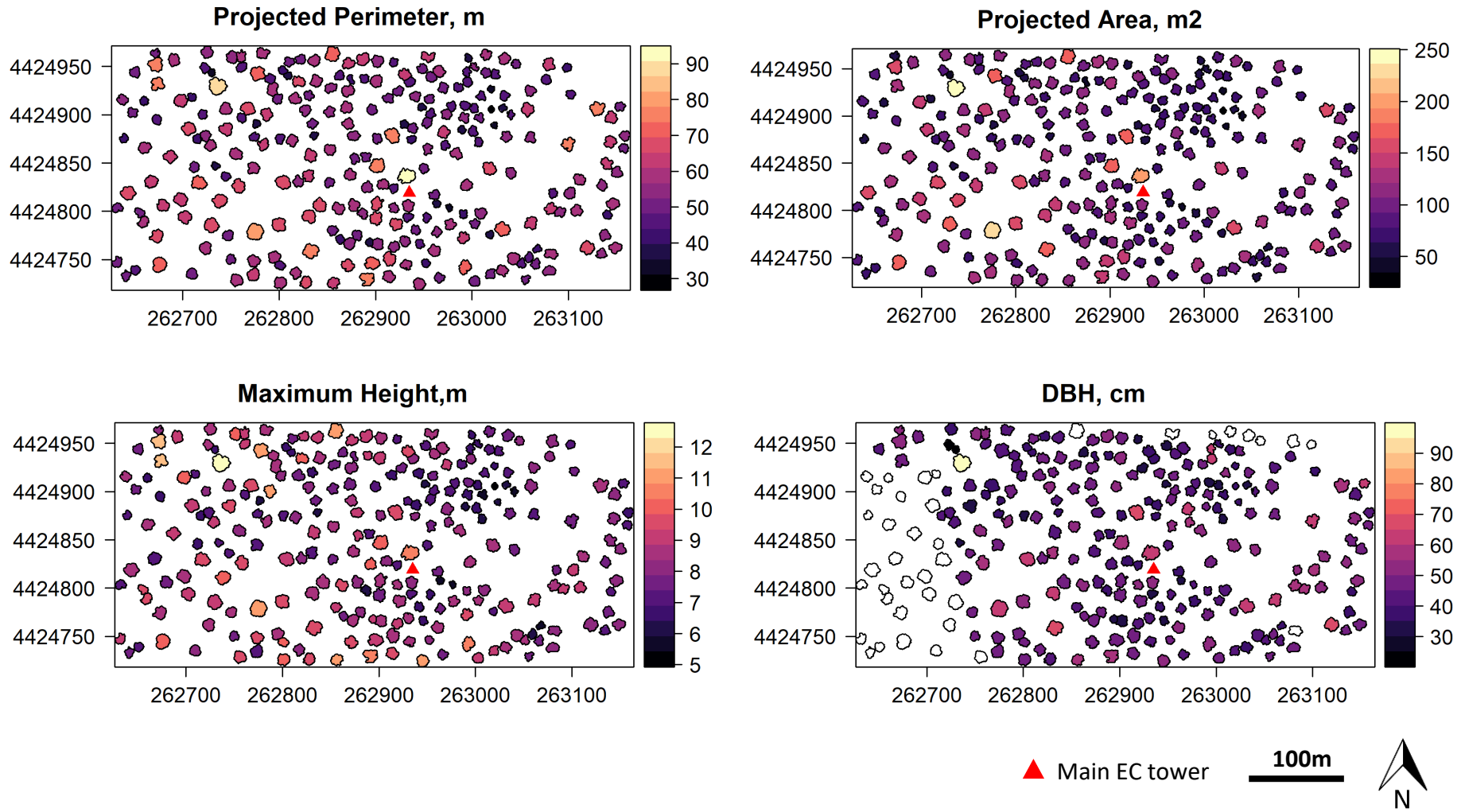
Figure 5-4: Spatial distribution of structural parameters on MT site
(own illustration)
white trees – no data.

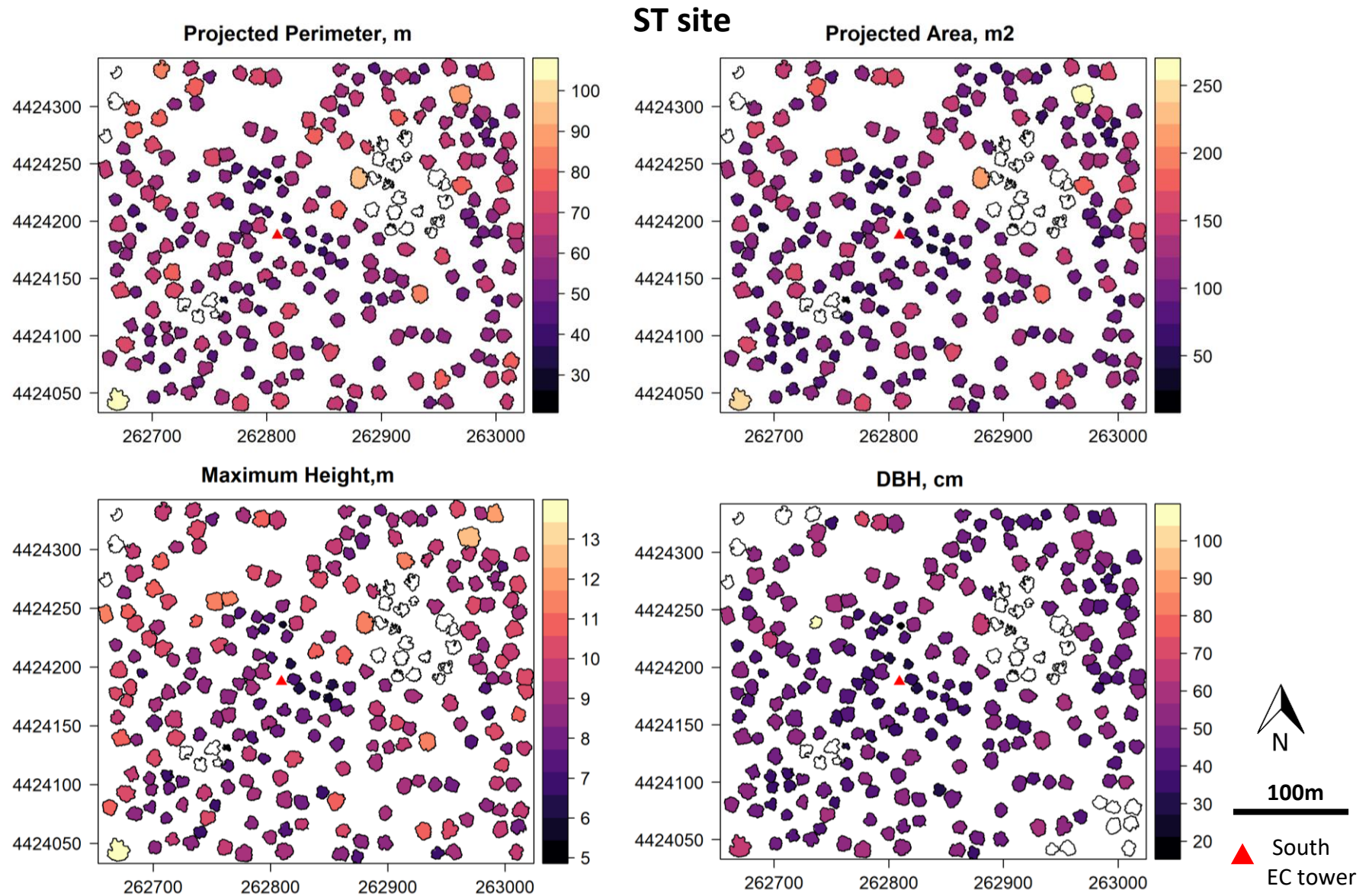Figure 5-5: Spatial distribution of structural parameters on ST site
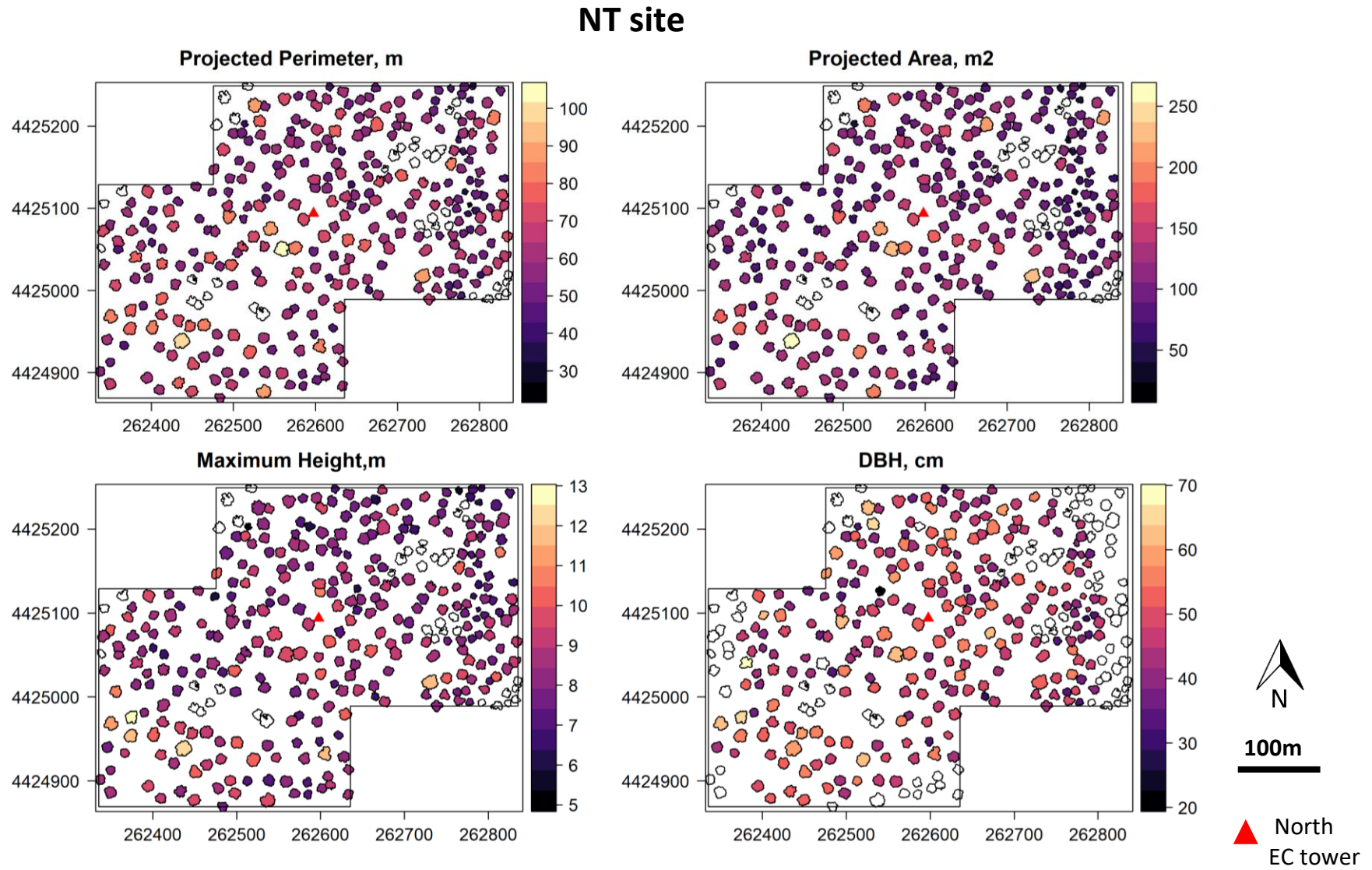(own illustration)
white trees - no data

NT site

Figure 5-6: Spatial distribution of structural parameters on NT site
(own illustration)
white trees – no data

Structural parameters are not evenly distributed: there are areas with high and low tree densities. From the plot it is clear that the trees with small crown perimeters and areas are located in regions with height tree density while the larger crowns concentrated in low tree density spots. This confer the degree of heterogeneity of the Dehesa and the importance in considering the polygon sizes and number of sampling required for a good representativeness.

Table 5-3 shows the average values together with standard deviation for each structural parameter and each plot size. Density distributions of tree structural parameters, tree density and tree canopy fraction are shown in Figure 5-7 and Figure 5-8. The histograms for each site and polygon size are presented in the appendix (Figure A-7 - Figure A-12). In general, all variables followed a normal distribution and their average values do not vary significantly with the polygon size. However, the standard deviation increases with a decreasing in polygon sizes. The MT site has the following characteristics: mean tree perimeter vary from 55.28 ± 3.71 m to 56.75 ± 9.76 m due to size of polygon, mean area - from 99.56 ± 14.25 m^2 to 104.41 ± 33.87 m^2, mean maximum height – from 8.07 ± 0.51 m to 8.25 ± 1.15 m, mean DBH from 46.30 ± 3.38 cm to 47.05 ± 9.10 cm. Tree canopy fraction vary from 18.91 ± 4.84% to 19.36 ± 17.24 %, tree density – from 19.40 ± 5.82 trees per ha to 19.38 ± 17.62 trees per ha.

Table 5-3: Results of random sampling

| Polygon size	Mean Perimeter (m)	Mean Area (m^2)	Mean Max Height (m)	Mean DBH (cm)	Mean Tree canopy fraction (%)	Mean Tree density (n*ha^{-1})
MT site: number of trees 260, sample size 200						
100	55.28 ± 3.71	99.56 ± 14.25	8.07 ± 0.51	46.30 ± 3.38	18.91 ± 4.84	19.40 ± 5.82
50	55.80 ± 6.22	101.79 ± 21.41	8.19 ± 0.75	46.90 ± 5.40	18.89 ± 7.79	19.50 ± 9.66
20	56.75 ± 9.76	104.41 ± 33.87	8.25 ± 1.15	47.05 ± 9.10	19.36 ± 17.24	19.38 ± 17.62
ST site: number of trees 260, sample size 200						
100	56.89 ± 2.93	102.50 ± 9.85	8.92 ± 0.45	47.17 ± 3.93	22.29 ± 3.39	22.09 ± 4.77
50	59.68 ± 5.54	110.60 ± 17.63	9.17 ± 0.73	48.35 ± 5.62	23.15 ± 7.83	21.68 ± 8.45
20	58.72 ± 9.77	107.25 ± 31.23	9.05 ± 1.17	47.67 ± 10.99	21.60 ± 20.27	20.50 ± 18.55
NT site: number of trees 298, sample size 300						
50	62.93 ± 6.52	120.90 ± 20.77	8.65 ± 0.63	47.85 ± 3.51	22.79 ± 6.44	19.35 ± 6.51
20	63.12 ± 9.58	120.96 ± 32.09	8.57 ± 1.02	48.64 ± 6.48	22.23 ± 19.61	18.83 ± 16.72
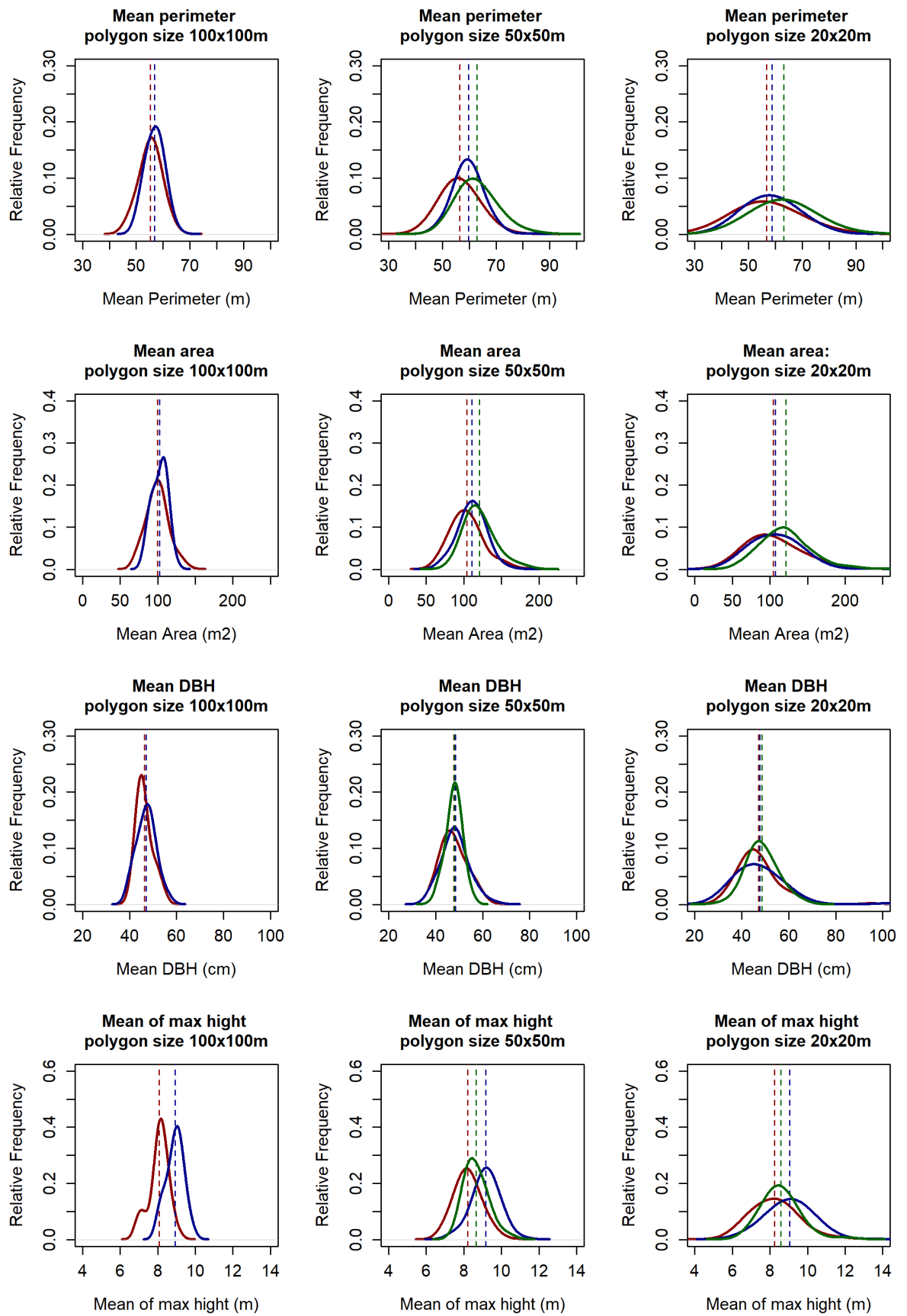
Figure 5-7: Density distribution of tree structural parameters

(own illustration)

red line – MT site; blue line – ST site; green line – NT site; solid lines – mean values
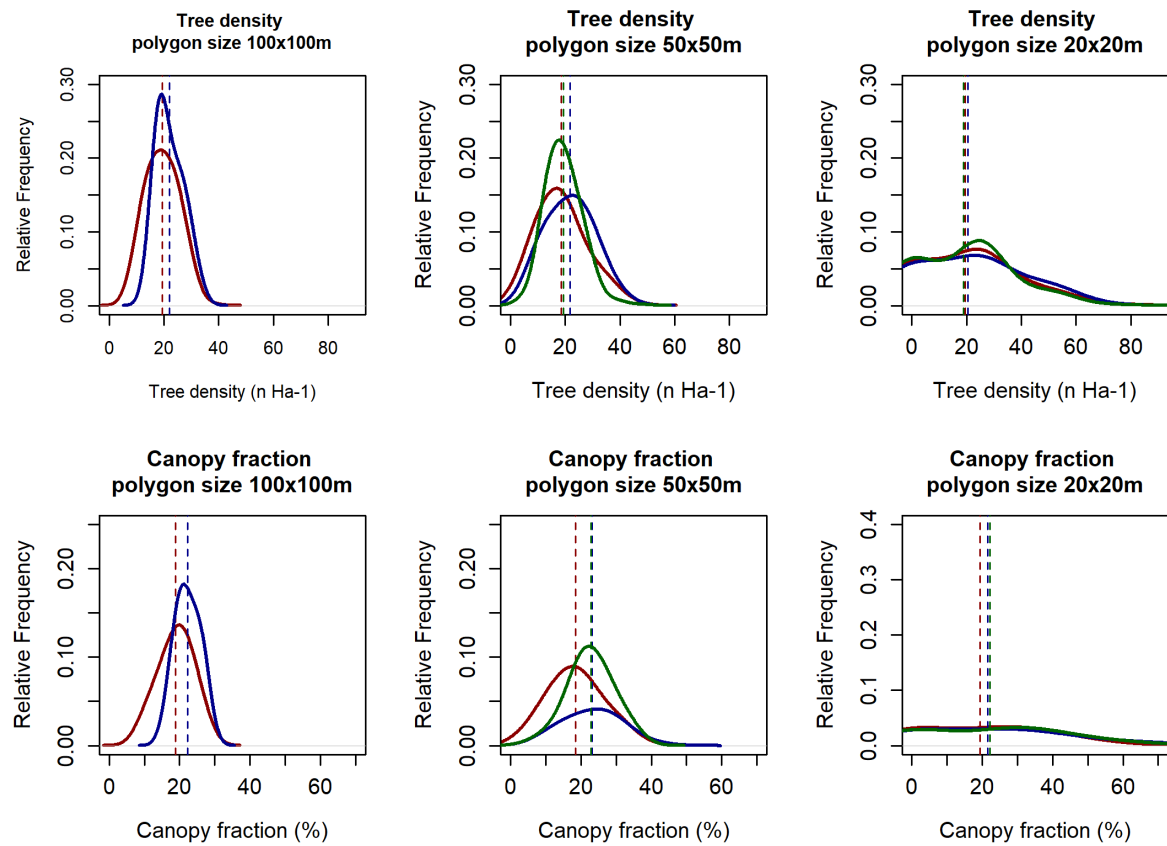
Figure 5-8. Density distribution of ecosystem structural parameters

(own illustration)

red line – MT site; blue line – ST site; green line – NT site; solid lines – mean values

On comparing the three eddy covariance sites under study, the trees at the MT site have larger canopies than the trees at the NT site: the mean perimeter of trees of NT site for 50x50 m polygon is 62.93 ± 6.52 m, area is 120.90 ± 20.77 m^2, while trees of MT site are characterized by mean perimeter of 55.80 ± 6.22 m and area of 101.79 ± 21.41 m^2. At the same time, tree density is similar to the MT site: 19.35 ± 6.51 trees per ha. Trees at the ST are slightly taller: mean maximum height is 8.92 ± 0.45 m (polygon size 100x100 m). The ST site has the higher tree density: 22.09 ± 4.77 trees per ha. There does not appear to be any outliers, except for the distribution of tree canopy fraction and tree density for a 20x20 m polygon size. Because of the small size of polygon and relative low tree density, there are several sample polygons without any trees inside.

Figure 5-9 shows the relationships between tree structural parameters, tree density and tree canopy fraction for all study sites. There is an expected strong correlation between mean perimeter and mean area (R=0.95), mean area and mean maximum height (R =0.88), mean perimeter and mean height (R =0.84) for the MT site.
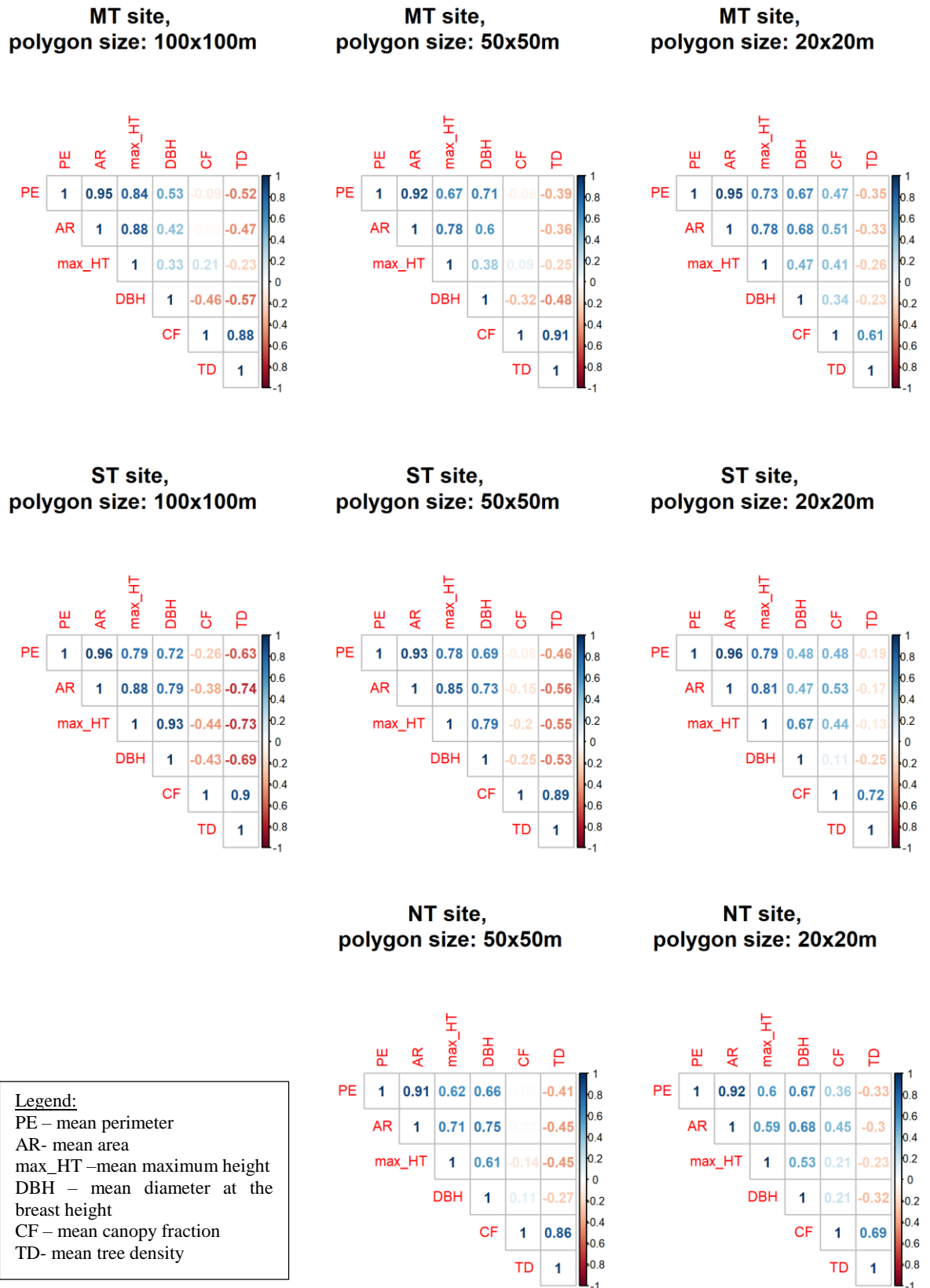
Figure 5-9: Relationships between tree and ecosystem structural parameters (own illustration)

The matrixes present spearman correlation coefficients, colours indicate the strength of the correlation (dark blue for high positive correlation coefficients and dark red for low negative correlation coefficients).

DBH is negatively correlated with canopy fraction and tree density, as well as with perimeter, area and tree height. Changing of the polygon size do not influence largely the strength of the relationships between tree height, area, perimeter and tree density. In contrast, correlation between structural parameters and canopy fraction vary from very weakly negative for large polygon size to weakly positive for 20x20m size. Similar relationships are found for ST and NT sites.

6 Discussion

6.1 Retrieval of structural parameters

One of the aims of this study was the retrieval of structural parameters of vegetation (tree height, canopy projected area and perimeter, diameter at the breast height, canopy clumping index) in the Mediterranean savanna ecosystem using TLS.

6.1.1 DBH

We have developed an approach to estimate DBH from TLS scans, which is based on delineation of the point cloud of trunk cuts. Although the common approach to estimate DBH is the cylinder fitting method (MOSKAL & ZHENG 2011, SRINIVASAN et al. 2015) we have demonstrated that this method can be subjected to uncertainties associated with the irregular cut shapes. Our results revealed that the proposed approaches CM and PM methods largely reduced such uncertainties for irregular shapes, where larger discrepancies were found between observations and estimates (Figure 5-2a). The results obtained from TLS using this approach showed good agreement with field measurements. PM seems to be more accurate, though, there is no difference in accuracy between the two methods. However, some factors influence the accuracy: i) the shape of trunk cut and ii) the point density of point cloud and slice thickness.

We have found the shape of tree cut from TLS point cloud is a critical parameter for accurate DBH estimation. In this study the shape can be explained from the standard deviation of average length of random perpendicular diameters: regular-formed cut shapes have the lowest standard deviation, because the length of perpendicular diameters is almost equal, at the same time irregular shaped cuts show relative high standard deviations. The irregular cut shape is a result of irregular shape of tree trunks that in most cases can be explained by tree inclination, i.e. the tree trunk is not perpendicular to the ground. This effect has been associated with environmental conditions (wind), mechanical damage or the influence of pathogens. Another factor is tree age: old trees have common irregular cross section (PULKKINEN 2012).

TLS point clouds of trees were sliced parallel to ground, while cross section of tree (even those that are tilted) is taken during field measurements perpendicular to the longitudinal axis of the trunk, i.e. regardless of slope to the ground. This can lead to a misrepresentation of cross section shape, e.g. an elliptical shape for a circular trunk cross section for non-vertical tree. This problem could be solved by rotating the point cloud of each tree to account for the inclination angle. However, this procedure is a higher

computational process that requires longer running times, especially in case of high tree count.

Another confounding factor is the density of point cloud and slice thickness. Based on visual inspections of point cloud, we concluded that some trees had a heterogeneous density along the cuts with more points on the one sides and less on the another (a.k.a. TLS occlusions). Although an optimal number of scan positions would always reduce this issue, the occlusion problem could be solved by increase slice thickness. The slice thickness does not affect trees with straight stems, in the case of tilted stem, it might be a source of error. Nevertheless, the low tree density of Dehesas makes LiDAR application quite efficient.

This study shows the ability of LiDAR to accurately determine the shape of cross section. This provides a means to evaluate potential pitfall of field techniques. For instance, BINOT et al. (1995) compared different measurement methods and concluded that the non-circular form of tree trunk cross section might be a reason for overestimation as compared to the use of tape, the diameter is determined from a measurement of the circumference, as "the circle is the geometric form with the shortest perimeter for a given area". Additionally, PULKKINEN (2012) analyzed the influence of shape of the cross section on basal area estimation. She defined convex and non-convex closures of cross section concluding that diameter measurements with calipers or measure tape do not take in account convexity of the cross section and therefore, this kind of measurements leads to an overestimate of the basal area and tree volume in case of non-convex closure. In our study tree "i" in Figure 5-2b is an example of non-convex closure. TLS is able to determine the "real" non-concavity shape of cross section. Therefore, estimation of cross section shape using TLS could be useful for dendromorphological studies of the influence of the cross sectional shape on estimations of basal area and tree volume without cutting a tree. Thus, LIANG et al. (2011) estimated the stem curve using TLS. Additionally, the standard deviation of perpendicular diameters, which are defined using PM calculation method, is an indicator of irregular shape of trunk cut, and, therefore, can be used for detection of inclined trees.

6.1.2 Clumping index

We have obtained the clumping index (Ω) from TLS scans using a novel approach proposed by GARCÍA et al. (2015). The main difference against the study by GARCÍA et al. (2015) lies on the fact that scans were performed with a different set up. We have demonstrated that the proposed method by GARCÍA et al. (2015) can be applied without

the need of taking the scans beneath the trees. This allows an optimal sampling rate for a given number of scans. In our case, we have demonstrated that with ~30 scans per site we were able to sample ~250 trees per site. Regardless this consideration, the 3D structure of the LiDAR scans provided a good estimation of the canopy architecture, in our case – gaps in canopy, because the Ω was calculated based on the gap fraction distribution. In order to evaluate the effect of voxel size on Ω, TLS scans of isolated trees were voxelized using different voxel sizes. Our results showed that Ω increased with decreasing voxel sizes. That corresponds with the results reported by GARCÍA et al. (2015). They compared TLS- and HP-derived clumping indices in the same study site (Majadas) and concluded that there was better agreement with smaller voxel sizes. This is mostly explained by the extent on which the distribution of gap fractions can be accurately determined upon the voxel size (small voxel size has more ability to capture small gaps, GARCÍA et al. (2015)). In addition, our results showed that Ω was affected by the zenith angle. We used two zenith angle ranges to calculate Ω, i.e. 55-60˚ and 30-60˚. According to the proposed parametrization, the most accurate result in our study is presented for a voxel size of 5 cm and a zenith angle range of 55-60˚. The calculated Ω values in 10 trees using these parameters were close to 1, which suggests a randomly distribution of the foliage elements inside the holm oaks canopies.

It is worth remarking here that there are some factors affecting the accuracy of Ω estimation with TLS: i) high noise at the edges of canopy because of its movement during scanning (wind flow), ii) occlusions effect in the upper canopy together with iii) decreasing of point cloud resolution with increasing distance from sensor, which tends to overestimate the canopy gap fraction (GARCÍA et al. 2015).

6.2   Spatial distribution of tree structural parameters and biometrical relationships

The second objective of this research was to study the spatial distribution of the vegetation structural parameters estimated with TLS and their biometrical relationships.

The manner that the respective parameters were spatially distributed was characterized using the probability distribution function obtained from the Monte Carlo analysis, which was used to evaluate the degree of heterogeneity upon the choice of the sampling areas. The results showed that the variables were normally distributed with the standard error associated with the sampling sizes. The normal distribution demonstrates a heterogeneity of structural properties of holm oaks for study area. With the reduction of polygon size spatial variability of these characteristics increases, that is demonstrated

especially well by polygon sizes of 20x20m. Thus, polygons with size 100x100m seemed to be too large to capture the whole spatial heterogeneity, whereas polygon sizes 50x50m are more suitable for this purpose.

Additionally, we tested relationship between tree structural parameters and found that tree height is positively related to crown size (area and perimeter) and DBH: the higher trees, the larger tree crown and diameter. At the same time a negative correlation was found between estimated tree structural parameters and tree density/tree canopy fraction. The trees with low DBH and smallest canopy size are concentrated in areas with high tree density, which indicates the presence of a competition between the trees. Our findings are in agreement with the research by SCHOLES & ARCHER (1997). They reviewed several studies of competition mechanisms in savannas. One of methods was to measure the spacing and size of trees. They showed a positive correlation between size of neighbouring trees and distance between them. In their research SCHOLES & ARCHER (1997) demonstrated self-thinning of trees in savannah as result of competition. They compared tree density in stands of trees having different age: young stands with small trees were characterized by higher tree density than older stands with large trees. Trees compete each other for water and nutrients and a clear spatial patterns is shown as a result soil moisture under tree canopies in areas with height density is lower due to an enhanced tree transpiration and rainfall interception (ANDERSON et al. 2001). Additionally, PLIENINGER et al. (2003) showed that trees in Dehesa have diameters related to the openness of the surrounding area. Result of competition on areas with high tree density affects negatively tree production. ABRAHAMSON & LAYNE (2003) showed lower acorn production of cork oak in stands with higher density and conversely trees in stands with lower density produced more acorn. They concluded also that the stand diameter distribution is also likely to affect acorn production. GREENBERG (2000) had similar conclusions: the larger tree DBH, the higher tree production.

We estimated tree canopy fraction based on tree delineation from CHM, i.e. elevation of canopies. LiDAR with its ability to capture 3D structure of an object has an advantage over optical sensors, as it is suitable for this purpose independently of the season, whereas the optical sensors focus on the spectral contrast between the trees and understory and are best utilized only in the dry season (CARREIRAS et al. 2006). The low tree density of study area allows one to delineate the trees accurately as there are fewer of the occlusion areas that are common for the areas with high tree density. However, the relative flat canopies of holm oaks complicate tree delineation. Further, noise in the data at the edge of canopies due to wind effects during measurement times may have an

influence on proper tree delineation and therefore perimeter and area estimation. Maximum tree height might be underestimated in case of TLS. Another problem of TLS-data is the large size of scans (for example, the size of MT scan is about 6.5 GB), which complicates quality checking of scans and requires high computer memory resources.

The spatial analysis provides valuable information could be useful for ecosystem research. Trees influence the soil structure and composition. Recycling of leaf litter and circulation of the nutrients thought the deep root system makes soils beneath the canopy rich in organic matter and nutrients (JOFFRE & RAMBAL 1993, VALLADARES & PUGNAIRE 1999). In particular, soils beneath the canopy are characterized by higher carbon stock in comparison to soils under open areas (HOWLETT et al. 2011, SIMÓN et al. 2013). SIMÓN et al. (2013) demonstrated that the carbon stock is positively correlated to tree crown projection and assume the crown projection to be a mechanism of organic carbon storage in soils under canopy cover. Another important factor that helps the understory survive during the dry season is tree influence on water balance: complex root system store the water during drought (SIMIONI et al. 2003). The trees affect light reaching beneath the canopy. Light reduction play an important role during dry season: it protect the plants beneath the tree canopy from the overheating and damage of the photosynthetic apparatus from too much light (VALLADARES & PUGNAIRE 1999). However, light reduction reaches 70% close to trunks, that can have negative effect on the photosynthesis of the understory plants (MARCOS et al. 2007, MONTERO et al. 2008).

7 Conclusions

We have demonstrated the ability of the TLS technique to retrieve trees structural parameters (DBH, clumping index, canopy projected perimeter, canopy projected area and tree maximum height) and their spatial distribution in a heterogeneous Mediterranean ecosystem characterized by sparse trees.

We have developed an improved approach to determine DBH from the delineated cuts of tree trunk point cloud. The two calculation methods were used: the first one is based on perimeter of cut (CM), while the second one is based on the on average value of random perpendicular diameters (PM). The PM method allows more accurate DBH estimates from TLS scans: the results showed very good agreement with field observations (r2= 0.92, RMSE = 2.4 cm). Residuals analysis revealed that factors, such as a tree inclination (which led to asymmetrical shapes of the cuts) and a low point density of the TLS point cloud are important source of uncertainties, e.g. the irregular shape of a cut can lead to residuals up to 5 cm. The proposed approach can be further improved using geometrical functions and aid to reduce the uncertainty related to tree inclination.

We used the method proposed by GARCÍA et al. (2015) to determine the clumping index (Ω) in a larger number of trees with different sizes and measurement setups (i.e. instruments positioned at different target distances to the trees). Our results were consistent with the results reported by GARCÍA et al. (2015): Ω was shown to be affected by the choice of critical parameters such as the voxel size and the zenith angle range. According to the proposed parameterization (a voxel size of 5 cm and a zenith angle range of 55-60˚), the value of Ω was close to 1, which suggests a randomly distribution of the foliage elements inside the holm oaks canopies.

Additionally, a random sampling technique was applied to describe the spatial distribution of the structural properties of the oak trees derived from the CHM. Although the mean of the main variables did not vary significantly upon the choice of the spatial polygon size, the results demonstrated that spatial variability is poorly captured with polygon sizes higher than 50x50m.

Our results also revealed the presence of a positive correlation between tree structural parameters among all polygon sizes: the higher trees, the larger tree crown and diameter (e.g. for maximum height and tree perimeter R=0.73 and R= 0.84 for polygon size 20x20m and 100x100m respectively). At the same time a negative correlation was obtained between estimated tree structural parameters and the spatial distribution of ecosystem properties (tree density and canopy fraction). The trees with low DBH and small canopy size were observed in areas with high tree density, which suggests the effect

of the competition between trees (correlation between tree structural properties and tree density stay negative with changing polygon size).

This study can be further applied for ecological modelling (e.g. half-hourly footprints of EC towers) and forestry inventory (tree volume and biomass accounting). TLS-derived vegetation parameters might be used for estimation biophysical properties of vegetation within half-hourly footprints of EC towers, since spatial variability of biophysical properties affects the uncertainty of the flux measurements (EL-MADANY et al. 2018). Important inventory parameters, such as tree volume and biomass can be quantified from allometric equations, which are parameterized with TLS-derived structural vegetation properties (e.g. DBH).

References

ABRAHAMSON, W. G. & J. N. LAYNE (2003): Long-term patterns of acorn production for five oak species in xeric Florida uplands. – Ecology, 84, 9, 2476-2492.

ALAGONA, P. S., A. LINARES, P. CAMPOS & L. HUNTSINGER (2013): History and recent trends. In: Campos, P., L. Huntsinger, J. L. Oviedo, P. F. Starrs, M. Díaz, R. B. Standiford & G. Montero (Hrsg.): Mediterranean Oak Woodland Working Landscapes. Dehesas of Spain and Ranchlands of California. Dordrecht: Springer, 25-58.

ANDERSON, L. J., M. S. BRUMBAUGH & R. B. JACKSON (2001): Water and tree–understory interactions: a natural experiment in a savanna with oak wilt. – Ecology, 82, 1, 33-49.

ASNER, G. P., J. M. SCURLOCK & J. A HICKE (2003): Global synthesis of leaf area index observations: implications for ecological and remote sensing studies. – Global Ecology and Biogeography, 12, 3, 191-205.

AXELSSON, P. (2000): DEM generation from laser scanner data using adaptive TIN models. – International archives of photogrammetry and remote sensing, 33, 4, 110-117.

BELSKY, A. J. (1994): Influences of trees on savanna productivity: tests of shade, nutrients, and tree-grass competition. – Ecology, 75, 4, 922-932.

BERINGER, J., L. B. HUTLEY, N. J. TAPPER & L. A. CERNUSAK (2007): Savanna fires and their impact on net ecosystem productivity in North Australia. – Global Change Biology, 13, 5, 990-1004.

BIENERT, A., C. HESS, H. MAAS & G. VON OHEIMB (2014): A voxel-based technique to estimate the volume of trees from terrestrial laser scanner data. – The International Archives of Photogrammetry, Remote Sensing and Spatial Information Sciences, 40, 5, 101-106.

BIENERT, A., H.-G. MAAS & S. SCHELLER (2006): Analysis of the information content of terrestrial laserscanner point clouds for the automatic determination of forest inventory parameters. Workshop on 3D Remote Sensing in Forestry. 14th-15th Feb 2006, Vienna: 1-7.

BIENERT, A., S. SCHELLER, E. KEANE, F. MOHAN & C. NUGENT (2007): Tree detection and diameter estimations by analysis of forest terrestrial laserscanner point clouds. ISPRS Workshop on Laser Scanning 2007 and SilviLaser 2007, Espoo, September 12-14, 2007, Finland: 50-55.

BINOT, J.-M., D. POTHIER & J. LEBEL (1995): Comparison of relative accuracy and time requirement between the caliper, the diameter tape and an electronic tree measuring fork. – The Forestry Chronicle, 71, 2, 197-200.

BREDA, N. J. (2003): Ground-based measurements of leaf area index: a review of methods, instruments and current controversies. – Journal of experimental botany, 54, 392, 2403-2417.

BROWN, S. & A. E. LUGO (1992): Aboveground biomass estimates for tropical moist forests of the Brazilian Amazon. – Interciencia, 17, 1, 8-18.

BUCKLEY, S. J., J. HOWELL, H. ENGE & T. KURZ (2008): Terrestrial laser scanning in geology: data acquisition, processing and accuracy considerations. – Journal of the Geological Society, 165, 3, 625-638.

CARREIRAS, J. M., J. M. PEREIRA & J. S. PEREIRA (2006): Estimation of tree canopy cover in evergreen oak woodlands using remote sensing. – Forest ecology and management, 223, 1-3, 45-53.

CHAVE, J., C. ANDALO, S. BROWN, M. A. CAIRNS, J. CHAMBERS, D. EAMUS, H. FÖLSTER, F. FROMARD, N. HIGUCHI & T. KIRA (2005): Tree allometry and improved estimation of carbon stocks and balance in tropical forests. – Oecologia, 145, 1, 87-99.

CHEN, J., T. BLACK & R. ADAMS (1991): Evaluation of hemispherical photography for determining plant area index and geometry of a forest stand. – Agricultural and forest meteorology, 56, 1-2, 129-143.

CHEN, J., C. MENGES & S. LEBLANC (2005): Global mapping of foliage clumping index using multi-angular satellite data. – Remote Sensing of Environment, 97, 4, 447-457.

CHEN, J. M. & T. BLACK (1992): Defining leaf area index for non-flat leaves. – Plant, Cell & Environment, 15, 4, 421-429.

CHEN, J. M. & J. CIHLAR (1995): Plant canopy gap-size analysis theory for improving optical measurements of leaf-area index. – Applied optics, 34, 27, 6211-6222.

CHEN, Q., D. BALDOCCHI, P. GONG & M. KELLY (2006): Isolating individual trees in a savanna woodland using small footprint lidar data. – Photogrammetric Engineering & Remote Sensing, 72, 8, 923-932.

CHO, M. A., R. MATHIEU, G. P. ASNER, L. NAIDOO, J. VAN AARDT, A. RAMOELO, P. DEBBA, K. WESSELS, R. MAIN & I. P. SMIT (2012): Mapping tree species composition in South African savannas using an integrated airborne spectral and LiDAR system. – Remote Sensing of Environment, 125, 214-226.

CHURNSIDE, J. H. (2013): Review of profiling oceanographic lidar. – Optical Engineering, 53, 5, 051405-1 - 051405-13.

COLGAN, M. S., C. A. BALDECK, J.-B. FÉRET & G. P. ASNER (2012): Mapping savanna tree species at ecosystem scales using support vector machine classification and BRDF correction on airborne hyperspectral and LiDAR data. – Remote Sensing, 4, 11, 3462-3480.

COLOMINA, I. & P. MOLINA (2014): Unmanned aerial systems for photogrammetry and remote sensing: A review. – ISPRS Journal of Photogrammetry and Remote Sensing, 92, 79-97.

COOPS, N. C. & T. R. TOOKE (2017): Introduction to Remote Sensing. In: Gergel, S. E. & M. G. Turner (Hrsg.): Learning landscape ecology: a practical guide to concepts and techniques. New York Springer, 3-19.

DARBOUX, F. & C.-H. HUANG (2003): An Instantaneous-Profile Laser Scanner to Measure Soil Surface Microtopography. – Soil Science Society of America Journal, 67, 1, 92-99.

DASSOT, M., T. CONSTANT & M. FOURNIER (2011): The use of terrestrial LiDAR technology in forest science: application fields, benefits and challenges. – Annals of Forest Science, 68, 5, 959-974.

DE RIGO, D. & G. CAUDULLO (2016): Quercus ilex in Europe: distribution, habitat, usage and threats. – European Atlas of Forest Tree Species; European Union: Luxembourg, 130-131.

DESLAURIERS, A., S. ROSSI & T. ANFODILLO (2007): Dendrometer and intra-annual tree growth: what kind of information can be inferred? – Dendrochronologia, 25, 2, 113-124.

DEVEREUX, B. J., G. S. AMABLE, P. CROW & A. D. CLIFF (2005): The potential of airborne lidar for detection of archaeological features under woodland canopies. – Antiquity, 79, 305, 648-660.

DÍAZ, M. (2009): Biodiversity in the dehesa. – Agroforestry systems as a technique for sustainable land management, 209-225.

DÍAZ, M., W. D. TIETJE & R. H. BARRETT (2013): Effects of management on biological diversity and endangered species. In: Campos, P., L. Huntsinger, J. L. Oviedo, P. F. Starrs, M. Díaz, R. B. Standiford & G. Montero (Hrsg.): Mediterranean Oak Woodland Working Landscapes. Dehesas of Spain and Ranchlands of California. Dordrecht: Springer, 213-243.

DONEUS, M., C. BRIESE, M. FERA & M. JANNER (2008): Archaeological prospection of forested areas using full-waveform airborne laser scanning. – Journal of Archaeological Science, 35, 4, 882-893.

EL-MADANY, T. S., M. REICHSTEIN, O. PEREZ-PRIEGO, A. CARRARA, G. MORENO, M. P. MARTÍN, J. PACHECO-LABRADOR, G. WOHLFAHRT, H. NIETO & U. WEBER (2018): Drivers of spatio-temporal variability of carbon dioxide and energy fluxes in a Mediterranean savanna ecosystem. – Agricultural and Forest Meteorology, 262, 258-278.

FERNÁNDEZ, M. P., J. F. L. CONTADOR, S. SCHNABEL, Á. G. GUTIÉRREZ & J. LOZANO-PARRA (2018): Changes in Land Management of Iberian Rangelands and Grasslands in the Last 60 Years and their Effect on Vegetation. In: Sebata, A. (Hrsg.): Vegetation. London: IntechOpen, 21-42.

FROMM, M., J. ALFRED, K. HOPPEL, J. HORNSTEIN, R. BEVILACQUA, E. SHETTLE, R. SERVRANCKX, Z. LI & B. STOCKS (2000): Observations of boreal forest fire smoke in the stratosphere by POAM III, SAGE II, and lidar in 1998. – Geophysical Research Letters, 27, 9, 1407-1410.

GAITAN, J. J., G. E. OLIVA, D. E. BRAN, F. T. MAESTRE, M. R. AGUIAR, E. G. JOBBAGY, G. G. BUONO, D. FERRANTE, V. B. NAKAMATSU & G. CIARI (2014): Vegetation structure is as important as climate for explaining ecosystem function across Patagonian rangelands. – Journal of Ecology, 102, 6, 1419-1428.

GARCÍA, M., J. GAJARDO, D. RIAÑO, K. ZHAO, P. MARTÍN & S. USTIN (2015): Canopy clumping appraisal using terrestrial and airborne laser scanning. – Remote Sensing of Environment, 161, 78-88.

GIBBS, H. K., S. BROWN, J. O. NILES & J. A. FOLEY (2007): Monitoring and estimating tropical forest carbon stocks: making REDD a reality. – Environmental Research Letters, 2, 4, 045023-1 - 045023-13.

GONSAMO, A. & P. PELLIKKA (2009): The computation of foliage clumping index using hemispherical photography. – Agricultural and Forest Meteorology, 149, 10, 1781-1787.

GOWER, S. T., C. J. KUCHARIK & J. M. NORMAN (1999): Direct and indirect estimation of leaf area index, fAPAR, and net primary production of terrestrial ecosystems. – Remote sensing of environment, 70, 1, 29-51.

GREENBERG, C. H. (2000): Individual variation in acorn production by five species of southern Appalachian oaks. – Forest Ecology and Management, 132, 2-3, 199-210.

GSCHWANTNER, T., K. SCHADAUER, C. VIDAL, A. LANZ, E. TOMPPO, L. DI COSMO, N. ROBERT, D. ENGLERT DUURSMA & M. LAWRENCE (2009): Common tree definitions for national forest inventories in Europe. – Silva Fennica 43, 5, 303-321.

HILL, M., N. HANAN, W. HOFFMANN, R. SCHOLES, S. PRINCE, J. FERWERDA, R. LUCAS, I. BAKER, A. ARNETH & S. HIGGINS (2011): Remote sensing and modeling of savannas: The state of the dis-union. Proceedings of the 34th International Symposium on Remote Sensing of the Environment (ISRSE), Sydney, NSW, Australia: 10-15.

HOGE, F. & R. SWIFT (1981):Application of the NASA airborne oceanographic lidar to the mapping of chlorophyll and other organic pigments. In: NASA: Langley Research Center Chesapeake Bay Plume Study 349-374.

HOPKINSON, C., L. CHASMER, C. YOUNG-POW & P. TREITZ (2004): Assessing forest metrics with a ground-based scanning lidar. – Canadian Journal of Forest Research, 34, 3, 573-583.

HORRILLO, A., M. ESCRIBANO, F. MESIAS, A. ELGHANNAM & P. GASPAR (2016): Is there a future for organic production in high ecological value ecosystems? – Agricultural Systems, 143, 114-125.

HOSOI, F., Y. NAKAI & K. OMASA (2013): Voxel tree modeling for estimating leaf area density and woody material volume using 3-D LIDAR data. – International Archives of the Photogrammetry, Remote Sensing and Spatial Information Sciences, II-5/W2, 115-120.

HOUGHTON, R., K. LAWRENCE, J. HACKLER & S. BROWN (2001): The spatial distribution of forest biomass in the Brazilian Amazon: a comparison of estimates. – Global Change Biology, 7, 7, 731-746.

HOWLETT, D. S., G. MORENO, M. R. M. LOSADA, P. R. NAIR & V. D. NAIR (2011): Soil carbon storage as influenced by tree cover in the Dehesa cork oak silvopasture of central-western Spain. – Journal of Environmental Monitoring, 13, 7, 1897-1904.

HUNTSINGER, L., P. CAMPOS, P. F. STARRS, J. L. OVIEDO, M. DÍAZ, R. B. STANDIFORD & G. MONTERO (2013): Working landscapes of the Spanish Dehesa and the California oak woodlands: an introduction. In: Campos, P., L. Huntsinger, J. L. Oviedo, P. F. Starrs, M. Díaz, R. B. Standiford & G. Montero (Hrsg.): Mediterranean Oak Woodland Working Landscapes. Dehesas of Spain and Ranchlands of California. Dordrecht: Springer, 3-23.

ISENBURG, M. (2014): Rasterizing Perfect Canopy Height Models from LiDAR. <https://rapidlasso.com/2014/11/04/rasterizing-perfect-canopy-height-models-from-lidar/> (Last updated: 04.11.2014) (Access: 10.04 2018).

JOFFRE, R. & S. RAMBAL (1993): How tree cover influences the water balance of Mediterranean rangelands. – Ecology, 74, 2, 570-582.

JOFFRE, R., J. VACHER, C. DE LOS LLANOS & G. LONG (1988): The dehesa: an agrosilvopastoral system of the Mediterranean region with special reference to the Sierra Morena area of Spain. – Agroforestry systems, 6, 1-3, 71-96.

KANNIAH, K. D., J. BERINGER & L. HUTLEY (2013): Exploring the link between clouds, radiation, and canopy productivity of tropical savannas. – Agricultural and forest meteorology, 182, 304-313.

KANNIAH, K. D., J. BERINGER & L. B. HUTLEY (2011): Environmental controls on the spatial variability of savanna productivity in the Northern Territory, Australia. – Agricultural and Forest Meteorology, 151, 11, 1429-1439.

KHOSRAVIPOUR, A., A. K. SKIDMORE & M. ISENBURG (2016): Generating spike-free digital surface models using LiDAR raw point clouds: A new approach for forestry applications. – International Journal of Applied Earth Observation and Geoinformation, 52, 104-114.

KHOSRAVIPOUR, A., A. K. SKIDMORE, M. ISENBURG, T. WANG & Y. A. HUSSIN (2014): Generating pit-free canopy height models from airborne lidar. – Photogrammetric Engineering & Remote Sensing, 80, 9, 863-872.

KOCH, B., U. HEYDER & H. WEINACKER (2006): Detection of individual tree crowns in airborne lidar data. – Photogrammetric Engineering & Remote Sensing, 72, 4, 357-363.

KOENIG, W. D., M. DÍAZ, F. PULIDO, R. ALEJANO, E. BEAMONTE & J. M. KNOPS (2013): Acorn production patterns. In: Campos, P., L. Huntsinger, J. L. Oviedo, P. F. Starrs, M. Díaz, R. B. Standiford & G. Montero (Hrsg.): Mediterranean Oak Woodland Working Landscapes. Dehesas of Spain and Ranchlands of California. Dordrecht: Springer, 181-209.

KRABILL, W., J. COLLINS, L. LINK, R. SWIFT & M. BUTLER (1984): Airborne laser topographic mapping results. – Photogrammetric Engineering and Remote Sensing, 50, 6, 685-694.

LEBLANC, S. G. (2002): Correction to the plant canopy gap-size analysis theory used by the tracing radiation and architecture of canopies instrument. – Applied Optics, 41, 36, 7667-7670.

LEDINGHAM, K. W. & M. CAMPBELL (1997): Laser-based sensors. In: Campbell, M. (Hrsg.): Sensor Systems for Environmental Monitoring. Volume One. Sensor Technologies. London: Blackie Academic and Professional, 65-99.

LEFSKY, M. A., W. B. COHEN, G. G. PARKER & D. J. HARDING (2002): Lidar remote sensing for ecosystem studies. – AIBS Bulletin, 52, 1, 19-30.

LEMMENS, M. (2011): Geo-information: technologies, applications and the environment. Springer Science & Business Media, Dordrecht. 1-348 S.

LENTILE, L. B., Z. A. HOLDEN, A. M. SMITH, M. J. FALKOWSKI, A. T. HUDAK, P. MORGAN, S. A. LEWIS, P. E. GESSLER & N. C. BENSON (2006): Remote sensing techniques to assess active fire characteristics and post-fire effects. – International Journal of Wildland Fire, 15, 3, 319-345.

LIANG, X., J. HYYPPÄ, V. KANKARE & M. HOLOPAINEN (2011): Stem curve measurement using terrestrial laser scanning: 1-6.

LIM, K., P. TREITZ, M. WULDER, B. ST-ONGE & M. FLOOD (2003): LiDAR remote sensing of forest structure. – Progress in physical geography, 27, 1, 88-106.

LIU, C., S. KANG, F. LI, S. LI & T. DU (2013): Canopy leaf area index for apple tree using hemispherical photography in arid region. – Scientia horticulturae, 164, 610-615.

LUDWIG BOLTZMANN INSTITUTE (2018): Filtering algorithm. <http://lbi-archpro.org/als-filtering/lbi-project/results/lastools/filtering-algorithm-2> (Last updated: not known) (Access: 01 June 2018).

MANNING, A. D., J. FISCHER & D. B. LINDENMAYER (2006): Scattered trees are keystone structures–implications for conservation. – Biological conservation, 132, 3, 311-321.

MARCOS, G. M., J. OBRADOR, E. GARCÍA, E. CUBERA, M. MONTERO, F. PULIDO & C. DUPRAZ (2007): Driving competitive and facilitative interactions in oak dehesas through management practices. – Agroforestry systems, 70, 1, 25-40.

MONTERO, M. J., G. MORENO & M. BERTOMEU (2008): Light distribution in scattered-trees open woodlands in Western Spain. – Agroforestry systems, 73, 3, 233.

MOORE, C., J. BERINGER, B. EVANS, L. HUTLEY, I. MCHUGH & N. TAPPER (2015): The contribution of trees and grasses to productivity of an Australian tropical savanna. – Biogeosciences, 12, 23, 2387-2403.

MOORTHY, I., J. R. MILLER, J. A. J. BERNI, P. ZARCO-TEJADA, B. HU & J. CHEN (2011): Field characterization of olive (Olea europaea L.) tree crown architecture using terrestrial laser scanning data. – Agricultural and Forest Meteorology, 151, 2, 204-214.

MORENO, G., J. W. BARTOLOME, G. GEA-IZQUIERDO & I. CAÑELLAS (2013): Overstory–Understory Relationships. In: Campos, P., L. Huntsinger, J. L. Oviedo, P. F. Starrs, M. Díaz, R. B. Standiford & G. Montero (Hrsg.): Mediterranean Oak Woodland Working Landscapes. Dehesas of Spain and Ranchlands of California. Dordrecht: Springer, 145-179.

MOSKAL, L. M. & G. ZHENG (2011): Retrieving forest inventory variables with terrestrial laser scanning (TLS) in urban heterogeneous forest. – Remote Sensing, 4, 1, 1-20.

NAIDOO, L., M. A. CHO, R. MATHIEU & G. ASNER (2012): Classification of savanna tree species, in the Greater Kruger National Park region, by integrating hyperspectral and LiDAR data in a Random Forest data mining environment. – ISPRS journal of Photogrammetry and Remote Sensing, 69, 167-179.

NEWNHAM, G. J., J. D. ARMSTON, K. CALDERS, M. I. DISNEY, J. L. LOVELL, C. B. SCHAAF, A. H. STRAHLER & F. M. DANSON (2015): Terrestrial laser scanning for plot-scale forest measurement. – Current Forestry Reports, 1, 4, 239-251.

OLOFSSON, K., J. HOLMGREN & H. OLSSON (2014): Tree stem and height measurements using terrestrial laser scanning and the RANSAC algorithm. – Remote Sensing, 6, 5, 4323-4344.

PEREIRA, L. G. & L. JANSSEN (1999): Suitability of laser data for DTM generation: a case study in the context of road planning and design. – ISPRS Journal of Photogrammetry and Remote Sensing, 54, 4, 244-253.

PEREZ-GUTIERREZ, C., J. MARTÍNEZ-FERNÁNDEZ, N. SANCHEZ & J. ALVAREZ-MOZOS (2007): Modeling of soil roughness using terrestrial laser scanner for soil moisture retrieval. IEEE: 1877-1880.

PLIENINGER, T., F. J. PULIDO & W. KONOLD (2003): Effects of land-use history on size structure of holm oak stands in Spanish dehesas: implications for conservation and restoration. – Environmental Conservation, 30, 1, 61-70.

POPESCU, S. C., R. H. WYNNE & J. A. SCRIVANI (2004): Fusion of small-footprint lidar and multispectral data to estimate plot-level volume and biomass in deciduous and pine forests in Virginia, USA. – Forest Science, 50, 4, 551-565.

POPESCU, S. C. & K. ZHAO (2008): A voxel-based lidar method for estimating crown base height for deciduous and pine trees. – Remote sensing of environment, 112, 3, 767-781.

PUESCHEL, P., H. BUDDENBAUM & J. HILL (2012): An efficient approach to standardizing the processing of hemispherical images for the estimation of forest structural attributes. – Agricultural and forest meteorology, 160, 1-13.

PULKKINEN, M. (2012): On non-circularity of tree stem cross-sections: Effect of diameter selection on cross-section area estimation, Bitterlich sampling and stem volume estimation in Scots pine. – Silva Fennica, 46, 5B, 747-986.

RIEGL-LASER-MANAGEMENT-SYSTEMS-GMBH (2017): Riegl VZ 2000 Data Sheet. <https://www.3dlasermapping.com/wp-content/uploads/2017/10/DataSheet_VZ-2000_2017-06-07.pdf> (Last updated: not known) (Access: 03.03. 2018).

ROERDINK, J. B. & A. MEIJSTER (2000): The watershed transform: Definitions, algorithms and parallelization strategies. – Fundamenta informaticae, 41, 1, 2, 187-228.

ROIG, S., R. R. EVETT, G. GEA-IZQUIERDO, I. CAÑELLAS & O. SÁNCHEZ-PALOMARES (2013): Climatic Influence on Oak Landscape Distributions. In: Campos, P., L. Huntsinger, J. L. Oviedo, P. F. Starrs, M. Díaz, R. B. Standiford & G. Montero (Hrsg.): Mediterranean Oak Woodland Working Landscapes. Dehesas of Spain and Ranchlands of California. Dordrecht: Springer, 61-89.

SABATÉ, S., A. SALA & C. A. GRACIA (1999): Leaf traits and canopy organization. In: Caldwell, M. M., G. Heldmaier, O. L. Lange, H. A. Mooney, E.-D. Schulze & U. Sommer (Hrsg.): Ecology of Mediterranean Evergreen Oak Forests. Berlin: Springer, 121-133.

SCHIESS, P. & F. KROGSTAD (2003): LiDAR-based topographic maps improve agreement between office-designed and field-verified road locations: 7-10.

SCHOLES, R. & S. ARCHER (1997): Tree-grass interactions in savannas. – Annual review of Ecology and Systematics, 28, 1, 517-544.

SIMIONI, G., J. GIGNOUX & X. LE ROUX (2003): Tree layer spatial structure can affect savanna production and water budget: results of a 3-D model. – Ecology, 84, 7, 1879-1894.

SIMÓN, N., F. MONTES, E. DÍAZ-PINÉS, R. BENAVIDES, S. ROIG & A. RUBIO (2013): Spatial distribution of the soil organic carbon pool in a Holm oak dehesa in Spain. – Plant and soil, 366, 1-2, 537-549.

SOUDARISSANANE, S. S. (2016): The geometry of terrestrial laser scanning: identification of errors, modeling and mitigation of scanning geometry. GILDEPRINT. 1-131 S.

SRINIVASAN, S., S. C. POPESCU, M. ERIKSSON, R. D. SHERIDAN & N.-W. KU (2014): Multi-temporal terrestrial laser scanning for modeling tree biomass change. – Forest Ecology and Management, 318, 304-317.

SRINIVASAN, S., S. C. POPESCU, M. ERIKSSON, R. D. SHERIDAN & N.-W. KU (2015): Terrestrial laser scanning as an effective tool to retrieve tree level height, crown width, and stem diameter. – Remote Sensing, 7, 2, 1877.

ST-ONGE, B., P. TREITZ & M. A. WULDER (2003): Tree and canopy height estimation with scanning LiDAR. In: Wulder, M. & S. E. Franklin (Hrsg.): Remote sensing of forest environments: concepts and case studies. New York: Springer Science & Business Media, 489-509.

TAKEUCHI, N. (2005): Elastic Lidar Measurement of the Troposphere. In: Fujii, T. & T. Fukuchi (Hrsg.): Laser Remote Sensing. Boca Raton: CRC Press Taylor & Francis Group 81-140.

TERRADAS, J. (1999): Holm oak and holm oak forests: an introduction. In: Caldwell, M. M., G. Heldmaier, O. L. Lange, H. A. Mooney, E.-D. Schulze & U. Sommer (Hrsg.): Ecology of Mediterranean evergreen oak forests. Berlin: Springer, 3-14.

TURNER, R., R. PANCIERA, M. A. TANASE, K. LOWELL, J. M. HACKER & J. P. WALKER (2014): Estimation of soil surface roughness of agricultural soils using airborne LiDAR. – Remote sensing of environment, 140, 107-117.

TURNER, W., S. SPECTOR, N. GARDINER, M. FLADELAND, E. STERLING & M. STEININGER (2003): Remote sensing for biodiversity science and conservation. – Trends in ecology & evolution, 18, 6, 306-314.

UTKIN, A., A. FERNANDES, F. SIMÕES, R. VILAR & A. LAVROV (2002): Forest-fire detection by means of lidar. Citeseer: 1-14.

VALLADARES, F. & F. I. PUGNAIRE (1999): Tradeoffs between irradiance capture and avoidance in semi-arid environments assessed with a crown architecture model. – Annals of Botany, 83, 4, 459-469.

VAN LAAR, A. & A. AKÇA (2007): Forest mensuration. Springer Science & Business Media, Dordrecht. S.

VAN LEEUWEN, M. & M. NIEUWENHUIS (2010): Retrieval of forest structural parameters using LiDAR remote sensing. – European Journal of Forest Research, 129, 4, 749-770.

VINCENT, L. & P. SOILLE (1991): Watersheds in digital spaces: an efficient algorithm based on immersion simulations. – IEEE Transactions on Pattern Analysis & Machine Intelligence, 6, 583-598.

WALTER, J.-M. N., R. A. FOURNIER, K. SOUDANI & E. MEYER (2003): Integrating clumping effects in forest canopy structure: an assessment through hemispherical photographs. – Canadian Journal of remote sensing, 29, 3, 388-410.

WANG, L., P. GONG & G. S. BIGING (2004): Individual tree-crown delineation and treetop detection in high-spatial-resolution aerial imagery. – Photogrammetric Engineering & Remote Sensing, 70, 3, 351-357.

WANG, Y., H. WEINACKER, B. KOCH & K. STERENCZAK (2008): Lidar point cloud based fully automatic 3D single tree modelling in forest and evaluations of the procedure. – International Archives of Photogrammetry, Remote Sensing and Spatial Information Sciences, 37, PART B6B, 45-51.

WIEZIK, M., A. WIEZIKOVÁ & M. SVITOK (2011): Vegetation structure, ecological stability, and low-disturbance regime of abandoned dry grasslands support specific ant assemblages in Central Slovakia. – Tuexenia, 31, 301-315.

YAO, W., P. KRZYSTEK & M. HEURICH (2012): Tree species classification and estimation of stem volume and DBH based on single tree extraction by exploiting airborne full-waveform LiDAR data. – Remote Sensing of Environment, 123, 368-380.

ZHENG, G. & L. M. MOSKAL (2009): Retrieving leaf area index (LAI) using remote sensing: theories, methods and sensors. – Sensors, 9, 4, 2719-2745.

Appendix
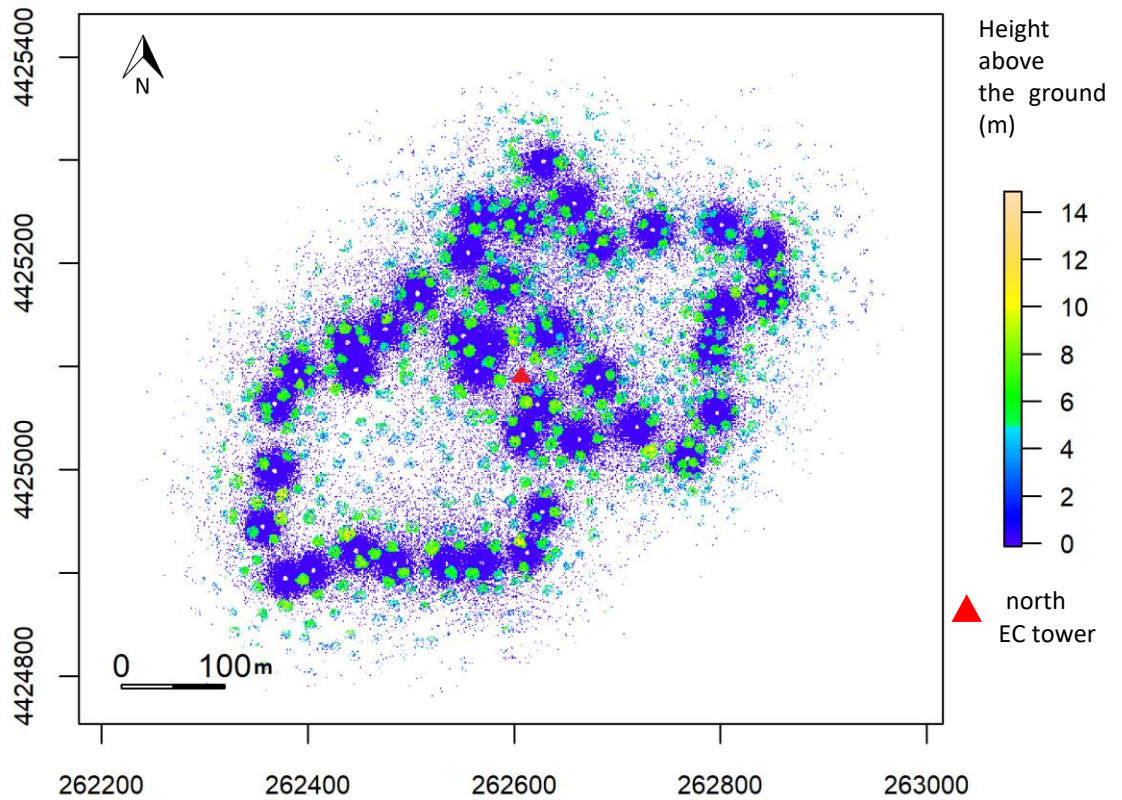
Figure A-1: Standard CHM: area around north EC tower
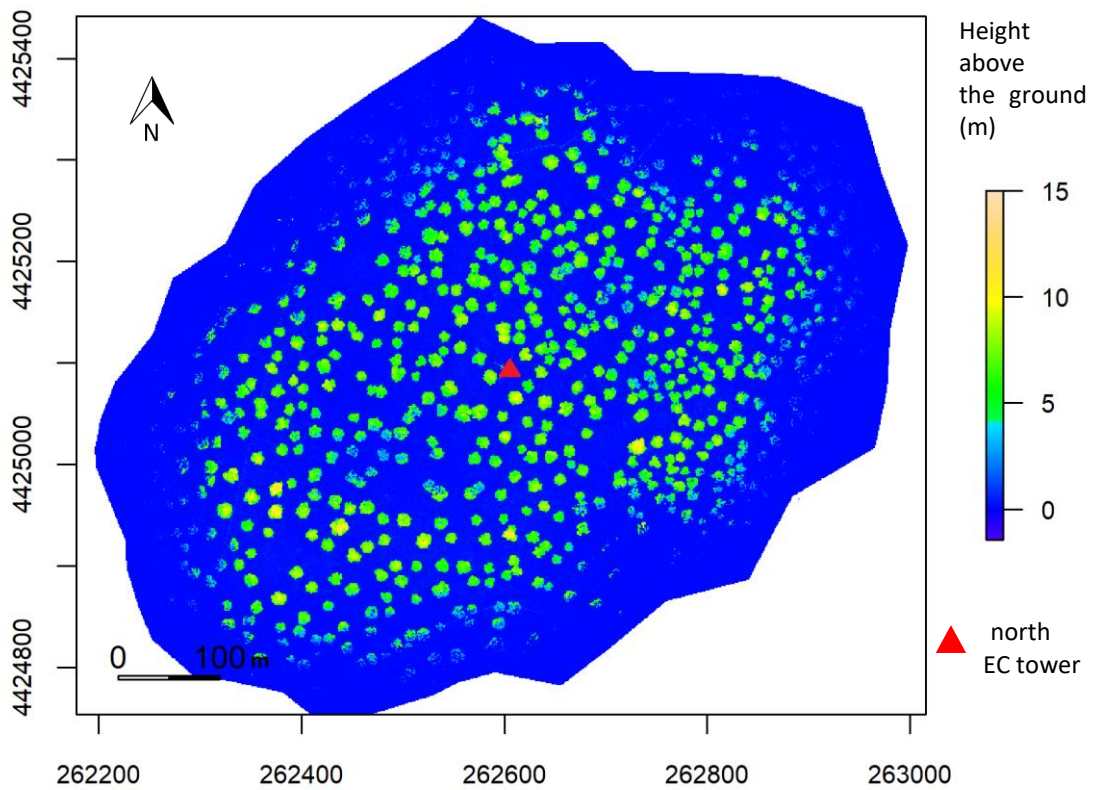
(own illustration)

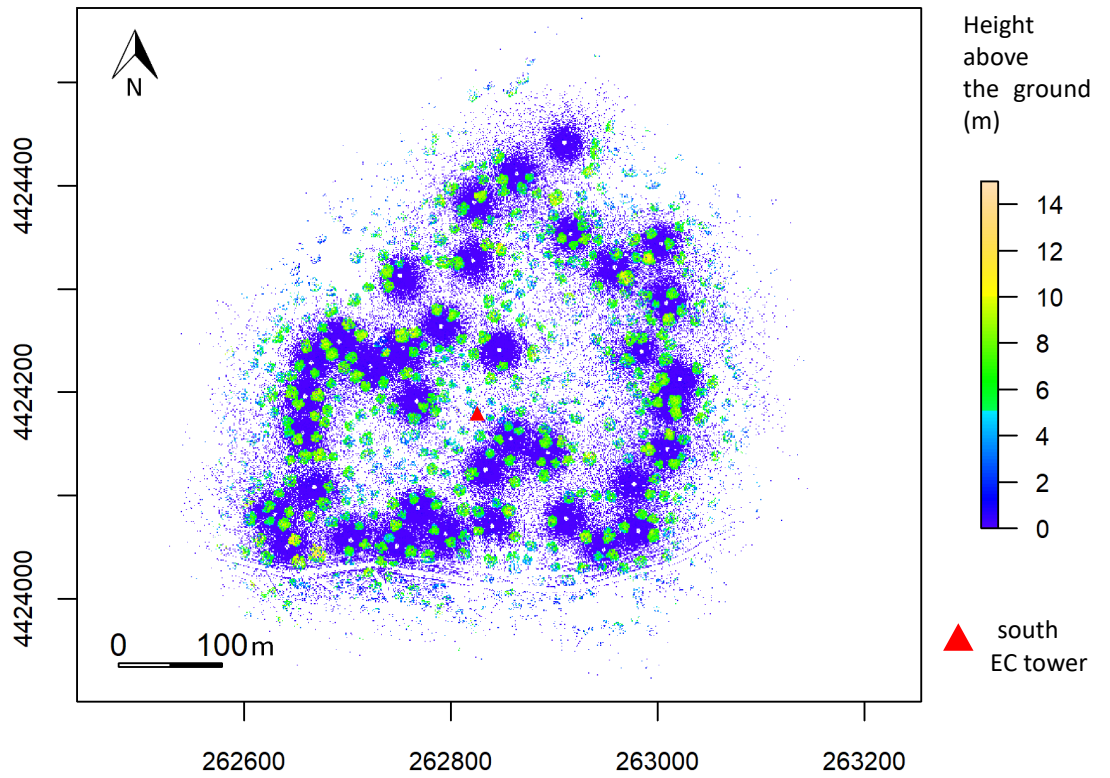Figure A-2: Pitt-free CHM: area around north EC tower

(own illustration)

Figure A-3: Standard CHM: area around south EC tower
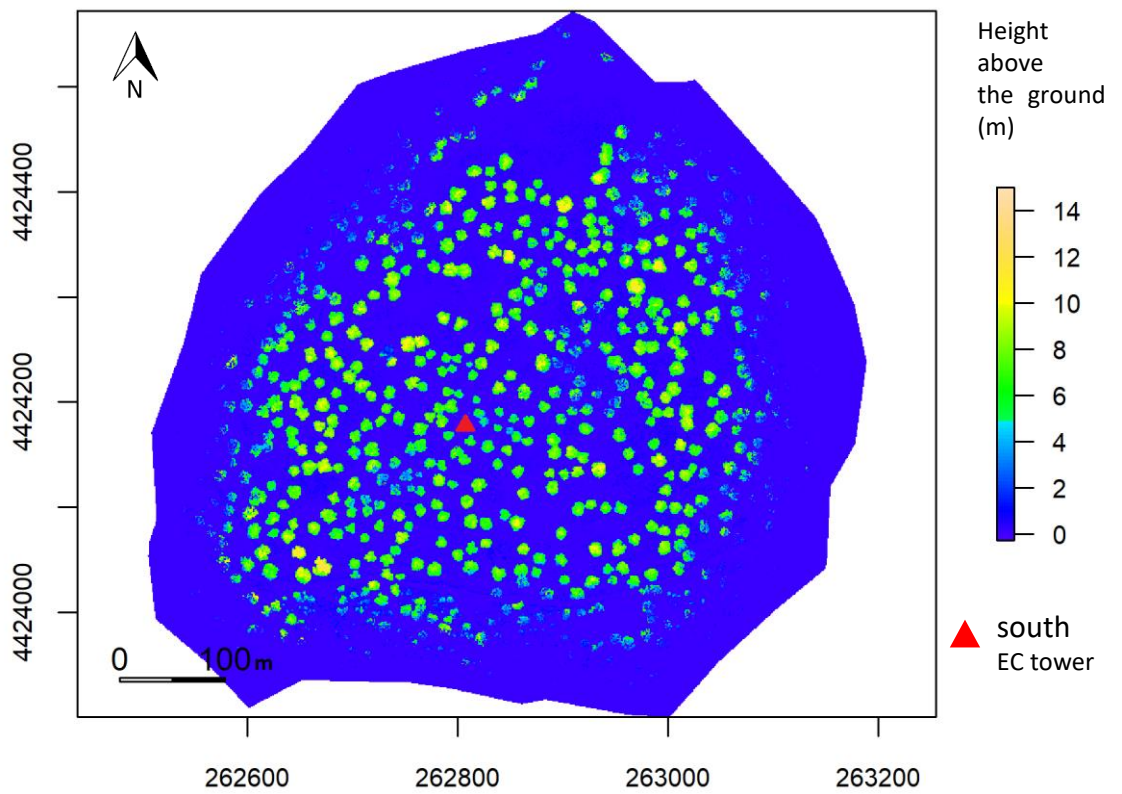
(own illustration)

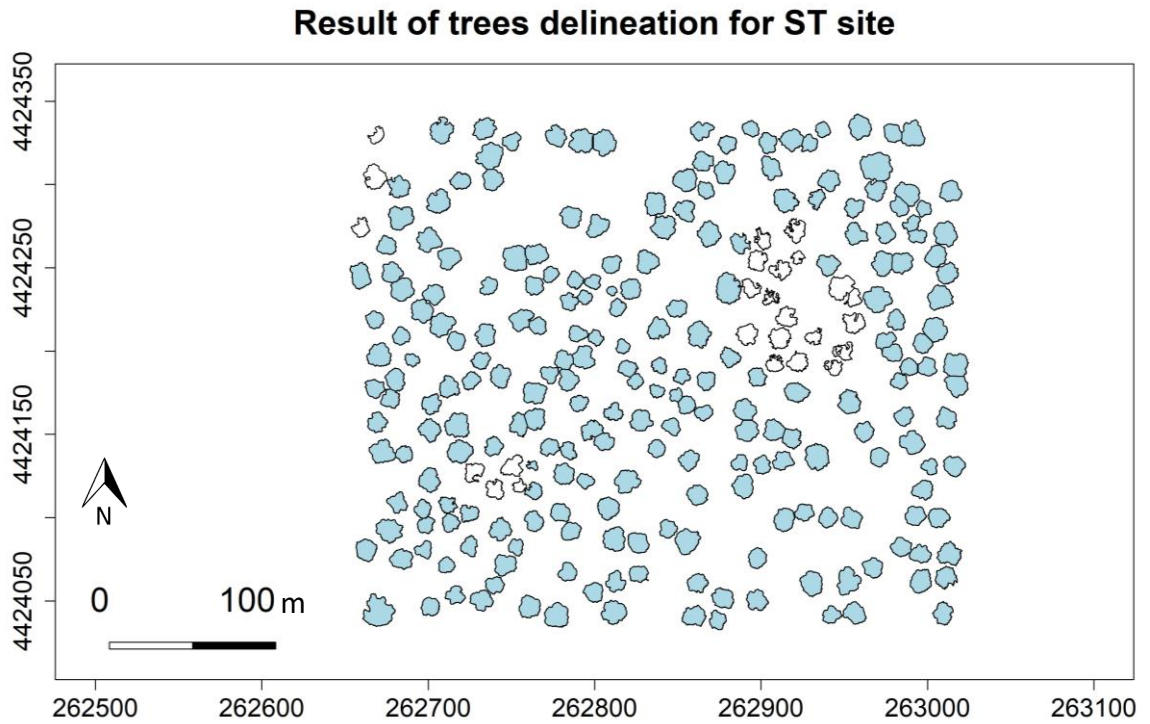Figure A-4: Pit-free CHM: area around south EC tower

(own illustration)

Figure A-5: Result of trees delineation for MT site
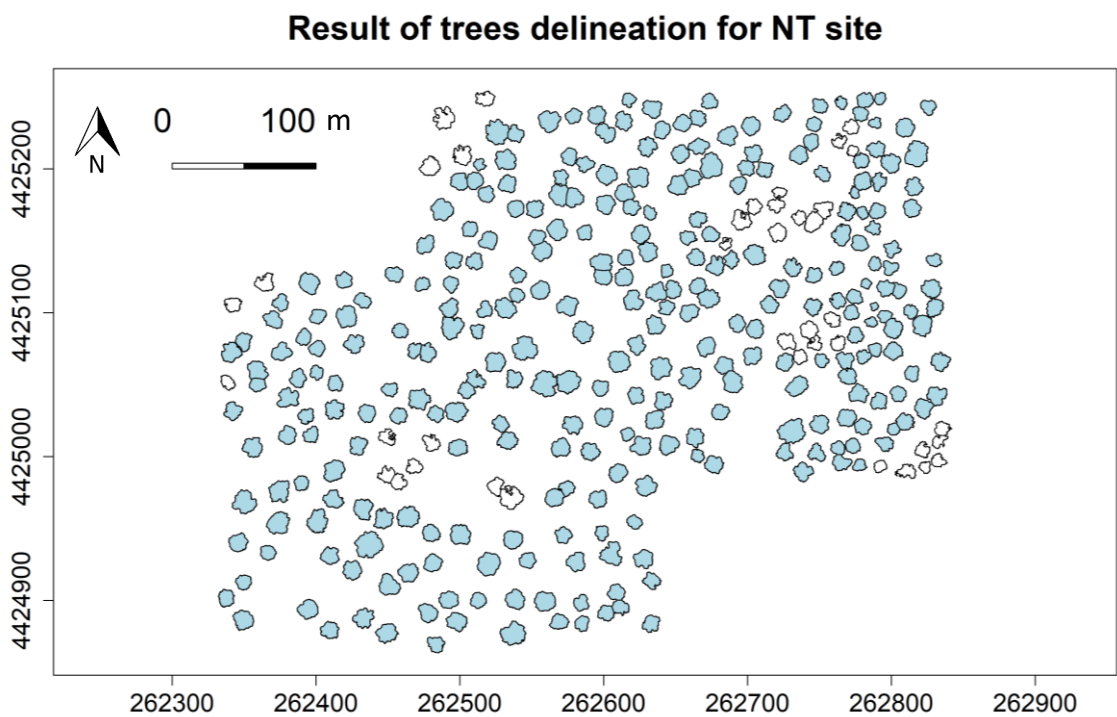
(own illustration)

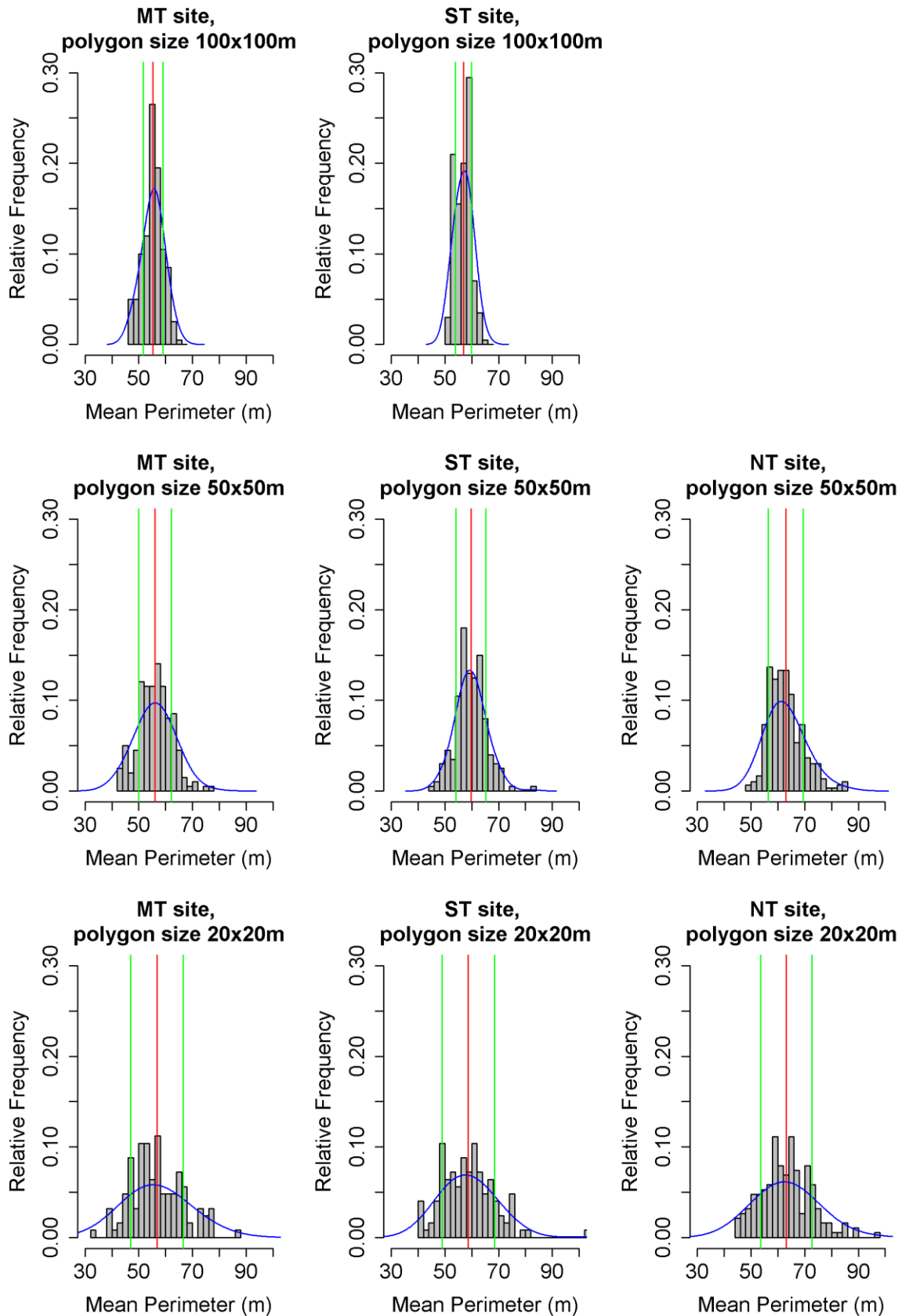Figure A-6: Result of trees delineation for NT site

(own illustration)

Figure A-7: Distribution of mean perimeter

(own illustration)

red line – mean value; green line – standard deviation; blue line – density curve
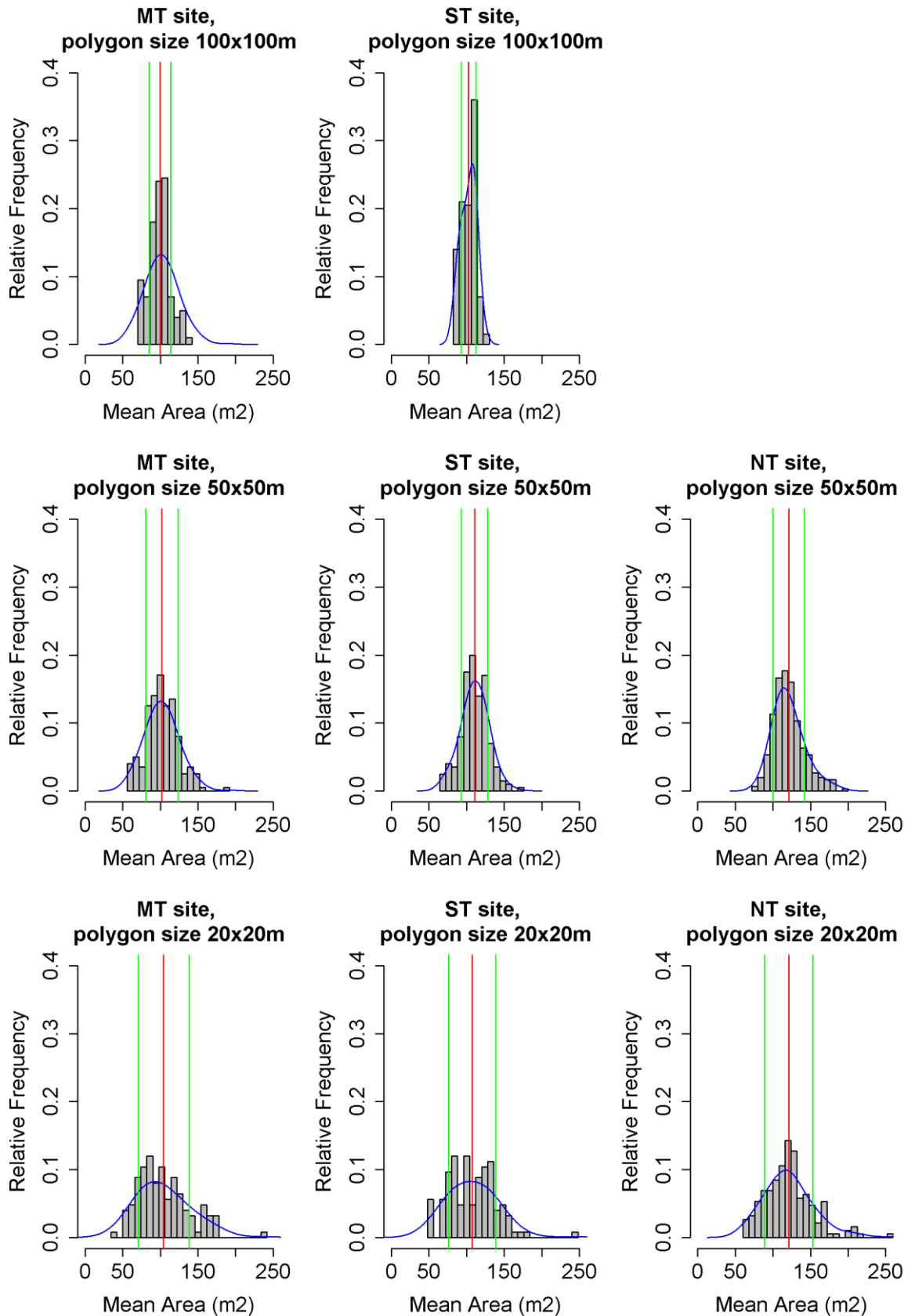
Figure A-8: Distribution of mean area

(own illustration)

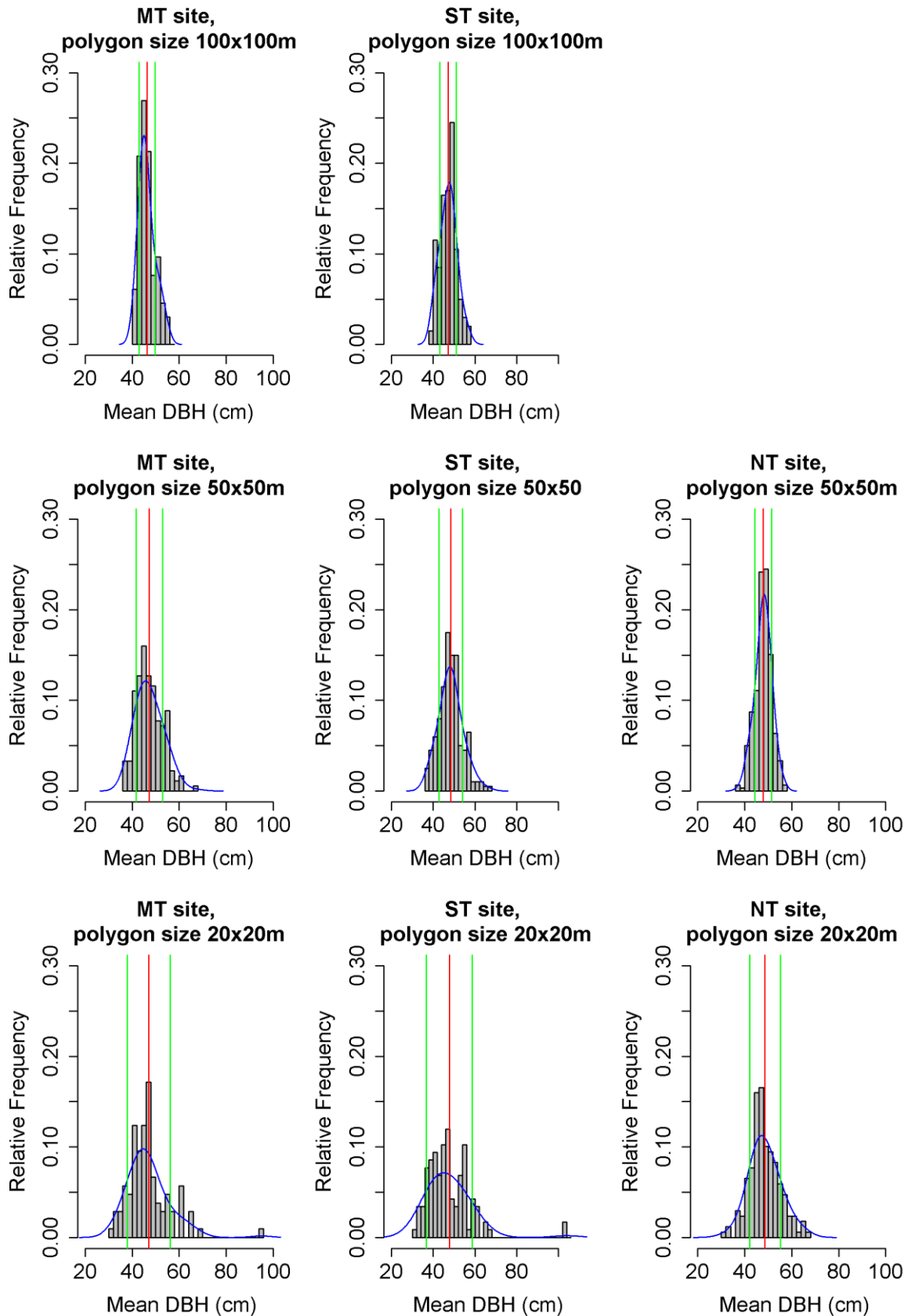red line – mean value; green line – standard deviation; blue line – density curve

Figure A-9: Distribution of mean DBH

(own illustration)

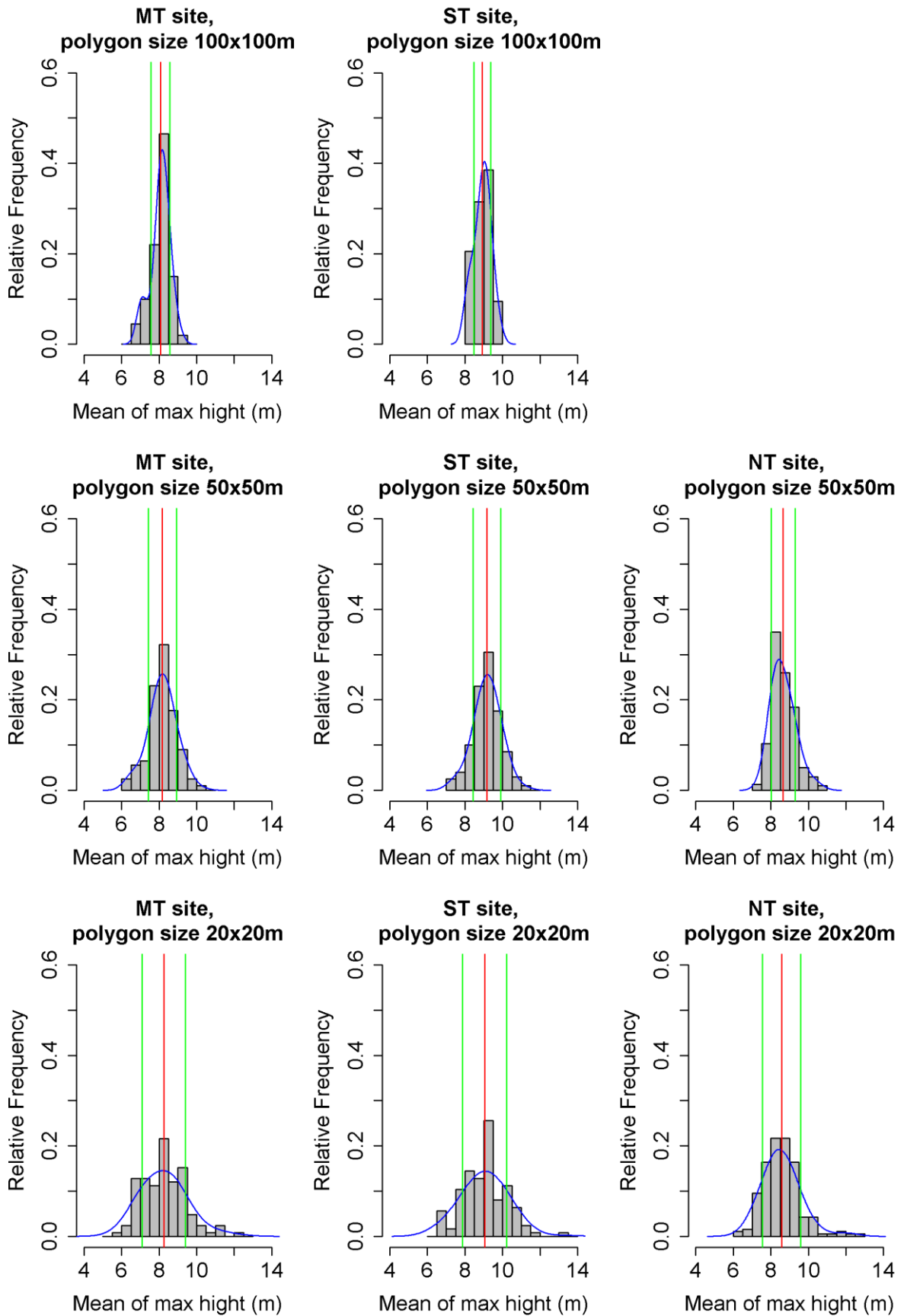red line – mean value; green line – standard deviation; blue line – density curve

Figure A-10: Distribution of mean maximum height

(own illustration)

red line – mean value; green line – standard deviation; blue line – density curve
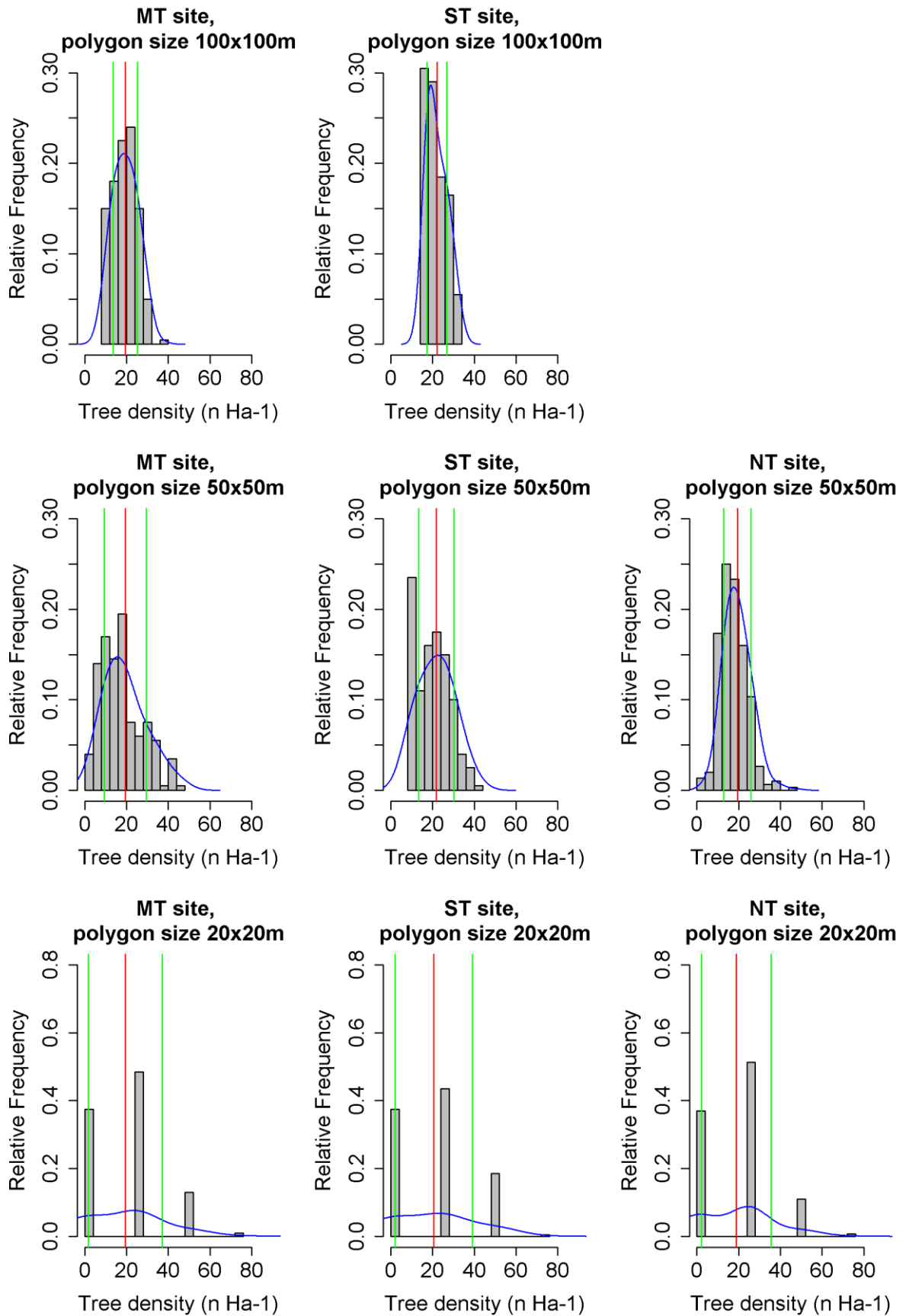
Figure A-11: Distribution of Tree density

(own illustration)

red line – mean value; green line – standard deviation; blue line – density curve
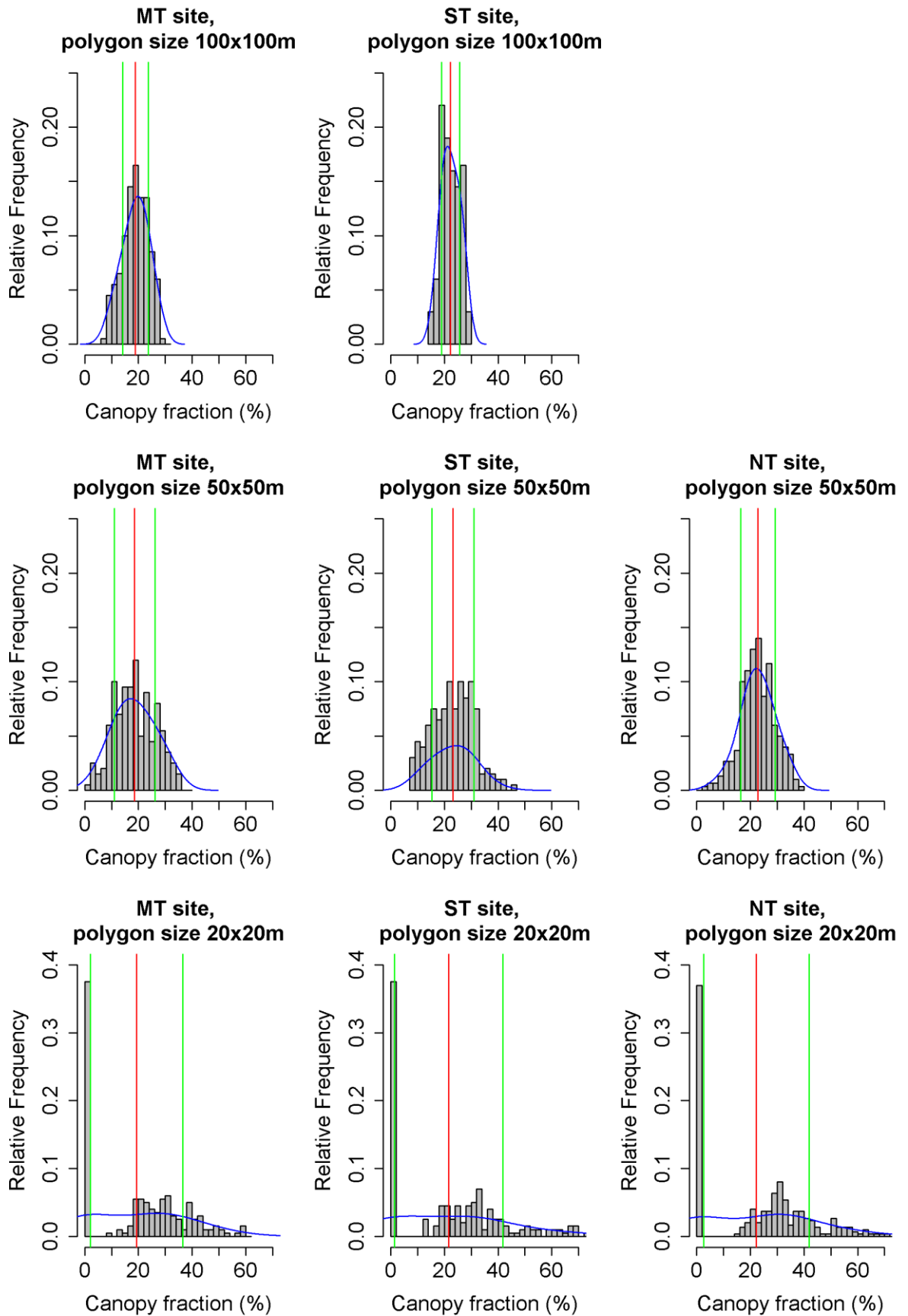
Figure A-12: Distribution of mean perimeter

(own illustration)

red line – mean value; green line – standard deviation; blue line – density curve

Declaration of Authorship

I hereby certify that this thesis has been composed by me and is based on my own work. All direct or indirect sources used are acknowledged as references. This thesis has never been submitted for examination elsewhere nor has it been published in German or any other language.

Place and Date	Signature